You may also like:

Adsorption Applications for Environmental Sustainability

Vortex-in-nanodot potentials in thin circular magnetic dots
G M Wysin

The classical two-dimensional XY model with in-plane magnetic field
M E Gouvea, F G Mertens, A R Bishop et al.

On the topological phase transition of the two-dimensional XY-model on the Voronoi–Delaunay lattice
N M Oliveira-Neto, S G Alves, R L Silva et al.

Free vortex and vortex-pair lifetimes in classical two-dimensional easy-plane magnets
D A Dimitrov and G M Wysin

Magnetic Excitations and Geometric Confinement
Theory and simulations
Gary Matthew Wysin

Chapter 9

Magnetic vortex core motion and internal dynamics

In this chapter some dynamic properties of individual vortices in 2D ferromagnets are presented. Analogous to 1D magnetic solitons, vortices have charges, momentum and mass. In addition, they possess a topological charge or gyrovector $\mathbf{G}$ that strongly governs the motion of the vortex core in response to applied forces. The Thiele equation, which describes vortex core motion via the gyrovector, is presented and its extension to include mass is discussed. The connection to Lagrangian mechanics for the core motion is also considered. Vortices also interact with spin waves and modify the spin wave spectrum. Oscillation of spin waves on top of a vortex background is considered its *internal dynamics*, which includes effects that can be studied theoretically and with simulations.

9.1 Thiele equations and vortex motion

In a complex system, a vortex is affected by an externally applied magnetic field and the far spin field of other vortices, as well as damping torques. Thiele [1, 2], and also Huber [3], developed a kind of collective coordinate equation that describes the motion of a domain wall or a vortex, treating it as a particle. The Thiele equation of motion gives the dynamics for the motion of the vortex core, which could have some time-dependent position $\mathbf{X}(t)$ and a corresponding time-varying velocity $\mathbf{V}(t) = \dot{\mathbf{X}}(t)$.

In the development of the dynamic equation by Thiele, it was assumed that the vortex structure for a moving vortex is the same as that for a static vortex, $\mathbf{S}(\mathbf{r})$, except for adding a uniform translation, $\mathbf{S} = \mathbf{S}(\mathbf{r} - \mathbf{X}(t))$. Here $\mathbf{r}$ is the location of a spin being measured (field point), whereas $\mathbf{X}$ is the location of the vortex center. If the position $\mathbf{X}(t)$ of the core translates uniformly, it is described by the equation,

$$\mathbf{X}(t) = \mathbf{V}t + \mathbf{X}_0. \tag{9.1}$$

But we have seen earlier that the vortex structure itself is changed in shape by the motion. In particular, the out-of-plane component develops an asymmetric structure

linearly proportional to **V**. Thus, we consider here the modification to the Thiele equation, when vortex shape variations that are dependent on **V** are included in the theory [4]. Then, the spin structure is assumed to have a form that has an explicit velocity-dependence, for unit spins,

$$\mathbf{s} = \mathbf{s}(\mathbf{r} - \mathbf{X}(t), \mathbf{V}(t)). \tag{9.2}$$

By translating, the spin at a given location is changed. Also, if the vortex changes its velocity, the vortex changes its structure and a spin at a given location is changed. This latter effect is represented by a dependence on **V**, the second parameter in this collective coordinate spin function. This means that the time derivative of the spin field is obtained from both a convective derivative term and an acceleration term:

$$\frac{d\mathbf{s}}{dt} = -\frac{d\mathbf{X}}{dt} \cdot \frac{\partial \mathbf{s}}{\partial \mathbf{r}} + \frac{d\mathbf{V}}{dt} \cdot \frac{\partial \mathbf{s}}{\partial \mathbf{V}} = -\mathbf{V} \cdot \frac{\partial \mathbf{s}}{\partial \mathbf{r}} + \mathbf{A} \cdot \frac{\partial \mathbf{s}}{\partial \mathbf{V}}. \tag{9.3}$$

The last term, proportional to the vortex acceleration $\mathbf{A} = \dot{\mathbf{V}}$, will lead to a vortex effective mass. The dot products indicate the sum over x-and y-components of both the coordinate and velocity gradients.

Equation (9.2) represents only the contributions to the spin field due to a particular vortex under consideration. In a real application, the spin field will be a nonlinear superposition of parts due to the vortex of interest, and all other contributions from say, other vortices at far away locations. It can be kept in mind, then, that the total spin field will not be translating as in (9.2). Indeed, the vortex of interest is influenced by the spin fields of all other vortices and other independent modes in the system.

9.1.1 Derivation of Thiele's equation of motion

The Thiele equation is derived from the Landau–Lifshitz equations, including Gilbert damping, by considering it as an equation with force-like terms (acting on the vortex). Wysin and Mertens [4] extended it to include acceleration effects, based on analysis of vortex momentum. First, we consider a derivation based on the Thiele approach, in which the damping is easily accounted for. The Landau–Lifshitz–Gilbert (LLG) equation (2.105) for **s** is

$$\dot{\mathbf{s}} = \mathbf{s} \times \gamma \mathbf{B} - \alpha \mathbf{s} \times \dot{\mathbf{s}}, \tag{9.4}$$

where

$$\gamma \mathbf{B} = -\frac{\delta H}{\delta \mathbf{S}} \tag{9.5}$$

is the effective field providing the torque (it could depend on **s**). The LLG equation can be expressed equivalently as

$$\mathbf{s} \times \mathbf{H}_{\text{net}} = 0 \tag{9.6a}$$

$$\mathbf{H}_{\text{net}} \equiv \gamma \mathbf{B} + (\mathbf{s} \times \dot{\mathbf{s}}) - \alpha \dot{\mathbf{s}}. \tag{9.6b}$$

Note that this works because spin length is conserved, which implies $\mathbf{s} \cdot \dot{\mathbf{s}} = 0$, used in the vector identity,

$$\mathbf{s} \times (\mathbf{s} \times \dot{\mathbf{s}}) = (\mathbf{s} \cdot \dot{\mathbf{s}})\mathbf{s} - (\mathbf{s} \cdot \mathbf{s})\dot{\mathbf{s}} = -\dot{\mathbf{s}}. \tag{9.7}$$

Equation (9.6a) proves that the fields $\mathbf{H}_{\text{net}}$ and $\mathbf{s}$ are parallel. Any change in $\mathbf{s}$ must be perpendicular to $\mathbf{s}$, i.e. $(\nabla \mathbf{s}) \cdot \mathbf{s} = 0$, where $\nabla = \hat{\mathbf{e}}_j \partial_j = \hat{\mathbf{e}}_j \frac{\partial}{\partial r_j}$, and the spin components are contracted by dot ($\cdot$) here, resulting in a vector. In this section repeated indices i, j, $k = 1$, 2, are summed over. Because $\mathbf{H}_{\text{net}}$ is parallel to $\mathbf{s}$, one has an expression that contains local force-like quantities as a conservation law:

$$-(\nabla \mathbf{s}) \cdot \mathbf{H}_{\text{net}} = -\left(\hat{\mathbf{e}}_j \partial_j \mathbf{s}\right) \cdot \left[\gamma \mathbf{B} + (\mathbf{s} \times \dot{\mathbf{s}}) - \alpha \dot{\mathbf{s}}\right] = 0. \tag{9.8}$$

A minus sign is included so that the resulting terms go directly as written into the Thiele equation being produced. The time derivatives contained here are taken in the convective form (9.3). It is more convenient to express this time derivative using index notation,

$$\dot{\mathbf{s}} = -V_k \partial_k \mathbf{s} + A_k \tilde{\partial}_k \mathbf{s}, \tag{9.9}$$

where $\tilde{\partial}_j \equiv \frac{\partial}{\partial V_j}$ is the velocity gradient and $\partial_k = \frac{\partial}{\partial r_k}$ is a component of the gradient with respect to the field point $\mathbf{r}$. This now gives

$$-\gamma \mathbf{B} \cdot \left(\hat{\mathbf{e}}_j \partial_j \mathbf{s}\right) - \mathbf{s} \cdot \left(\partial_j \mathbf{s} \times \partial_k \mathbf{s}\right)\hat{\mathbf{e}}_j V_k - \alpha\left(\partial_j \mathbf{s}\right) \cdot (\partial_k \mathbf{s})\hat{\mathbf{e}}_j V_k$$
$$+ \mathbf{s} \cdot (\partial_j \mathbf{s} \times \tilde{\partial}_k \mathbf{s})\hat{\mathbf{e}}_j A_k + \alpha\left(\partial_j \mathbf{s}\right) \cdot (\tilde{\partial}_k \mathbf{s})\hat{\mathbf{e}}_j A_k = 0. \tag{9.10}$$

The terms in the first line give Thiele's original equation; the second line contains the modifications caused by velocity-dependent structure changes. This then motivates the definitions of integrals over a vortex structure, which are collective properties of a vortex that act to describe the dynamics.

The first term in the first line of (9.10) is related to an effective force $\mathbf{F}$ acting on the vortex. Consider using the definition (9.5) of the effective field $\gamma \mathbf{B}$, and integrating over 2D space,

$$-\int d^2 r \; \gamma \mathbf{B} \cdot \left(\hat{\mathbf{e}}_j \partial_j \mathbf{s}\right) = \frac{1}{S}\hat{\mathbf{e}}_j \int d^2 r \; \frac{\delta H}{\delta \mathbf{S}} \cdot \frac{\partial \mathbf{S}}{\partial r_j}$$
$$= \frac{v_{\text{cell}}}{S}\hat{\mathbf{e}}_j \int \frac{d^2 r}{v_{\text{cell}}} \frac{\delta H}{\delta \mathbf{S}} \cdot \left(-\frac{\partial \mathbf{S}}{\partial X_j}\right)$$
$$= -\frac{v_{\text{cell}}}{S}\hat{\mathbf{e}}_j \frac{\partial}{\partial X_j} \int \frac{d^2 r}{v_{\text{cell}}} \; \mathcal{H} = -\frac{v_{\text{cell}}}{S} \frac{\partial H}{\partial \mathbf{X}}. \tag{9.11}$$

In the second line of (9.11), the gradient $\partial \mathbf{S}/\partial \mathbf{r}$ has been replaced by $-\partial \mathbf{S}/\partial \mathbf{X}$, and the area per spin, v_{cell}, has been included into the integrand. The last line of (9.11) is written as a gradient of the total Hamiltonian, *with respect to the vortex core location* $\mathbf{X}$. That defines the force acting on the vortex,

$$\mathbf{F} = -\frac{\partial H}{\partial \mathbf{X}}. \tag{9.12}$$

Therefore this first term in (9.10) is summarized as

$$-\int d^2 r \; \gamma \mathbf{B} \cdot \left(\hat{\mathbf{e}}_j \partial_j \mathbf{s}\right) = \frac{1}{\sigma} \mathbf{F}, \qquad \sigma \equiv \frac{S}{v_{\text{cell}}}. \tag{9.13}$$

The factor σ is spin density per area and v_{cell} is the area occupied by one spin in the system. In many papers the factor $1/\sigma$ on $\mathbf{F}$ is instead expressed equivalently as γ/m_0, where $m_0 = \gamma S/v_{\text{cell}}$ is the magnetic dipole moment per unit area.

The second term in the first line of (9.10) leads to an anti-symmetric gyrotensor G_{jk} and gyrovector $\mathbf{G} = G_i \hat{\mathbf{e}}_i$ derived from it (both taken as dimensionless here):

$$\mathsf{G}_{jk} \equiv \int d^2r \; \mathbf{s} \cdot \left(\partial_j \mathbf{s} \times \partial_k \mathbf{s} \right) \tag{9.14a}$$

$$G_i = \frac{1}{2}\epsilon_{ijk}\mathsf{G}_{jk}. \tag{9.14b}$$

Because j and k can only take the values 1 or 2, in application for a 2D system the only non-zero elements of the gyrotensor are $\mathsf{G}_{12} = -\mathsf{G}_{21}$. Then, the gyrovector only has an out-of-plane component, $\mathbf{G} = G_3 \hat{\mathbf{e}}_3$, where $G_3 = \mathsf{G}_{12}$, and it can also be expressed in a form using the canonical variables (see the derivation of (9.28) below),

$$\mathbf{G} = G_3 \hat{\mathbf{e}}_3 = \int d^2r \; \nabla\phi \times \nabla s^z. \tag{9.15}$$

Some algebra is aided by the result of the following exercise.

Exercise 9.1. From (9.14b) and the identity for the Levi–Civita symbol,

$$\epsilon_{ijk}\epsilon_{ilm} = \delta_{jl}\delta_{km} - \delta_{jm}\delta_{kl} \tag{9.16}$$

show the additional relation,

$$\mathsf{G}_{jk} = \epsilon_{ijk}G_i. \tag{9.17}$$

With the result (9.17) for G_{jk}, the corresponding term in (9.10) becomes

$$-\mathsf{G}_{jk}\hat{\mathbf{e}}_j V_k = -\epsilon_{ijk}G_i\hat{\mathbf{e}}_j V_k = +\epsilon_{jik}\hat{\mathbf{e}}_j G_i V_k = \mathbf{G} \times \mathbf{V}. \tag{9.18}$$

As the gyrovector $\mathbf{G}$ points perpendicular to the plane, this *gyrotropic force* $\mathbf{G} \times \mathbf{V}$ then produces forces on the vortex acting within the 2D plane. It is the most important physical effect that results from the gyrovector.

The next collective property from the first line of (9.10) is a symmetric dissipation tensor with components D_{jk} (also dimensionless),

$$\mathsf{D}_{jk} \equiv -\alpha \int d^2r \left(\partial_j \mathbf{s} \right) \cdot \left(\partial_k \mathbf{s} \right). \tag{9.19}$$

This can define a dyadic object, $\mathsf{D} = \mathsf{D}_{jk}\hat{\mathbf{e}}_j\hat{\mathbf{e}}_k$, that operates on $\mathbf{V}$. Then using only these vortex properties, the original form of the Thiele equation is

$$\frac{1}{\sigma}\,\mathbf{F} + \mathbf{G} \times \mathbf{V} + \mathsf{D} \cdot \mathbf{V} = 0. \tag{9.20}$$

This equation describes the dynamics of the vortex core motion, assuming the internal spin structure of a vortex is unaffected by velocity. All terms in the equation have dimensions of velocity. Note that the gyrovector will vanish for an in-plane vortex. Then, in the absence of dissipation, this equation is inadequate for the

dynamics of an in-plane vortex, because it becomes $\mathbf{F} = 0$, which is not necessarily true if the vortex is exposed to some external field. This is an important reason why the acceleration terms must be included.

9.1.2 Including vortex mass effects

Now consider the velocity-dependent vortex structure changes. The first term in the second line of (9.10) motivates definition of an effective mass tensor $\mathbf{M} = \mathsf{M}_{jk}\hat{\mathbf{e}}_j\hat{\mathbf{e}}_k$, with elements

$$\mathsf{M}_{jk} \equiv -\int \mathrm{d}^2r \; \mathbf{s} \cdot (\partial_j\mathbf{s} \times \tilde{\partial}_k\mathbf{s}). \tag{9.21}$$

This definition gives $\mathbf{M}$ dimensions of time. A vortex mass tensor $\mathbf{m}$ in units of kilograms would be obtained by including a factor of the spin density,

$$\mathbf{m} \equiv \sigma\mathbf{M}. \tag{9.22}$$

Also one has another term, a new type of dissipation tensor $\tilde{\mathbf{D}} = \tilde{\mathsf{D}}_{jk}\hat{\mathbf{e}}_j\hat{\mathbf{e}}_k$, with elements

$$\tilde{\mathsf{D}}_{jk} \equiv -\alpha\int \mathrm{d}^2r \left(\partial_j\mathbf{s}\right) \cdot (\tilde{\partial}_k\mathbf{s}). \tag{9.23}$$

The addition of these leads to a modified Thiele equation, including acceleration effects,

$$\frac{1}{\sigma} \mathbf{F} + \mathbf{G} \times \mathbf{V} + \mathbf{D} \cdot \mathbf{V} = \mathbf{M} \cdot \mathbf{A} + \tilde{\mathbf{D}} \cdot \mathbf{A}. \tag{9.24}$$

While both $\mathbf{M}$ and $\tilde{\mathbf{D}}$ appear in the same way in the equation, one expects that the 2×2 matrices associated with them have different structures, leading to quite different physical effects. The effect of $\tilde{\mathbf{D}}$ is expected to be small, compared to the damping caused by D.

The factor of σ dividing the force can be moved to the other terms, defining ones with more natural units. Thus we could write this modified Thiele equation with all terms having force dimensions as

$$\mathbf{F} + \mathbf{g} \times \mathbf{V} + \mathbf{d} \cdot \mathbf{V} = \mathbf{m} \cdot \mathbf{A} + \tilde{\mathbf{d}} \cdot \mathbf{A}. \tag{9.25}$$

σ has been used to make the gyrovector, dissipation tensors and mass tensor with physically reasonable units:

$$\mathbf{g} = \sigma\mathbf{G} = S\int \frac{\mathrm{d}^2r}{v_{\text{cell}}} \; \mathbf{s} \cdot \left(\partial_1\mathbf{s} \times \partial_2\mathbf{s}\right)\hat{\mathbf{e}}_3 \tag{9.26a}$$

$$\mathbf{d} = \sigma\mathbf{D} = -\alpha S\int \frac{\mathrm{d}^2r}{v_{\text{cell}}}\left(\partial_j\mathbf{s}\right) \cdot \left(\partial_k\mathbf{s}\right)\hat{\mathbf{e}}_j\hat{\mathbf{e}}_k \tag{9.26b}$$

$$\mathbf{m} = \sigma\mathbf{M} = -S\int \frac{\mathrm{d}^2r}{v_{\text{cell}}} \; \mathbf{s} \cdot (\partial_j\mathbf{s} \times \tilde{\partial}_k\mathbf{s})\hat{\mathbf{e}}_j\hat{\mathbf{e}}_k \tag{9.26c}$$

$$\tilde{\mathbf{d}} = \sigma\tilde{\mathbf{D}} = -\alpha S\int \frac{\mathrm{d}^2r}{v_{\text{cell}}}\left(\partial_j\mathbf{s}\right) \cdot (\tilde{\partial}_k\mathbf{s})\hat{\mathbf{e}}_j\hat{\mathbf{e}}_k. \tag{9.26d}$$

Next, it is necessary to discuss the values of these collective properties of a vortex, contrasting the results for in-plane versus out-of-plane vortices.

9.1.3 Calculation of vortex gyrovector and other properties

The expression in (9.14) is not so convenient for calculation of the gyrovector components, $G_3 = \mathsf{G}_{12} = -\mathsf{G}_{21}$, just as (9.21) is not particularly good for calculation of M_{jk}. It is better to find their expressions in terms of the in-plane and out-of-plane angles (ϕ, θ). Letting $\mathbf{s} = (\cos\theta\cos\phi, \cos\theta\sin\phi, \sin\theta)$, one has the components of a space or velocity gradient, where ∂ represents any of $\partial/\partial r_j$ or $\partial/\partial V_k$,

$$\partial\mathbf{s} = (-\sin\theta\cos\phi\ \partial\theta - \cos\theta\sin\phi\ \partial\phi, -\sin\theta\sin\phi\ \partial\theta + \cos\theta\cos\phi\ \partial\phi, \cos\theta\ \partial\theta)$$
$$= (-\sin\theta\cos\phi, -\sin\theta\sin\phi, \cos\theta)\partial\theta + (-\sin\phi, \cos\phi, 0)\cos\theta\ \partial\phi$$
$$= \hat{\boldsymbol{\theta}}\ \partial\theta + \hat{\boldsymbol{\phi}}\cos\theta\ \partial\phi. \tag{9.27}$$

The unit vectors $\hat{\boldsymbol{\theta}}$ and $\hat{\boldsymbol{\phi}}$ implicitly defined in the second line are oriented in the directions of increasing θ and ϕ, respectively. Their cross product is $\hat{\boldsymbol{\phi}} \times \hat{\boldsymbol{\theta}} = \hat{\mathbf{r}} = \mathbf{s}$. The relation (9.27) represents how the unit vector $\mathbf{s}$ can only change as its tip moves on the unit sphere. This gradient can be combined with another general gradient component, $\partial'\mathbf{s}$, leading to

$$\mathbf{s}\cdot(\partial\mathbf{s}\times\partial'\mathbf{s}) = \mathbf{s}\cdot\left[\left(\hat{\boldsymbol{\theta}}\ \partial\theta + \hat{\boldsymbol{\phi}}\cos\theta\ \partial\phi\right)\times\left(\hat{\boldsymbol{\theta}}\ \partial'\theta + \hat{\boldsymbol{\phi}}\cos\theta\ \partial'\phi\right)\right]$$
$$= \cos\theta\left(\partial\phi\ \partial'\theta - \partial\theta\ \partial'\phi\right)$$
$$= \partial\phi\partial's^z - \partial s^z\partial'\phi. \tag{9.28}$$

Choosing $\partial \to \partial_j$ and $\partial' \to \partial_k$ (two space gradients), expression (9.14) becomes

$$G_{jk} = \int \mathrm{d}^2r\left(\partial_j\phi\ \partial_k s^z - \partial_j s^z\partial_k\phi\right). \tag{9.29}$$

Finally, using this to find $G_3 = G_{12}$ gives the angular formula for the gyrovector (9.15).

For static in-plane vortices with $S^z = 0$, and even for moving ones, with S^z anti-symmetric about the direction of motion, (9.15) gives $\mathbf{G} = 0$. For out-of-plane vortices, consider the static profile, and assume that the change in $\mathbf{G}$ will be essentially zero for moving out-of-plane vortices. The in-plane angle $\phi(\varphi)$ changes by $2\pi q$ around the core, and the out-of-plane spin component $s^z(r)$ takes the value $s^z(0) = p = \pm 1$ at the core and $s^z = 0$ as $r \to \infty$. Then (9.15) becomes

$$\mathbf{G} = \int_0^{2\pi}\mathrm{d}\varphi\int_0^{\infty} r\mathrm{d}r\ \frac{1}{r}\frac{\partial\phi}{\partial\varphi}\hat{\boldsymbol{\varphi}}\times\frac{\partial s^z}{\partial r}\hat{\mathbf{r}} = \int_0^{2\pi}\mathrm{d}\varphi\int_0^{\infty} r\mathrm{d}r\ \frac{q}{r}\frac{\partial s^z}{\partial r}(-\hat{\mathbf{z}}) = 2\pi pq\hat{\mathbf{z}}. \tag{9.30}$$

This gives $G = \pm 2\pi$, which is the solid angle on the unit sphere covered by the vortex spin distribution. This defines the topological charge $Q = G = 2\pi pq$ of a vortex.

For components of the mass tensor, choose $\partial \to \partial_j$ (space gradient) and $\partial' \to \tilde{\partial}_k$ (velocity gradient), which then gives from (9.21) the angular formulation,

$$\mathbf{M}_{jk} = -\int \mathrm{d}^2r(\partial_j\phi\ \tilde{\partial}_k s^z - \partial_j s^z\ \tilde{\partial}_k\phi). \tag{9.31}$$

One can see that $\mathbf{M}_{jk}$ is not anti-symmetric. As a result it is not possible to write its contraction with the acceleration $\mathbf{A}$ as a cross product. To estimate $\mathbf{M}_{jk}$, we can use the result $s^z \approx \sin\theta_1$ in (8.39) for the leading corrections to the static vortex structure, due to motion. Also, the in-plane angle does not depend on $\mathbf{V}$, to leading order, so $\tilde{\partial}_k\phi \approx 0$. The non-zero velocity gradient is that of s^z, which is

$$\tilde{\partial}_k s^z = \frac{\partial}{\partial V_k}\left[-\frac{\mathbf{V}\cdot\nabla\phi}{JS(4\delta - q^2/r^2)}\right] = \frac{-\partial_k\phi}{JS(4\delta - q^2/r^2)} \approx \frac{-1}{4\delta\,JS}\partial_k\phi. \tag{9.32}$$

The last approximation uses the field far from the core. This reduces the mass tensor to

$$\mathbf{M}_{jk} \approx \frac{1}{4\delta\,JS}\int d^2r\,\partial_j\phi\,\partial_k\phi. \tag{9.33}$$

From (8.8), with $\nabla\phi = q\hat{\boldsymbol{\varphi}}/r$, we have

$$\left(\partial_1\phi, \partial_2\phi\right) = \frac{q}{r}\left(-\sin\varphi, \cos\varphi\right). \tag{9.34}$$

Upon integration over the plane, $\sin\varphi$ and $\cos\varphi$ are orthogonal functions, and only the diagonal terms of $\mathbf{M}_{jk}$ survive. With lower and upper radial cutoffs r_0 and R, they are

$$\mathbf{M}_{jk} = \frac{\delta_{jk}}{4\delta JS}\int_0^{2\pi}d\varphi\,\sin^2\varphi\int_{r_0}^R r\,dr\,\frac{q^2}{r^2} = \frac{\pi q^2}{4\delta JS}\ln\left(\frac{R}{r_0}\right)\delta_{jk}. \tag{9.35}$$

This has the same logarithmic dependence on system size as the static in-plane vortex energy. Although calculated from the in-plane vortex structure, the mass tensor for out-of-plane vortices should be nearly identical.

The dissipation tensor $\mathbf{D}_{jk}$ can be written with the help of (9.27) as

$$\mathbf{D}_{jk} = -\alpha\int dr^2\left(\hat{\boldsymbol{\theta}}\,\partial_j\theta + \hat{\boldsymbol{\phi}}\cos\theta\,\partial_j\phi\right)\cdot\left(\hat{\boldsymbol{\theta}}\,\partial_k\theta + \hat{\boldsymbol{\phi}}\cos\theta\,\partial_k\phi\right)$$

$$= -\alpha\int dr^2\left(\partial_j\theta\,\partial_k\theta + \cos^2\theta\,\partial_j\phi\,\partial_k\phi\right). \tag{9.36}$$

For an in-plane vortex, the contribution from gradients of θ will be proportional to V^2, so we consider it small. Then the main contribution comes from the gradients of ϕ, and using $\cos\theta \approx 1$,

$$\mathbf{D}_{jk} \approx -\alpha\int dr^2\,\partial_j\phi\,\partial_k\phi = -\alpha\pi q^2\delta_{jk}\ln\frac{R}{r_0} \qquad \text{(in-plane vortex)}. \tag{9.37}$$

For an in-plane vortex, the damping tensor is directly proportional to the mass tensor. One can see that the negative sign here is physically reasonable. In the presence of very strong damping, the vortex motion (with $\mathbf{G} = 0$) will follow $\mathbf{V} = \mathbf{F}/|\mathbf{D}|$, which gives a motion of the vortex in the same direction as the force.

For an out-of-plane vortex, both terms in the integrand of (9.36) can contribute. The part with gradients of θ is larger near the core ($r < r_v$) where θ approaches $\pm\pi/2$. Far from the core, at radius $r > r_v$, the part with gradients of ϕ is larger, where $\cos\theta \approx 1$. We can use the asymptotic forms found for the static out-of-plane vortex

to obtain an estimate to these two contributions in the separate regions $r < r_v$ and $r > r_v$. For $q^2 = 1$ and using (8.19a), the core region's contribution (integral only over $r < r_v$) is found to be

$$\mathsf{D}_{jk,\mathrm{core}} = -\alpha \pi A_0^2 \delta_{jk}. \tag{9.38}$$

Note that there is no lower cutoff r_0 present, because the out-of-plane vortex does not have a singularity at $r \to 0$. For the region exterior to the core (integral only over $r > r_v$), one obtains

$$\mathsf{D}_{jk,\,\mathrm{ext}} = -\alpha \pi \delta_{jk} \left\{ \ln \frac{R}{r_v} + A_\infty^2 \left[\frac{1}{4} e^{-2} + \frac{3}{2} E_1(2) \right] \right\} \tag{9.39}$$

where the last part involves the exponential integral with value $E_1(2) \approx 0.0489$, defined from

$$E_1(x) \equiv \int_x^\infty \mathrm{d}t \, \frac{e^{-t}}{t}. \tag{9.40}$$

Note that the logarithmic term does have a dependence on a large radius cutoff R, but it is scaled by r_v rather than r_0 as in the in-plane vortex. Then the total damping constant is the sum of these parts,

$$\mathsf{D}_{jk} = -\alpha \pi \delta_{jk} \left\{ A_0^2 + \ln \frac{R}{r_v} + A_\infty^2 \left[\frac{1}{4} e^{-2} + \frac{3}{2} E_1(2) \right] \right\}$$

$$\approx -\alpha \pi \delta_{jk} \left(\ln \frac{R}{r_v} + 1.20 \right) \qquad \text{(out-of-plane vortex)}. \tag{9.41}$$

The dominant term here can be the logarithm, unless r_v is fairly large. As a result, one sees that especially as λ approaches closer to 1, causing a larger value of r_v, the tendency will be for out-of-plane vortices to have weaker damping than in-plane vortices.

Finally we can calculate the additional damping factor $\tilde{\mathsf{D}}$, based on transforming the definition to angular variables,

$$\tilde{\mathsf{D}}_{jk} = -\alpha \int \mathrm{d}r^2 \left(\partial_j \theta \, \tilde{\partial}_k \theta + \cos^2 \theta \, \partial_j \phi \, \tilde{\partial}_k \phi \right) \approx -\alpha \int \mathrm{d}r^2 \partial_j \theta \, \tilde{\partial}_k \theta. \tag{9.42}$$

This is reduced to the last form because to leading order in $\mathbf{V}$ the in-plane angle does not change with velocity. Assuming the velocity-dependent changes in θ are small and given from (9.32), then

$$\cos \theta \, \tilde{\partial}_k \theta \approx \tilde{\partial}_k s^z \approx \frac{-1}{4\delta JS} \partial_k \phi. \tag{9.43}$$

Then this damping parameter is determined by the integral

$$\tilde{\mathsf{D}}_{jk} = \frac{\alpha}{4\delta JS} \int \mathrm{d}r^2 \sec^2 \theta (\partial_j \theta)(\partial_k \phi). \tag{9.44}$$

However, this integral is identically zero, because $\theta = \theta(r)$ while $\phi = \phi(\varphi)$. One has specifically,

$$\left(\partial_1 \theta, \, \partial_2 \theta \right) = \frac{\partial \theta}{\partial r} (\cos \varphi, \, \sin \varphi) \tag{9.45}$$

and together with relation (9.34), the orthogonality of the sine and cosine functions integrated over the plane leads to $\tilde{\mathbf{D}} = 0$. Then, for most situations the main modification of the original Thiele equation is only the mass term. Vortex dynamics for both in-plane and out-of-plane vortices should be fairly well described by a *modified* Thiele equation with mass,

$$\frac{1}{\sigma}\,\mathbf{F} + \mathbf{G} \times \mathbf{V} + \mathbf{D} \cdot \mathbf{V} = \mathbf{M} \cdot \mathbf{A}. \tag{9.46}$$

Exercise 9.2. From the definition (9.36) of the dissipation tensor D_{jk}, (a) verify the results (9.38) and (9.39) for the contributions from interior and exterior regions of an out-of-plane vortex. (b) Check the total result for the damping tensor, equation (9.41). Compare the result to that in (9.37) for in-plane vortices. You may need to assume a cutoff length.

9.2 Relation of vortex momentum to the Thiele equations

The vortex mass and gyrovector can also be related to considerations of vortex linear momentum. There are various uses of the word 'momentum' for slightly different concepts, including canonical momentum, kinetic momentum and momentum as a generator of translations. For instance, the kinetic momentum $\mathbf{p} = m\mathbf{v}$ of an electron in a magnetic field is not the same as the canonical momentum $\mathbf{P}$; these are different by a term dependent on the vector potential. A similar situation applies to vortices, which can cause a lot of confusion. Here we consider how to define both the kinetic and canonical momenta of a vortex, in such a way as to be consistent with the undamped Thiele equation [5].

A vortex kinetic momentum $\mathbf{p}$ (dependent only on vortex velocity and not on position) can be defined tentatively like that for solitons [6], based on the kinetic integral in the Lagrangian (see (2.126*b*)) and its application (7.51) for a 1D chain), for a translating structure,

$$K = \int \frac{\mathrm{d}^2 r}{v_{\text{cell}}}\, S^z\, \dot{\phi} = \mathbf{V} \cdot \mathbf{p}, \tag{9.47}$$

where the kinetic momentum is then defined as

$$\mathbf{p} = -\int \frac{\mathrm{d}^2 r}{v_{\text{cell}}}\, S^z\, \nabla\phi = -\sigma \int \mathrm{d}^2 r\, s^z\, \nabla\phi. \tag{9.48}$$

This is the 2D generalization of kink momentum, (7.55) for a magnetic chain, where v_{cell} is the area per spin. One can see that $\mathbf{p}$ is zero for a stationary vortex, where S^z is either zero or circularly symmetric, while $\nabla\phi$ is anti-symmetric around the vortex center. Motion of the vortex leads to an asymmetric part of S^z, that combined with $\nabla\phi$ leads to non-zero momentum. The evaluation is left as an exercise.

Exercise 9.3. Use the small out-of-plane perturbation (8.39) for moving in-plane vortices to obtain the estimate of their kinetic momentum,

$$\mathbf{p} \approx \frac{\pi q^2 \sigma}{4\delta JS} \ln\left(\frac{R}{r_0}\right) \mathbf{V} = \frac{\pi q^2}{4\delta J v_{\text{cell}}} \ln\left(\frac{R}{r_0}\right) \mathbf{V}. \tag{9.49}$$

This result for $\mathbf{p}$ is the same as $\mathbf{p} \approx \mathsf{m}\mathbf{V}$ using a scalar mass m (units of kg) derived from (9.35),

$$\mathsf{m}_{jk} = \mathsf{m}\delta_{jk} = \sigma\mathsf{M}_{jk}. \tag{9.50}$$

At this basic level the definitions of mass and kinetic momentum, for in-plane vortices, are consistent. One can also show that the primary contribution to vortex energy due to non-zero velocity is of the expected form, $\frac{1}{2}\mathsf{m}\mathbf{V}^2$. While these results point to this momentum being the usual kinetic or mechanical momentum, it is important to analyze its dynamic properties, with the aim of seeing its connection to the canonical momentum, $\mathbf{P}$. At the same time, one needs to see how the momentum for out-of-plane vortices, with non-zero gyrovector, compares with momentum of in-plane vortices.

9.2.1 Poisson bracket of kinetic momentum components

One interesting property of $\mathbf{p}$ is the Poisson bracket (PB, recall the definition (2.63)) between its two components, as considered in [5]. For a canonical momentum $\mathbf{P}$, the two components are expected to be independent and have a zero PB, $\{P_x, P_y\} = 0$. For a continuum system, the fundamental PB that replaces $\{\phi_i, S_j^z\} = \delta_{ij}$ for spins on discrete sites is

$$\{\phi(\mathbf{r}), S^z(\mathbf{r}')\} = v_{\text{cell}}\delta(\mathbf{r} - \mathbf{r}'). \tag{9.51}$$

Then using the definition (2.131), we want to check the PB of the xy-components of the above kinetic momentum by calculating

$$\{p_x, p_y\} = \int \frac{\mathrm{d}^2 r}{v_{\text{cell}}}\left(\frac{\delta p_x}{\delta\phi}\frac{\delta p_y}{\delta S^z} - \frac{\delta p_x}{\delta S^z}\frac{\delta p_y}{\delta\phi}\right). \tag{9.52}$$

The required functional derivatives of p_x are found by applying (2.129) for two space dimensions to the x-component of (9.48), using subscripts on the fields to indicate partial derivatives,

$$\frac{\delta p_x}{\delta\phi} = \left(\partial_\phi - \partial_x\partial_{\phi_x} - \partial_y\partial_{\phi_y}\right)\left(-S^z\ \partial_x\phi\right) = \partial_x S^z \tag{9.53a}$$

$$\frac{\delta p_x}{\delta S^z} = \left(\partial_{S^z} - \partial_x\partial_{S_x^z} - \partial_y\partial_{S_y^z}\right)\left(-S^z\ \partial_x\phi\right) = -\partial_x\phi. \tag{9.53b}$$

With similar results for the derivatives of p_y, we have the PB,

$$\{p_x, p_y\} = \int \frac{\mathrm{d}^2 r}{v_{\text{cell}}}\left(-\partial_x S^z\partial_y\phi + \partial_x\phi\partial_y S^z\right) = \sigma\mathsf{G}_{12} = \sigma G_3. \tag{9.54}$$

The RHS is identified with σ times the gyrovector by comparing with relation (9.29). Note that a similar results holds for an electric charge in a magnetic field; the PB of two kinetic momentum components is proportional to the third component of the magnetic induction. This behavior is not typical of a canonical momentum.

One could also obtain this same result by changing to a definition of $\mathbf{p}$ based on discrete differences of spin components on lattice sites, avoiding the functional derivatives. For instance, for a square lattice with spins at sites labeled by indices (n, m) for (x, y)-directions respectively, the discrete lattice definitions, using central differences, are

$$p_x = -\sum_{nm} S_{n,m}^z \partial_x \phi_{n,m} = -\frac{1}{2}\sum_{n,m} S_{n,m}^z \left(\phi_{n+1,m} - \phi_{n-1,m}\right) \tag{9.55a}$$

$$p_y = -\sum_{nm} S_{n,m}^z \partial_y \phi_{n,m} = -\frac{1}{2}\sum_{n,m} S_{n,m}^z \left(\phi_{n,m+1} - \phi_{n,m-1}\right). \tag{9.55b}$$

Then the needed PB is a sum of terms, using primed indices in the p_y sum,

$$\{p_x, p_y\} = \frac{1}{4}\sum_{n,m,n',m'} \left\{ S_{n,m}^z\left(\phi_{n+1,m} - \phi_{n-1,m}\right), S_{n',m}^z\left(\phi_{n',m'+1} - \phi_{n',m'-1}\right)\right\}. \tag{9.56}$$

Using the canonical PBs (2.101), only limited terms are non-zero here, giving

$$\{p_x, p_y\} = \frac{1}{4}\sum_{n,m,n',m'} \left[S_{n,m}^z\left(\phi_{n',m'+1} - \phi_{n',m'-1}\right)\left(\delta_{n+1,n'} - \delta_{n-1,n'}\right)\delta_{m,m'}\right.$$
$$\left. + \left(\phi_{n+1,m} - \phi_{n-1,m}\right)S_{n',m}^z\delta_{n,n'}\left(\delta_{m,m'+1} - \delta_{m,m'-1}\right)\right]. \tag{9.57}$$

Employing the deltas to eliminate the primed indices leads to

$$\{p_x, p_y\} = \frac{1}{4}\sum_{n,m}\left[S_{n,m}^z\left(\phi_{n+1,m+1} - \phi_{n+1,m-1} - \phi_{n-1,m+1} + \phi_{n-1,m-1}\right)\right.$$
$$\left. + \left(\phi_{n+1,m} - \phi_{n-1,m}\right)\left(S_{n,m+1}^z - S_{n,m-1}^z\right)\right]. \tag{9.58}$$

Finally, shifting n by ± 1 on the first line changes nothing, but leads to a result that is equivalent to the discretized gyrovector density, whose sum gives back the gyrovector:

$$\{p_x, p_y\} = \frac{1}{4}\sum_{n,m}\left[-\left(S_{n+1,m}^z - S_{n-1,m}^z\right)\left(\phi_{n,m+1} - \phi_{n,m-1}\right)\right.$$
$$\left. + \left(\phi_{n+1,m} - \phi_{n-1,m}\right)\left(S_{n,m+1}^z - S_{n,m-1}^z\right)\right]$$
$$= \sum_{n,m}\left(-\partial_x S_{n,m}^z \partial_y \phi_{n,m} + \partial_x \phi_{n,m} \partial_y S_{n,m}^z\right) = \sigma G_3. \tag{9.59}$$

This is a good check that the PB obtained via functional derivatives is correct.

9.2.2 The momentum conjugate to X

Suppose there is another momentum $\mathbf{P}$ that is conjugate to the vortex position $\mathbf{X}$. The canonical PBs between these should then be

$$\left\{X_i, P_j\right\} = \delta_{ij}, \qquad \left\{X_i, X_j\right\} = 0, \qquad \left\{P_i, P_j\right\} = 0. \tag{9.60}$$

It is interesting to suppose a transformation from $\mathbf{p}$ to $\mathbf{P}$, that will ensure these canonical PBs and reproduce (9.54):

$$\mathbf{p} = \mathbf{P} - \frac{1}{2}\sigma\mathbf{G} \times \mathbf{X} = \left(P_x + \frac{1}{2}\sigma G_3 Y, \; P_y - \frac{1}{2}\sigma G_3 X\right). \tag{9.61}$$

Then one sees that this produces the PB already obtained above for the kinetic momentum components,

$$\{p_x, p_y\} = \left\{P_x + \frac{1}{2}\sigma G_3 Y, \; P_y - \frac{1}{2}\sigma G_3 X\right\}$$

$$= \frac{1}{2}\sigma G_3\left\{Y, P_y\right\} - \frac{1}{2}\sigma G_3\left\{P_x, X\right\} = \sigma G_3. \tag{9.62}$$

The transformation produces the correct PB, while at the same time giving a new momentum $\mathbf{P}$ that is conjugate to vortex core position,

$$\mathbf{P} = \mathbf{p} + \frac{1}{2}\sigma\mathbf{G} \times \mathbf{X}. \tag{9.63}$$

9.2.3 Momentum as a generator of translations

Next, consider the translational property of $\mathbf{p}$, by evaluating its PB with an arbitrary function of the spin field, $f(\mathbf{x}) \equiv f(\mathbf{S}(\mathbf{x})) = f(\phi(\mathbf{x}), S^z(\mathbf{x}))$. Then following the same rules for PBs, we have the algebra for one component,

$$\left\{p_j, f(\mathbf{x})\right\} = \int \frac{\mathrm{d}^2 r}{v_{\text{cell}}}\left(\frac{\delta p_j}{\delta\phi}\frac{\delta f}{\delta S^z} - \frac{\delta p_j}{\delta S^z}\frac{\delta f}{\delta\phi}\right). \tag{9.64}$$

The function f can be written as a functional by including a delta function:

$$f(\mathbf{x}) = \int \frac{\mathrm{d}^2 r}{v_{\text{cell}}} f\big(\phi(\mathbf{r}), \, S^z(\mathbf{r})\big)v_{\text{cell}}\delta(\mathbf{r} - \mathbf{x}), \tag{9.65}$$

which allows calculation of its derivatives (at the location $\mathbf{r}$ needed in (9.64)) as

$$\frac{\delta f}{\delta\phi} = \frac{\partial f}{\partial\phi}\,v_{\text{cell}}\delta(\mathbf{r} - \mathbf{x}), \qquad \frac{\delta f}{\delta S^z} = \frac{\partial f}{\partial S^z}\,v_{\text{cell}}\delta(\mathbf{r} - \mathbf{x}). \tag{9.66}$$

Then we obtain

$$\left\{p_j, f(\mathbf{x})\right\} = \int \frac{\mathrm{d}^2 r}{v_{\text{cell}}}\left(\frac{\partial S^z}{\partial r_j}\frac{\partial f}{\partial S^z} + \frac{\partial\phi}{\partial r_j}\frac{\partial f}{\partial\phi}\right)v_{\text{cell}}\delta(\mathbf{r} - \mathbf{x}) = \frac{\partial f}{\partial x_j}. \tag{9.67}$$

If the function depends on a vortex spin field in the form $\mathbf{S}(\mathbf{x} - \mathbf{X})$, where $\mathbf{X}$ is the core location, then with $\partial/\partial x_j = -\partial/\partial X_j$, the result is

$$\{\mathbf{p}, f(\mathbf{x} - \mathbf{X})\} = \frac{\partial f}{\partial \mathbf{x}} = -\frac{\partial f}{\partial \mathbf{X}}. \tag{9.68}$$

Compare the expansion of $f(\mathbf{x} - \mathbf{X})$ for small displacement $\mathbf{X}$,

$$f(\mathbf{x} - \mathbf{X}) \approx f(\mathbf{x}) - \mathbf{X} \cdot \frac{\partial f}{\partial \mathbf{X}}. \tag{9.69}$$

The shift in position $\mathbf{X}$ then acts on $\{\mathbf{p}, f\}$ to produce the change in f due to a small translation. Therefore, the kinetic momentum $\mathbf{p}$ is a generator of space translations on arbitrary functions of the spin field. Note that it is analogous to the translations in time that are generated by the Hamiltonian, according to the PB relation,

$$\{H, f(\mathbf{S})\} = -\frac{\mathrm{d}f}{\mathrm{d}t}. \tag{9.70}$$

The *canonical momentum* $\mathbf{P}$ found earlier in (9.61), which is conjugate to vortex location $\mathbf{X}$, has the same translational property, as found for one component:

$$\left\{ P_j, f(\mathbf{x} - \mathbf{X}) \right\} = \left\{ p_j + \frac{1}{2}\sigma \mathbf{G} \times \mathbf{X}, f(\mathbf{x} - \mathbf{X}) \right\} = \left\{ p_j, f(\mathbf{x} - \mathbf{X}) \right\} = -\frac{\partial f}{\partial X_j}. \tag{9.71}$$

This is the same as expected from a general chain rule such as (2.66a) for PBs,

$$\left\{ P_j, f(\mathbf{x} - \mathbf{X}) \right\} = \left\{ P_j, X_k \right\} \frac{\partial f}{\partial X_k} = -\delta_{jk} \frac{\partial f}{\partial X_k} = -\frac{\partial f}{\partial X_j}. \tag{9.72}$$

9.2.4 Time derivative of kinetic momentum p

The dynamics of $\mathbf{p}$ is important for comparison to the Thiele equation. Thus, we ask what is $\dot{\mathbf{p}}$? This can be answered by appealing to PB algebra again[1]. The time derivative of a component of $\mathbf{p}$ is determined from a PB with the Hamiltonian, which can be expressed as

$$\dot{p}_j = \left\{ p_j, H \right\} = \int \frac{\mathrm{d}^2 r}{v_{\text{cell}}} \left(\frac{\delta p_j}{\delta \phi} \frac{\delta H}{\delta S^z} - \frac{\delta p_j}{\delta S^z} \frac{\delta H}{\delta \phi} \right)$$

$$= \int \frac{\mathrm{d}^2 r}{v_{\text{cell}}} \left(\frac{\partial S^z}{\partial r_j} \frac{\delta H}{\delta S^z} + \frac{\partial \phi}{\partial r_j} \frac{\delta H}{\delta \phi} \right) = -\frac{\partial}{\partial X_j} \int \frac{\mathrm{d}^2 r}{v_{\text{cell}}} \mathcal{H} = -\frac{\partial H}{\partial X_j} = F_j. \tag{9.73}$$

Our earlier results (9.53a) for the functional derivatives of p_j were used, as well as the ansatz that the spin field is assumed of the form $\mathbf{S}(\mathbf{r} - \mathbf{X})$, or $\frac{\partial}{\partial r_j} = -\frac{\partial}{\partial X_j}$. This result gives a simple principle,

---

[1] One can also try to differentiate through the integral of the original definition (9.48). This has technical difficulties, however, because of the singularity at the vortex core, which can lead to nonsensical or poorly defined results. This seems to be the difficulty in some earlier works [4, 5].

$$\dot{\mathbf{p}} = \mathbf{F}. \tag{9.74}$$

The rate of change of the defined kinetic momentum is the force on the vortex.

The expression for $\dot{p}_j$ can be expressed differently, using instead the canonical equations (2.130) to replace the functional derivatives of H in the integrand:

$$\dot{p}_j = \int \frac{\mathrm{d}^2 r}{v_{\text{cell}}} \left(\frac{\delta p_j}{\delta \phi} \frac{\delta H}{\delta S^z} - \frac{\delta p_j}{\delta S^z} \frac{\delta H}{\delta \phi} \right) = \int \frac{\mathrm{d}^2 r}{v_{\text{cell}}} \left(\left(\partial_j S^z \right) \left(\dot{\phi} \right) - \left(-\partial_j \phi \right) \left(-\dot{S^z} \right) \right). \tag{9.75}$$

Now replacing the spin time derivatives with the convective form (9.9) gives

$$\dot{p}_j = V_k \int \frac{\mathrm{d}^2 r}{v_{\text{cell}}} \left(\partial_j \phi \partial_k S^z - \partial_j S^z \partial_k \phi \right) - A_k \int \frac{\mathrm{d}^2 r}{v_{\text{cell}}} \left(\partial_j \phi \tilde{\partial}_k S^z - \partial_j S^z \tilde{\partial}_k \phi \right). \tag{9.76}$$

This contains the gyrotensor (9.29) and the mass tensor (9.31), and comparing with (9.18), it is summarized as

$$\dot{\mathbf{p}} = -\sigma \mathbf{G} \times \mathbf{V} + \sigma \mathbf{M} \cdot \mathbf{A}. \tag{9.77}$$

Although no damping is included, these results reproduce the modified Thiele equation (9.46), once $\dot{\mathbf{p}}$ is replaced by the force $\mathbf{F}$ on the vortex. This derivation based on the canonical equations of motion and classical PBs is much more direct than our earlier derivation starting from the LLG equations, although the former allowed the inclusion of damping directly. A slightly different approach was used in [5], but required differentiation of the integral definition for $\mathbf{p}$, which is not a well-defined mathematical operation, because of the singularity at the core. The derivations here have avoided that procedure. Using the scalar value $\mathsf{m} = \sigma \mathsf{M}$ from a diagonal mass tensor, the modified Thiele equation is

$$\mathbf{F} + \sigma \mathbf{G} \times \mathbf{V} = \mathsf{m} \mathbf{A}. \tag{9.78}$$

These last results show that Thiele equation dynamics can be considered from the point of view of momentum conservation. However, the system contains an additional momentum term $\sigma \mathbf{G} \times \mathbf{X}$, whose time derivative appears here in the force equation. This extra momentum depends on the choice of origin, however, a shift in the origin simply gives an irrelevant constant, whose time derivative is zero.

9.2.5 Comparison of vortex dynamics to electric charge dynamics

The modified Thiele equation in the form (9.78), without damping, can be seen to be equivalent to the non-relativistic equation of motion for an electric charge e with velocity $\mathbf{v}$ and acceleration $\mathbf{a}$, affected by combined electric and magnetic forces (Lorentz force):

$$e\mathbf{E} + e\mathbf{v} \times \mathbf{B} = m\mathbf{a}. \tag{9.79}$$

The equivalence requires $\mathbf{F}$ in the Thiele equation to be identified with only the electric part of the Lorentz force, and the gyrovector must be identified with the negative magnetic induction, while spin density σ needs to be equivalent to the charge:

$$\mathbf{F} \to e\mathbf{E}, \qquad \sigma \mathbf{G} \to -e\mathbf{B}. \tag{9.80}$$

This maps vortex dynamics directly onto charge dynamics. We can see that both $\mathbf{F}$ and $\sigma\mathbf{G} \times \mathbf{V}$ in the vortex problem should be considered forces in some general sense, whose net sum gives the vortex acceleration. The contribution to $\mathbf{F}$ is only due to space variations of H, while the *gyroforce* $\sigma\mathbf{G} \times \mathbf{V}$ is analogous to the magnetic Lorentz force. We can also see how this equivalence relates to canonical momentum.

For vortices, refer again to the connection between kinetic and canonical momentum found in (9.61). Combining with (9.74) and the modified Thiele equation as (9.77), leads to three equivalent ways to write the time derivative of kinetic momentum:

$$\dot{\mathbf{p}} = \mathbf{F} = \dot{\mathbf{P}} - \frac{1}{2}\sigma\mathbf{G} \times \mathbf{V} = -\sigma\mathbf{G} \times \mathbf{V} + m\mathbf{A}. \qquad (9.81)$$

This is then solved to give two equivalent expressions for $\dot{\mathbf{P}}$:

$$\dot{\mathbf{P}} = \mathbf{F} + \frac{1}{2}\sigma\mathbf{G} \times \mathbf{V} \qquad (9.82a)$$

$$\dot{\mathbf{P}} = m\mathbf{A} - \frac{1}{2}\sigma\mathbf{G} \times \mathbf{V}. \qquad (9.82b)$$

While $\dot{\mathbf{P}}$ does not appear in the equations for vortex or charge dynamics, but rather acts as more of a calculational aid, some insight is obtained by comparing the relations in the two systems.

It is well known that a Lagrangian for a point charge of mass m in non-relativistic motion can be written as

$$L = \frac{1}{2}m\mathbf{v}^2 - e\Phi + e\mathbf{v} \cdot \mathcal{A}, \qquad (9.83)$$

where Φ is the scalar potential and $\mathcal{A}$ is the vector potential. The resulting canonical momentum is defined by

$$\mathbf{P} = \frac{\partial L}{\partial \mathbf{v}} = m\mathbf{v} + e\mathcal{A} = m\mathbf{v} + \frac{1}{2}e\mathbf{B} \times \mathbf{x}, \qquad (9.84)$$

where the vector potential $\mathcal{A}(\mathbf{x})$ associated with a uniform magnetic induction is

$$\mathcal{A} = \frac{1}{2}\mathbf{B} \times \mathbf{x} = \frac{1}{2}\epsilon_{jkl}\hat{\mathbf{e}}_j B_k x_l. \qquad (9.85)$$

The Euler–Lagrange equation of motion for one component is

$$\dot{P}_i = \frac{\mathrm{d}}{\mathrm{d}t}\left(\frac{\partial L}{\partial \dot{x}_i}\right) = \frac{\partial L}{\partial x_i} = -e\frac{\partial \Phi}{\partial x_i} + ev_j\frac{\partial \mathcal{A}_j}{\partial x_i}. \qquad (9.86)$$

The needed gradients of the vector potential are

$$\frac{\partial A_j}{\partial x_i} = \frac{\partial}{\partial x_i}\left(\frac{1}{2}\epsilon_{jkl}B_k x_l\right) = \frac{1}{2}\epsilon_{jki}B_k. \qquad (9.87)$$

Then with $v_j \epsilon_{jki} B_k = \epsilon_{ijk} v_j B_k = (\mathbf{v} \times \mathbf{B})_i$, this leads to the first way to write the momentum's time derivative,

$$\dot{\mathbf{P}} = \frac{\partial L}{\partial \mathbf{x}} = -e\frac{\partial \Phi}{\partial \mathbf{x}} - \frac{1}{2}e\mathbf{B} \times \mathbf{v}. \qquad (9.88)$$

Note that this equivalent to (9.82a), under the mappings in (9.80). The other way to obtain a result for $\dot{\mathbf{P}}$ is to time differentiate its expression (9.84) directly[2]:

$$\dot{\mathbf{P}} = \frac{\mathrm{d}}{\mathrm{d}t}\frac{\partial L}{\partial \mathbf{v}} = m\mathbf{a} + e\frac{1}{2}\mathbf{B} \times \mathbf{v} + e\frac{\partial \mathcal{A}}{\partial t}. \qquad (9.89)$$

Changing $e\mathbf{B} \to -\sigma\mathbf{G}$, and assuming static fields, this is seen to be equivalent to (9.82b) for the vortex problem. Then equating the two expressions for $\dot{\mathbf{P}}$ eliminates that variable, and leads to the Lorentz force equation (9.79).

These results then indicate that the force $\mathbf{F}$ in the vortex problem is analogous to *only* the electrostatic force for the charge problem. With the mappings in (9.80) the two systems have essentially equivalent time derivatives of canonical momenta. The connection between their kinetic momenta, however, is less obvious. For a charge one can identify a kinetic momentum $\mathbf{p} = m\mathbf{v}$, with time derivative $\dot{\mathbf{p}} = m\mathbf{a}$, however, that is not an element directly used in the derivations of the Lorentz force law dynamics. For *in-plane* vortices that have $\mathbf{G} = 0$, we were able to show that the kinetic momentum is $\mathbf{p} \approx \mathsf{m}\mathbf{V}$, however, that is not necessarily true for out-of-plane vortices. We were able to use PBs to obtain $\dot{\mathbf{p}}$ as in (9.77), containing $\mathsf{m}\mathbf{A}$ as well as a gyrotropic contribution. This strongly contrasts $\dot{\mathbf{p}} = m\mathbf{a}$ in the charge dynamics problem and is a significant difference in the dynamics.

9.2.6 Lagrangian mechanics for vortex core motion

The ideas in the last section have mapped vortex motion approximately onto the motion of a charge in combined electric and magnetic fields. The results can be collected together by determination of a Lagrangian that will reproduce the undamped modified Thiele equation (9.78). To achieve this, make the usual transformation from Hamiltonian to Lagrangian, using the canonical momentum,

$$L = \mathbf{P} \cdot \dot{\mathbf{X}} - H. \qquad (9.90)$$

Based on time integration of (9.82b), we take the canonical momentum to be defined up to an arbitrary constant as

$$\mathbf{P} = \mathsf{m}\mathbf{V} - \frac{1}{2}\sigma\mathbf{G} \times \mathbf{X}. \qquad (9.91)$$

This is consistent with canonical momentum expression (9.84) for a charge in a field, changing $e\mathbf{B}$ to $-\sigma\mathbf{G}$. This gives the vortex Lagrangian, with $\dot{\mathbf{X}} = \mathbf{V}$,

---

[2] For the electrodynamic problem the term $\frac{\partial \mathcal{A}}{\partial t}$ contributes to $\mathbf{E}(\mathbf{x}, t) = -\nabla\Phi - \frac{\partial \mathcal{A}}{\partial t}$. The contributions to both $\mathbf{E}$ and $\mathbf{B}$ in the Lorentz force law are split between the two ways to write $\dot{\mathbf{P}}$. The mapping from the vortex problem to a charge system only requires a situation with static electric and magnetic fields.

$$L = m\mathbf{V}^2 - \frac{1}{2}\sigma\,(\mathbf{G} \times \mathbf{X}) \cdot \mathbf{V} - H. \tag{9.92}$$

Note that the second term has the form $+\sigma\mathcal{A} \cdot \mathbf{V}$, with an effective vector potential,

$$\mathcal{A} = -\frac{1}{2}\mathbf{G} \times \mathbf{X}. \tag{9.93}$$

The interaction term can also be written as $\mathcal{A} \cdot \mathbf{V} = +\frac{1}{2}(\mathbf{G} \times \mathbf{V}) \cdot \mathbf{X}$, which is useful later for differentiation. To apply L and check that the correct equation of motion results, it is necessary to assume that the Hamiltonian has a kinetic energy contribution of $\frac{1}{2}m\mathbf{V}^2$. This will ensure as well that the canonical momentum is correctly derived from L by $\mathbf{P} = \frac{\partial L}{\partial \mathbf{V}}$. In addition, H can have other parts that depend on vortex position, whose negative gradient leads to the force $\mathbf{F}$. The Euler–Lagrange equation for one component is

$$\frac{\partial L}{\partial X_j} = \frac{\mathrm{d}}{\mathrm{d}t}\left(\frac{\partial L}{\partial V_j}\right). \tag{9.94}$$

This requires the derivatives,

$$\frac{\partial L}{\partial X_j} = -\frac{\partial H}{\partial X_j} + \frac{1}{2}\sigma(\mathbf{G} \times \mathbf{V})_j \tag{9.95a}$$

$$\frac{\partial L}{\partial V_j} = 2m V_j - \frac{\partial H}{\partial V_j} - \frac{1}{2}\sigma(\mathbf{G} \times \mathbf{X})_j = m V_j - \frac{1}{2}\sigma(\mathbf{G} \times \mathbf{X})_j. \tag{9.95b}$$

Then it is clear that the Euler–Lagrange equations (9.94) for all components give the correct equation,

$$-\frac{\partial H}{\partial \mathbf{X}} + \sigma\mathbf{G} \times \mathbf{V} = m\mathbf{A} \tag{9.96}$$

once the negative gradient of H is identified as the force $\mathbf{F}$. Thus the stated Lagrangian (9.92) is appropriate for analyzing dynamics of vortices, including vortex mass effects. In the case of in-plane vortices, the gyrovector is not present, and the mass effects should dominate (for very weak damping). In the case of out-of-plane vortices, the mass effects could be relatively weak; setting m to zero can give a leading approximation for out-of-plane vortex dynamics in some potential contained in H.

9.3 Vortex forces and motions

The basic dynamics of vortex core motion has been interesting to study in terms of comparing numerical simulations to predictions of the modified Thiele equation (9.46). For quasi-2D ferromagnets, a number of simple situations have been studied, including individual vortices near a boundary, and pairs of vortices in a larger system with a far away boundary. Here we give a short summary of some of the possible motions, and indicate when a non-zero vortex mass reveals its presence.

The force $\mathbf{F}$ acting on a vortex is one of the most relevant factors that determines the motion. There are three direct ways that forces are produced, including externally applied fields, the interaction of a vortex with other vortices or anti-vortices, and the interaction of a vortex with the boundary of the system. Let us estimate $\mathbf{F}$ for the most obvious situations.

9.3.1 Force due to applied field

The first way to generate force is to apply a magnetic induction $\mathbf{B}_{\text{ext}}$, especially, within the easy place. The interaction of $\mathbf{B}_{\text{ext}}$ with the spins will cause an induced magnetization and also an energy gradient. Although the vortex will become slightly deformed by an applied field, we suppose that deformation is small, which will be true as long as $\mathbf{B}_{\text{ext}}$ is much weaker than the nearest neighbor exchange fields. This means our the calculation will slightly over-estimate the force. The force comes only from the negative space gradient of the Zeeman energy,

$$U_B = -\sum_n \boldsymbol{\mu}_n \cdot \mathbf{B}_{\text{ext}} = -\sum_n \gamma \mathbf{S}_n \cdot \mathbf{B}_{\text{ext}}, \tag{9.97}$$

which is easy to estimate for the vortex as a whole. For stationary in-plane and out-of-plane vortices, the component S^z is circularly symmetric around the vortex core position $\mathbf{X}$, while (8.7) describes the in-plane angle.

Uniform applied field

If the whole system is exposed to a *spatially uniform field*, then only the in-plane components of $\mathbf{B}_{\text{ext}}$ can contribute to the force. Suppose the applied field of strength B_{ext} makes an angle ϕ_B to the x-axis. For the vortex, expression (8.7) for $\phi(\mathbf{r})$ is extended to a vortex with core position (X, Y),

$$\phi(\mathbf{r}) = q \tan^{-1}\left(\frac{x - X}{y - Y}\right) + \phi_0. \tag{9.98}$$

For an in-plane vortex, the Zeeman energy in continuum theory then becomes

$$
\begin{aligned}
U_B &= -\gamma S B_{\text{ext}} \int \frac{d^2r}{v_{\text{cell}}} \cos\left(q\varphi + \phi_0 - \phi_B\right) \\
&= -\gamma S B_{\text{ext}} \int \frac{d^2r}{v_{\text{cell}}} \left\{ \cos(q\varphi) \cos\left(\phi_0 - \phi_B\right) - \sin(q\varphi) \sin\left(\phi_0 - \phi_B\right) \right\} \\
&= -q\gamma S B_{\text{ext}} \int \frac{d^2r}{v_{\text{cell}}} \left\{ \frac{x - X}{\rho} \cos\left(\phi_0 - \phi_B\right) - \frac{y - Y}{\rho} \sin\left(\phi_0 - \phi_B\right) \right\}, \quad (9.99)
\end{aligned}
$$

where the last line applies only to $q = \pm 1$ and ρ is the radius measured from the vortex center,

$$\rho = \sqrt{(x - X)^2 + (y - Y)^2}. \tag{9.100}$$

Integration over an infinite system leads to constant U_B, and no force. However, we must consider a finite system, wherein an infinitesimal vortex displacement causes

one set of spins to become more aligned with $\mathbf{B}_{\text{ext}}$ and another set of spins to become less aligned with $\mathbf{B}_{\text{ext}}$. The spins in the region of the core are the ones most affected.

For the force F_x, the gradient of U_B with respect to X requires the following derivatives,

$$\frac{\mathrm{d}}{\mathrm{d}X}\left(\frac{x-X}{\rho}\right) = -\frac{(y-Y)^2}{\rho^3}, \qquad \frac{\mathrm{d}}{\mathrm{d}X}\left(\frac{y-Y}{\rho}\right) = -3\frac{(x-X)(y-Y)}{\rho^3}. \quad (9.101)$$

Then this gives

$$F_x = -q\gamma S B_{\text{ext}} \int \frac{\mathrm{d}^2 r}{v_{\text{cell}}} \left\{ \frac{(y-Y)^2}{\rho^3} \cos(\phi_0 - \phi_B) - 3\frac{(x-X)(y-Y)}{\rho^3} \sin(\phi_0 - \phi_B) \right\}.$$
$$(9.102)$$

This is still indeterminant, because the boundary of the system must be specified. Let us take the simplest case: a circular system of radius R and the vortex at the center of the system. One can later consider the vortex slightly displaced from the center as a perturbation. Then, putting $X = Y = 0$, then $\rho = r$, one has some simple integrations over the circular system:

$$\int \mathrm{d}^2 r \frac{(y-Y)^2}{\rho^3} = \int_0^{2\pi} \mathrm{d}\varphi \int_0^R r\mathrm{d}r \, \frac{1}{r} \sin^2 \varphi = \pi R. \quad (9.103)$$

The second term of (9.102) involves a product $\sin\varphi \cos\varphi$ which integrates to zero. A similar calculation applies to finding F_y, then, the resulting force on an in-plane vortex in a uniform magnetic field is

$$\mathbf{F} = -q\pi R\sigma\gamma B_{\text{ext}}\left(\cos(\phi_0 - \phi_B), -\sin(\phi_0 - \phi_B)\right). \quad (9.104)$$

To interpret this result, recall that ϕ_0 is the angle the spins make with the positive x-axis, along that axis. When $\phi_0 = 0$, the spin field is of a vortex ($q = +1$) is radially outward from the core: it has the appearance of the electric field of a positive electric charge. Then in that case, the force is opposite to the direction of $\mathbf{B}_{\text{ext}}$:

$$\mathbf{F} = -q\pi R\sigma\gamma B_{\text{ext}}\left(\cos\phi_B, \sin\phi_B\right) = -q\pi R\sigma\gamma \, \mathbf{B}_{\text{ext}}, \qquad \phi_0 = 0. \quad (9.105)$$

Conversely, the force on an anti-vortex ($q = -1$) will be parallel to $\mathbf{B}_{\text{ext}}$ if $\phi_0 = 0$. It is easy to check that a small displacement along the force direction for these spin configurations will lead to greater alignment of spins with the field.

A more interesting case is when the spin field has $\phi_0 = 90°$, giving the appearance of a magnetic field around a current-carrying wire. Now, the force becomes

$$\mathbf{F} = -q\pi R\sigma\gamma B_{\text{ext}}\left(\sin\phi_B, -\cos\phi_B\right) = q\pi R\sigma\gamma \, \hat{\mathbf{z}} \times \mathbf{B}_{\text{ext}}, \qquad \phi_0 = 90°. \quad (9.106)$$

If the vortex were to slide sideways to the field, in the direction of $q\hat{\mathbf{z}} \times \mathbf{B}_{\text{ext}}$, one can see that it will cause more spins to align with the field, lowering the Zeeman energy. Again, the force is oppositely directed on anti-vortices when compared to vortices. In small magnetic particles this is the more probable vortex structure, because of demagnetization energy causing the spins to follow close to the direction of a boundary.

The result (9.104) has been calculated for in-plane vortices only. If this calculation is repeated for out-of-plane vortices, then near the vortex core, the non-zero S^z causes the lengths of the in-plane components to be smaller. It is clear that the contribution to Zeeman energy from the core region is reduced, and hence so is the force. Without an exact expression for $S^z(\rho)$ (measuring from the vortex core location), only an approximate value for $\mathbf{F}$ can be found. The Zeeman energy in the case of out-of-plane vortices interacting with an *in-plane* magnetic induction is now

$$U_B = -\gamma S B_{\text{ext}} \int \frac{\mathrm{d}^2 r}{v_{\text{cell}}} \left[1 - (s^z)^2 \right]^{1/2} \cos\left(q\varphi + \phi_0 - \phi_B \right). \tag{9.107}$$

The result of this extra factor is that the core region has a much weaker contribution to the interaction; the spins are nearly perpendicular to $\mathbf{B}_{\text{ext}}$ there. This effect can be incorporated approximately by using the vortex core radius r_v in (8.18) as the lower cutoff of the radial integration. This means that (9.104) can be extended to the case of out-of-plane vortices, provided that R is replaced by $R - r_v$. For a system large compared to r_v, the force on out-of-plane vortices will be nearly the same as on in-plane vortices.

Non-uniform applied field

Another way to exert a force on a vortex is via the out-of-plane spin component, in a *non-uniform* out-of-plane applied field $B_{\text{ext}}^z(\mathbf{r})$. This applies only to out-of-plane vortices. Start from only the z-component's contribution to Zeeman energy,

$$U_B = -q\gamma S \int \frac{\mathrm{d}^2 r}{v_{\text{cell}}} \, s^z(\mathbf{r}) \cdot B_{\text{ext}}^z(\mathbf{r}). \tag{9.108}$$

The s^z spin field is circularly symmetric around the vortex core, so a uniform B_{ext}^z would not produce any force. Suppose B_{ext}^z is a constant plus a uniform gradient along the x-direction[3],

$$B_{\text{ext}}^z(x, y) = B_0 + \left(\frac{\partial B^z}{\partial x} \right)_0 x. \tag{9.109}$$

The zero subscripts refer to the values at the origin. Consider again a circular system, with its center at the origin. Then the estimate of the force is expressed as

$$F_x = -\frac{\partial U_B}{\partial X} = \gamma\sigma \int \mathrm{d}^2 r \, \frac{\partial s^z}{\partial \rho} \frac{\partial \rho}{\partial X} \left[B_0 + \left(\frac{\partial B^z}{\partial x} \right)_0 x \right]$$

$$= \gamma\sigma \int \mathrm{d}^2 r \, \frac{\partial s^z}{\partial \rho} \left[\frac{-(x - X)}{\rho} \right] \left[B_0 + \left(\frac{\partial B^z}{\partial x} \right)_0 x \right]. \tag{9.110}$$

---

[3] Maxwell's equation $\nabla \cdot \mathbf{B} = 0$ would imply also non-zero in-plane components of $\mathbf{B}_{\text{ext}}$. We suppose that these extra components can be ignored to leading order.

When the vortex is at the center of the system with $X = 0$ and $\rho = r$, only the gradient part is seen to contribute, being dependent on $x^2 = r^2 \cos^2 \varphi$,

$$F_x = -\gamma\sigma \int_0^{2\pi} d\varphi \int_0^R dr \; r \frac{\partial s^z}{\partial r} \cos\varphi \left(\frac{\partial B^z}{\partial x}\right)_0 r \cos\varphi$$

$$= -\pi\gamma\sigma \left(\frac{\partial B^z}{\partial x}\right)_0 \int_0^R dr \; r^2 \frac{\partial s^z}{\partial r} = 2\pi\gamma\sigma \left(\frac{\partial B^z}{\partial x}\right)_0 \int_0^R dr \; r \; s^z(r). \quad (9.111)$$

The last step involved integration by parts, assuming that $s^z(R) \approx 0$ on the system boundary. To evaluate further, it is necessary to have $s^z(r)$. An estimate can be made based on the approximate solutions (8.19) found earlier, for the two regions $r < r_v$ and $r > r_v$, which is an exercise.

Exercise 9.4. From the approximate out-of-plane component (8.19), check the evaluation of the following integrals for force contributions from the core region and the far field region of an out-of-plane vortex,

$$\int_0^{r_v} dr \; r \; s^z(r) \approx p\left(\frac{r_v}{A_0}\right)^2 \left(A_0 \sin A_0 + \cos A_0 - 1\right) \approx 0.3943 p r_v^2 \quad (9.112a)$$

$$\int_{r_v}^R dr \; r \; s^z(r) \approx p A_\infty r_v^2 \left(e^{-1} + \frac{1}{2}\sqrt{\pi} \; \text{erfc}(1)\right) \approx 0.8664 p r_v^2. \quad (9.112b)$$

These depend on the core polarization $p = \pm 1$ and the constants A_0 and A_∞ that define the approximate structure of $s^z(r)$; 'erfc' is the complementary error function.

The core contributes about 1/3 and the far region about 2/3 of the total force. Then combining these contributions, and generalizing to a gradient of B^z in any direction, the force is found to be

$$\mathbf{F} \approx 1.26 \times 2\pi\gamma\sigma p r_v^2 (\nabla B^z)_0. \quad (9.113)$$

The 0 subscript means the gradient is measured at the location of the vortex center. Although this has been calculated for a vortex centered in a circular system, one could also find the small corrections if the vortex is offset away from the center. Note the dependence on core polarization p, which shows that the force is in the direction appropriate to increase the alignment of spins with $\mathbf{B}_{ext}$ for $p = +1$, or reduce the amount of anti-alignment for $p = -1$. Thus, a small gradient in $\mathbf{B}_{ext}$ might be used to separate vortices of opposite polarizations.

In the case of strong damping, a displacement of the vortex will take place in the same direction as the calculated force. If the damping is weak, then at least initially, an out-of-plane vortex will make some gyrotropic motion, typically perpendicular to the instantaneous force.

9.3.2 Vortex pair forces

The second way forces are generated is through the interactions between pairs of vortices or anti-vortices. First, consider a pair of in-plane vortices, one of vorticity q_1, and phase angle ϕ_{01} at the origin, and a second of vorticity q_2 and phase angle ϕ_{02} at a position $\mathbf{X} = (X, 0)$ along the x-axis (chosen as the axis from one vortex to the other). With only in-plane spin components, the total in-plane angle is a superposition of the two vortices,

$$\phi = \phi_1 + \phi_2, \quad \text{where} \quad \begin{cases} \phi_1 = q_1 \tan^{-1}\left(\dfrac{y}{x}\right) + \phi_{01} \\[2mm] \phi_2 = q_2 \tan^{-1}\left(\dfrac{y}{x - X}\right) + \phi_{02}. \end{cases} \tag{9.114}$$

In the Hamiltonian (8.4) the energy density depends only on the square of $\nabla\phi = \nabla\phi_1 + \nabla\phi_2$, which is independent of the phase angles, and determined from

$$\nabla\phi_1 = q_1 \frac{\hat{\mathbf{z}} \times \mathbf{r}}{r^2} = \frac{q_1}{x^2 + y^2}(-y, x) \tag{9.115a}$$

$$\nabla\phi_2 = q_2 \frac{\hat{\mathbf{z}} \times (\mathbf{r} - \mathbf{X})}{|\mathbf{r} - \mathbf{X}|^2} = \frac{q_2}{(x - X)^2 + y^2}(-y, x - X). \tag{9.115b}$$

Its absolute square has two direct terms (single vortex) and cross terms (the interaction),

$$|\nabla\phi|^2 = \frac{q_1^2}{x^2 + y^2} + \frac{q_2^2}{(x - X)^2 + y^2} + 2q_1 q_2 \frac{x(x - X) + y^2}{\left(x^2 + y^2\right)\left[(x - X)^2 + y^2\right]}. \tag{9.116}$$

When integrated over the system, the first two terms are the single vortex energies; only the last term will be the pair interaction energy that depends on the separation X. This pair interaction potential U_{pair} is obtained, writing the integration in circular coordinates,

$$U_{\text{pair}} = \frac{1}{2} J S^2 \int d^2r \; |\nabla\phi|^2_{\text{pair}}$$

$$= J S^2 q_1 q_2 \int_0^{2\pi} d\varphi \int_0^R r \, dr \frac{r^2 - rX \cos\varphi}{r^2\left[r^2 - 2rX \cos\varphi + X^2\right]}. \tag{9.117}$$

Doing the radial integration first, a change of variable to $u = r^2 - 2rX \cos\varphi + X^2$, with $du = 2(r - X \cos\varphi)dr$, transforms the radial integral to logarithmic form,

$$U_{\text{pair}} = J S^2 q_1 q_2 \int_0^{2\pi} d\varphi \int \frac{1}{2} \frac{du}{u}$$

$$= J S^2 q_1 q_2 \int_0^{2\pi} d\varphi \frac{1}{2} \ln\left[r^2 - 2rX \cos\varphi + X^2\right]_0^R = 2\pi J S^2 q_1 q_2 \ln\left(\frac{R}{X}\right). \tag{9.118}$$

Note the similarity to the in-plane single vortex energy (8.15), but with an extra factor of 2 and the separation X replacing the short radius cutoff r_0.

Then the negative gradient gives the force, which is along the line connecting the vortices:

$$F_x = -\frac{\partial U_{\text{pair}}}{\partial X} = \frac{2\pi J S^2 q_1 q_2}{X}.$$ (9.119)

Not surprisingly, the dependence on $1/X$ is analogous to the force (per unit length) between a pair of current-carrying wires, which produce a magnetic field of the same geometry as the vortex in-plane spin field. Opposite signed vortices produce attractive forces while like-signed vortices produce repulsive forces.

For out-of-plane vortices, the result must be corrected due to the non-zero value of $S^z(r)$. These corrections will come mostly from the core region, $r < r_v$. If the core regions of the pair overlap, then this correction could be significant, yet there is no simple calculation based on the energy (8.4). Generally speaking, as long as the core regions do not overlap, expression (9.119) should be a good approximation for the force between out-of-plane vortices.

Exercise 9.5. Two out-of-plane vortices with opposite polarizations $p_2 = -p_1$ are separated by distance X_{12}. Suppose their gyrovectors are anti-parallel; they have equal vorticities. That arrangement causes them to make a parallel translational motion, as found from the Thiele equation, see figure 9.8. Discuss whether it would be possible to use some applied magnetic field arrangement to stop that motion and freeze the vortices in place. If there is a possible solution, also analyze whether it would be stable.

9.3.3 Vortex image forces

A third effect that produces a force on a vortex is the interaction with the boundary of the system. A boundary has a tendency to polarize the spins in such a way that is equivalent to the field of an image vortex across the boundary, outside the system. Depending on boundary conditions, it is possible to determine the location and charge of the image and then determine the force as that for a pair interaction.

Free boundary conditions

The first type of boundary condition is *free boundary conditions*. This means that the system is sharply cut off at the boundary, and the spins along the edge are lacking a nearest neighbor in the direction $\hat{\mathbf{n}}$ pointing outward from the system. In a discrete lattice system, the equations of motion are of a form,

$$\dot{\mathbf{S}}_i = \mathbf{S}_i \times \mathcal{F}_i,$$ (9.120)

where $\mathcal{F}_i$ is the effective field due to the sites that are neighbors of site i. Across the boundary, it is conceptually useful to imagine fictitious spins on the other side, from which the boundary condition and the image vortex can be analyzed. A missing neighbor due to a boundary can be set to the value of the spin $\mathbf{S}_i$ itself, without changing the dynamics, since $\mathbf{S}_i \times \mathbf{S}_i = 0$. This is equivalent to saying that the spin field within the system will adjust itself quasi-statically so that its gradient

perpendicular to the boundary becomes zero. This is the concept of minimal changes in $\mathbf{S(r)}$ as one moves from the real spins within the system to the fictitious ones outside. So for free boundary conditions, we assume the quasi-static boundary conditions, where subscript 'b' indicates evaluation at the boundary,

$$(\hat{\mathbf{n}} \cdot \nabla)\mathbf{S}|_{b} = \frac{\partial \mathbf{S}}{\partial n}\bigg|_{b} = 0 \tag{9.121}$$

In fact, $\mathbf{S}(n)$ is continuous and has a zero slope across a boundary, where n is a coordinate measured through the boundary. This is equivalent to two equations for the angular coordinates,

$$\frac{\partial \theta}{\partial n}\bigg|_{b} = 0, \qquad \frac{\partial \phi}{\partial n}\bigg|_{b} = 0. \tag{9.122}$$

Applied to the component $S^{z} = S \sin \theta$, it means that an out-of-plane vortex with polarization p has an image vortex across the boundary with the *same polarization.*

For either an out-of-plane or in-plane vortex, the condition on ϕ determines the vorticity of the image vortex, as follows. A vortex produces a field $\nabla\phi$ given in (8.8) that can be derived from a vector potential as $\nabla\phi = \nabla \times \mathcal{A}$, which determines $\mathcal{A}$ according to

$$\nabla\phi = \frac{q}{r}\hat{\boldsymbol{\varphi}} = \nabla \times \mathcal{A} = \left(\frac{\partial \mathcal{A}_{r}}{\partial z} - \frac{\partial \mathcal{A}_{z}}{\partial r}\right)\hat{\boldsymbol{\varphi}}. \tag{9.123}$$

Only a z-component of $\mathcal{A}$ is required, which is solved as

$$\mathcal{A}_{z} = -q \ln r. \tag{9.124}$$

That is the potential for a vortex at the origin; it is easy to shift this to another center. Then, assume a vortex q at position $\mathbf{X}$ inside the system requires an image q' outside the system at position $\mathbf{X}'$. Their combined vector potential is

$$\mathcal{A}_{z} = -q \ln|\mathbf{r} - \mathbf{X}| - q' \ln|\mathbf{r} - \mathbf{X}'|. \tag{9.125}$$

It is helpful to apply this to the case of a *straight boundary*, and then generalize to other cases. Suppose there is an infinite straight boundary along the line $x = x_{b}$ parallel to the y-axis, as in figure 9.1, while the vortex is placed at $x = X$, $y = 0$. The boundary condition at $x = x_{b}$ is obtained by the curl component,

$$\frac{\partial \phi}{\partial x}\bigg|_{x_{b}} = (\nabla \times \mathcal{A})_{x} = \frac{\partial \mathcal{A}_{z}}{\partial y} = 0. \tag{9.126}$$

This says that the value of $\mathcal{A}_{z}$ *along the boundary* is a constant. Then expressing it in Cartesian coordinates, we have

$$\mathcal{A}_{z}(x_{b}, y) = -\frac{1}{2}\left\{q \ln\left[(x_{b} - X)^{2} + y^{2}\right] + q' \ln\left[(x_{b} - X')^{2} + y^{2}\right]\right\} = \text{constant.} \tag{9.127}$$

One can verify that (9.126) and this last expression are satisfied, with $\mathcal{A}_{z}(x_{b}, y) = 0$, only if

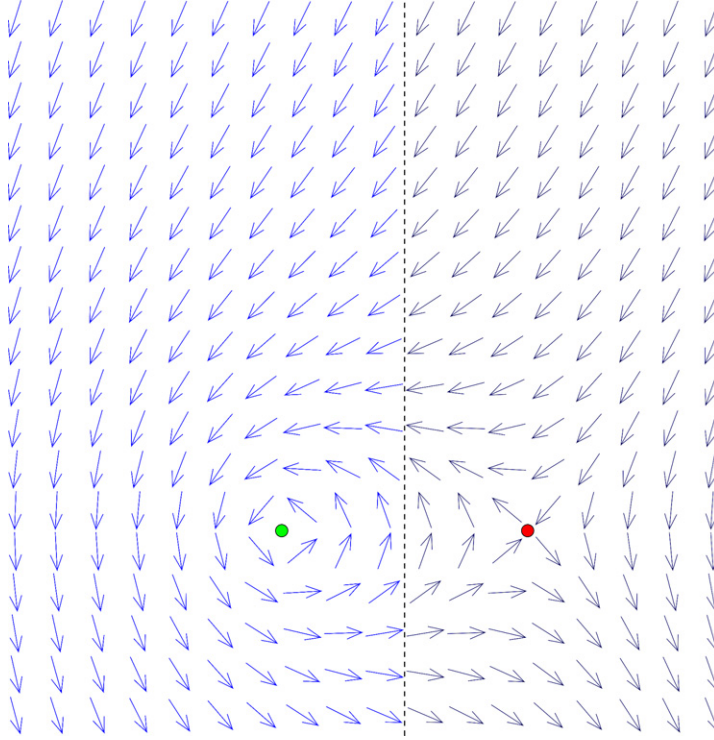$$q' = -q \quad \text{and} \quad X' - x_{b} = x_{b} - X. \tag{9.128}$$

Figure 9.1. The effect of free boundary conditions on a vortex (green dot, for $q = +1$) within a system, which is the region left of the dashed line, is as if there are fictitious spins outside the system (gray arrows) whose field is that of an anti-vortex (red dot, for $q' = -1$) equidistant from the boundary. This causes the gradient of the spin field perpendicular to the boundary to be zero there. The vortex is attracted to the boundary.

Then, the image vorticity is *opposite* to that of the original vortex, and the image is located equidistant from the boundary on the outside of the system. In figure 9.1 the $q = +1$ vortex is depicted with a green dot, while its $q' = -1$ image is displayed as a red dot. This result is identical to an electrostatics image for an electric charge near a grounded infinite plane. If we let the distance from vortex to the boundary be denoted $d_b \equiv |x_b - X|$, then our previous result (9.119) for the interaction of a pair of vortices separated by $2d_b$ gives an estimate of the force due to the boundary,

$$F_x = \frac{\pi J S^2 q^2}{d_b}. \tag{9.129}$$

A positive value here indicates a force of attraction towards the boundary.

In the case of an arbitrary *curved boundary*, the condition on the curl of $\mathcal{A}$ contains both components relative to the normal to the boundary, $\hat{\mathbf{n}}$, according to

$$\frac{\partial \phi}{\partial n}\bigg|_b = \hat{\mathbf{n}} \cdot \nabla \phi = \hat{\mathbf{n}} \cdot (\nabla \times \mathcal{A}) = n_x \partial_y \mathcal{A}_z - n_y \partial_x \mathcal{A}_z = (\hat{\mathbf{n}} \times \nabla)_z \mathcal{A}_z = 0. \tag{9.130}$$

If $\hat{\mathbf{n}}$ is normal to the boundary, then $\hat{\mathbf{n}} \times \nabla$ is the component of gradient directed *along the boundary*. Then for any boundary, this demonstrates that a constant value
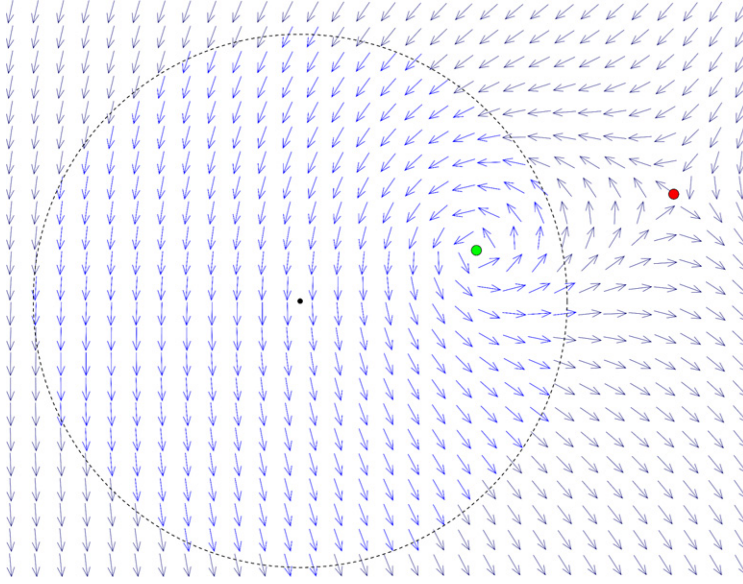
Figure 9.2. The effect of free boundary conditions on a vortex ($q = +1$, green dot) within a circular system. One can imagine fictitious spins outside the system whose field is that of an anti-vortex ($q' = -1$, red dot) at radius given by (9.132) outside the boundary. The gradient of the spin field perpendicular to the boundary is zero at the boundary and the vortex is attracted to the boundary.

of $\mathscr{A}_z$ along the boundary will be required. The image problem then requires making $\mathscr{A}_z$ constant on the boundary, regardless of its exact shape.

An example of a curved boundary is a vortex q at position $\mathbf{X} = (X, 0)$ within a circular system of radius R, similar to that in figure 9.2. The image charge q' is assumed by symmetry to be at $\mathbf{X}' = (X', 0)$. In circular coordinates the total vector potential can be expressed as

$$\mathscr{A}_z = -q \ln\left[r^2 - 2rX \cos\varphi + X^2\right] - q' \ln\left[r^2 - 2rX' \cos\varphi + X'^2\right]. \quad (9.131)$$

This needs to be independent of angular location φ at the system edge $r = R$. The derivative with respect to φ being zero leads to an expected result, $q' = -q$. Thus the image is of opposite vorticity. Imposing the boundary condition at radius R then gives the result for the position of the image,

$$X' = \frac{R^2}{X}, \quad (9.132)$$

which is similar to that for an electrostatic image outside a grounded cylinder or even a grounded sphere. Thus we can then find that the image force on a vortex in a circular system is radially outward, for free boundary conditions, determined by the vortex–image separation,

$$F_r = F_x = \frac{2\pi JS^2 q^2}{X' - X} = \frac{2\pi JS^2 q^2}{\dfrac{R^2}{X} - X}. \quad (9.133)$$

Again, the vortex is attracted towards the boundary, with a spin field such as that in figure 9.2. Of course, the motion itself need not be towards the boundary, due to gyrotropic effects. The result is only valid for out-of-plane vortices if the vortex is not within a vortex core radius (r_v) of the system edge. If the vortex is close to the center of the system ($X \ll R$), one sees that the force is linearly proportional to X, away from the center.

Exercise 9.6. Consider the vector potential due to a vortex and its image given in (9.131). (a) Show that $q' = -q$ is needed to make the potential constant on the circular boundary at $r = R$. (b) Show that the image location is related to the vortex location by $XX' = R^2$.

Strong demagnetization or fixed boundary conditions

Another type of boundary condition is that where demagnetization effects are strong along the boundary. This may not be important for an individual layer of spins, but could be important as more layers are added to build up a mesoscopic thin film (i.e. a micromagnetic system). If one supposes that the demagnetization energy should be reduced to its minimum, this implies that no surface magnetic charges should be present on the system boundaries. Based on the definition (3.23), for our purpose here we take an edge magnetic charge density as $\sigma_S = \mathbf{S} \cdot \hat{\mathbf{n}}$. The requirement of $\sigma_S = 0$ means that the spins need to follow the path of the boundary at an edge, which can be summarized as

$$\hat{\mathbf{n}} \cdot \mathbf{S}|_b = 0. \tag{9.134}$$

It should be kept in mind that this is a rather strong assumption. It may require a certain minimum system size in order to be true.

As an example, consider first a *linear edge*, again at $x = x_b$ along a line parallel to the y-axis, with a charge q vortex at position $\mathbf{X} = (X, 0)$ near this boundary. This is depicted in figure 9.3. In contrast to free boundary conditions where A_z was found to be constant (and zero) on the boundary, now the x-component of $\mathbf{S}(\mathbf{r})$ is assumed to be zero. Note that for free boundary conditions only $\nabla\phi$ was determined; an arbitrary constant angle could be added to that solution to fully determine the spin field. Here, consider the in-plane spin angle (not $\nabla\phi$) as a superposition of the original vortex field and an image, including a constant:

$$\phi = \phi_1 + \phi_2, \quad \text{where} \begin{cases} \phi_1 = q \tan^{-1} \dfrac{y}{x - X} + \phi_0 \\ \phi_2 = q' \tan^{-1} \dfrac{y}{x - X'}. \end{cases} \tag{9.135}$$

The image q' is assumed to be at $\mathbf{X}' = (X', 0)$. With $\hat{\mathbf{n}} = \hat{\mathbf{x}}$, we want here only the x-component of $\mathbf{S}$ to be forced to be zero at $x = x_b$. It is possible to imagine that this requires either $q' = q$ or $q' = -q$. Further, it simplifies the calculation by already assuming $\phi_0 = \pm\frac{\pi}{2}$, which makes the original vortex field point in a circular right- or
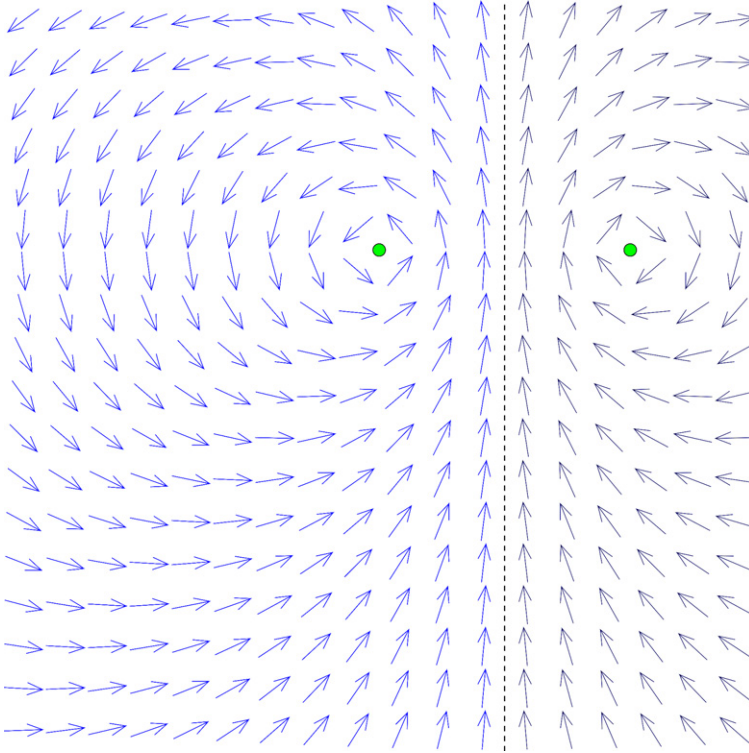
Figure 9.3. The effect of strong demagnetization boundary conditions (or fixed boundary conditions) on a vortex (green dot for $q = +1$) within a system, which is the region left of the dashed line. One can consider fictitious spins outside the system (gray arrows) whose field is that of an image vortex (also $q' = +1$) equidistant from the boundary. This causes the spin field to follow the boundary, eliminating the pole density there. The vortex is repelled from the boundary.

left-hand sense around the core point **X**. Rotating the original vortex field by $\pm\frac{\pi}{2}$, it becomes

$$\phi_1 = q \tan^{-1}\frac{x - X}{-y}.$$ (9.136)

Then the total in-plane angle is obtained from the tangent sum formula,

$$\tan\phi = \frac{\tan\phi_1 + \tan\phi_2}{1 - \tan\phi_1\tan\phi_2} = \frac{\dfrac{q(x - X)}{-y} + \dfrac{q'y}{x - X'}}{1 + qq'\dfrac{x - X}{x - X'}}$$

$$= \frac{q'y^2 - q(x - X)(x - X')}{y[(x - X') + qq'(x - X)]}.$$ (9.137)

To force the spins to follow this straight boundary parallel to $\hat{\mathbf{y}}$, one needs $\phi = 90°$ along $x = x_b$, meaning the denominator must vanish. That is seen to be

possible only if $q' = q$, in which case the image is found to be equidistant from the boundary as the original vortex:

$$d_b = X' - x_b = x_b - X. \tag{9.138}$$

The result is shown in figure 9.3, where both the real vortex and its image are depicted with green dots, to indicate their positive vorticity. Then, as the image has the same sign of vorticity as the vortex, the force between them is *repulsive*, but of the same magnitude as in expression (9.129). Thus we see the details of the boundary conditions will have a strong influence on dynamics.

This example can easily be extended to the case of a *curved boundary*, for a vortex q at position $\mathbf{X} = (X, 0)$ within a circular system of radius R, similar to that in figure 9.4. The image q' is again assumed to be at position $\mathbf{X}' = (X, 0)$. Expression (9.137) still applies in this case, but now the resulting angle ϕ evaluated on the circular boundary at $r = R$ must follow the boundary direction, which is the angular coordinate φ shifted by $\phi_0 = \pm\frac{\pi}{2}$, according to the sense of the spins' rotation:

$$\phi|_b = \varphi \pm \frac{\pi}{2}. \tag{9.139}$$

This means the tangent needed is

$$\tan\phi|_b = \frac{\sin\left(\varphi \pm \dfrac{\pi}{2}\right)}{\cos\left(\varphi \pm \dfrac{\pi}{2}\right)} = \frac{\cos\varphi}{-\sin\varphi} = -\cot\varphi = \frac{x}{-y}. \tag{9.140}$$
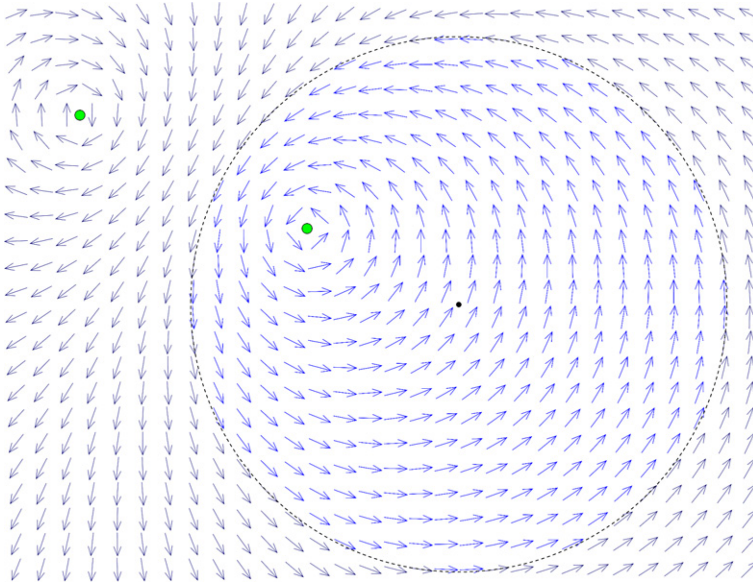

Figure 9.4. The effect of strong demagnetization boundary conditions on a $q = +1$ vortex (green for positive vorticity) in a circular system. The fictitious spins outside the system (gray arrows) make a field of an image vortex (also $q' = +1$) at the radius given by (9.144) outside the boundary. The spin field is forced to follow the boundary and the vortex is repelled from the boundary.

Then the boundary condition (9.134) will be satisfied provided at the boundary we have

$$\tan\phi\,|_b = \frac{q'y^2 - q(x - X)(x - X')}{y[(x - X') + qq'(x - X)]} = \frac{x}{-y}.$$

(9.141)

With $x = R\cos\varphi$ and $y = R\sin\varphi$, this can be rearranged into

$$(1 + qq' - q)R^2\cos^2\varphi + q'R^2\sin^2\varphi + \big[q(1 - q')X + (q - 1)X'\big]R\cos\varphi = qXX'.$$

(9.142)

The equation needs to be made valid and independent of φ by appropriate choices of q' and X'. The coefficient of $\cos\varphi$ must be zero to accomplish this, which is seen to give

$$q = q' = 1.$$

(9.143)

It is an intriguing result, that shows that the boundary condition can be satisfied *only for a vortex excitation*, not an anti-vortex. This makes sense, because the anti-vortex field is not capable of having its spin direction follow a circular boundary. Then with the image of the same sign, the vortex is repelled from the boundary, just as for a straight edge. Once the charges are determined, the remaining terms lead to a familiar result for the image location,

$$X' = \frac{R^2}{X}.$$

(9.144)

The situation is depicted in figure 9.4, where the combination of the fields of the original vortex and image vortex do follow the path of the boundary. Note that in the most general case, this requires a particular choice of the phase angle ϕ_0 as well. Then the force on a vortex ($q = +1$ only) due to its image is in the inward radial direction and is obtained from (9.119) as

$$F_r = F_x = -\frac{2\pi JS^2}{X' - X} = -\frac{2\pi JS^2}{\dfrac{R^2}{X} - X}.$$

(9.145)

In the limit of $X \ll R$, this is a linear restoring force that confines the vortex close to the center of the circle,

$$F_r \approx -\frac{2\pi JS^2}{R^2}X, \quad \text{for } X \ll R.$$

(9.146)

This is a result that could be of great use in the study of vortex motion in magnetic nanodots. It is worth noting that the force constant varies as the inverse square of the radius.

Exercise 9.7. (a) Check that the strong demagnetization boundary condition in the form (9.141) is transformed to (9.142). (b) Show that $q' = q = +1$ is required to satisfy the boundary condition at $r = R$. Then, it is impossible to satisfy the boundary condition with an anti-vortex. (c) Show that the image location is related to the vortex location by $XX' = R^2$, the same as for free boundary conditions.

9.4 Some simple examples of vortex dynamics

Here we look at some simple few-vortex situations and consider the dominant forces and the resulting motions, as described by the modified Thiele equation (9.46). Out-of-plane vortices are considered, because their dynamics is most interesting due to the presence of their non-zero gyrovector $\mathbf{G}$. For single vortices, the simplest situations are when they are interacting with their images caused by a boundary. The boundary may be straight or curved; in the latter case we assume a circular shape. For pairs of vortices in a system (two vortices or a vortex and an anti-vortex), there would be the direct force between the two as the primary driving force, and the image effects could be secondary, if the vortices are far from the system boundary. These kinds of motions have been verified in simulations of vortex pairs in rectangular systems [7] and individual vortices in circular systems.

9.4.1 An individual vortex near a straight boundary

Suppose a vortex of charge q, polarization p and gyrovector $\mathbf{G} = G\hat{\mathbf{z}} = 2\pi pq\hat{\mathbf{z}}$ finds itself a distance d_b from a straight boundary such as that in figure 9.1 or figure 9.3. In the case of free boundary conditions, the force on the vortex due to its image is towards the boundary, regardless of the sign of q. In the case of strong demagnetization (fixed) boundary conditions, the force is away from the boundary. Strong demagnetization requires the spins to point along the direction of the boundary, and that is possible only for vortices with $q = +1$; it is impossible to satisfy the requirement of zero pole density on the boundary if $q = -1$.

Suppose $\hat{\mathbf{n}}$ is a normal vector pointing *outward* from the system (from q towards its image q'). In both the cases of free and fixed boundary conditions, we can write the force on the vortex, due to its image outside the system in the following form, based on (9.129),

$$\mathbf{F} = -\frac{\pi JS^2 qq'}{d_b}\hat{\mathbf{n}}, \qquad q' = \nu_{bc}q, \tag{9.147}$$

where the index ν_{bc} that determines the image charge depends on boundary conditions,

$$\nu_{bc} = \begin{cases} -1 & \text{free boundaries} \\ +1 & \text{fixed boundaries.} \end{cases} \tag{9.148}$$

A free (fixed) boundary condition produces an image of the opposite (same) vorticity, attracting (repelling) the vortex to (from) the boundary[4].

---

[4] Note that the unit vector $\hat{\mathbf{n}}$ points towards the image vortex. Then, $-\hat{\mathbf{n}}$ points from the image towards q. The notation $\hat{\mathbf{R}}$ is used later in (9.181), in place of $-\hat{\mathbf{n}}$, for the unit vector pointing towards the charge of interest, when forces between vortex pairs inside a system are considered.

Steady-state uniform motion without damping

If there is no damping, a steady-state solution of the Thiele equation at constant velocity $\bar{\mathbf{V}}$ is then found by applying a cross product with the gyrovector (with acceleration $\mathbf{A} = 0$),

$$\mathbf{G} \times \left[\frac{1}{\sigma}\mathbf{F} + \mathbf{G} \times \bar{\mathbf{V}} \right] = 0, \tag{9.149}$$

which then leads to the steady-state undamped velocity

$$\bar{\mathbf{V}} = \frac{\mathbf{G} \times \mathbf{F}}{\sigma G^2} = -\nu_{\mathrm{bc}} \frac{\pi J S^2 q^2}{\sigma 2\pi p q d_{\mathrm{b}}} \, \hat{\mathbf{z}} \times \hat{\mathbf{n}}. \tag{9.150}$$

For later analysis, it is useful to put this result in the following form:

$$\bar{\mathbf{V}} = -\frac{C}{G d_{\mathrm{b}}} \, \hat{\mathbf{z}} \times \hat{\mathbf{n}}, \tag{9.151}$$

where C is a force constant between the vortex q and its image $q' = \nu_{\mathrm{bc}}q$,

$$C = qq'\pi\sigma^{-1}JS^2. \tag{9.152}$$

In terms of this constant, the force on the vortex, per unit spin density, is

$$\mathbf{f} = \sigma^{-1}\mathbf{F} = -\frac{C}{d_{\mathrm{b}}}\hat{\mathbf{n}}. \tag{9.153}$$

This stationary solution, depicted in figure 9.5, represents a uniform translational motion parallel to the boundary. Its direction is determined by the combination of q, p and ν_{bc}. The speed will be all the greater for a vortex closer to the boundary. However, the result will apply only as long as the distance d_{b} is greater than the vortex core radius r_{v}. For given $G = 2\pi qp$, the two different types of boundary conditions give motions in opposite directions. Some interesting examples can be
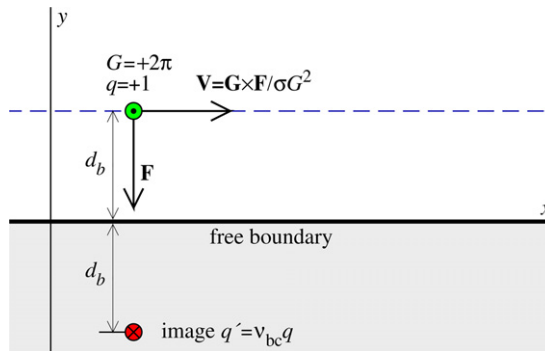

Figure 9.5. Coordinate system for a vortex q moved by the force of its image q' outside the system boundary. The vortex has $q = +1$ (shown as green), $p = +1$ and $G = +2\pi$ (shown with $\odot$), being attracted to the boundary with a force according to (9.147). For a free boundary ($\nu_{\mathrm{bc}} = -1$), its image is of opposite sign, $q' = -1$ (shown as red), with $p' = +1$ and then $G' = -2\pi$ (shown with $\otimes$). The steady-state vortex velocity results from the Thiele equation (9.20) without damping; see also (9.150).

seen in figure 3 of [7], where the closer a vortex is to a boundary, the faster it moves as it interacts with its image outside the system.

Steady-state motion with damping

Now, consider the effect of damping, including a damping term $\mathsf{D}_{jk}V_k$ in the Thiele equation. As seen earlier, the damping matrix is diagonal, with negative elements, so it is helpful to write it as $\mathsf{D}_{jk} \equiv -\mathsf{D}\delta_{jk}$, including the minus sign so that the constant D is positive. A little consideration shows that in fact, the presence of damping already forces there to be components of $\mathbf{V}$ both parallel and perpendicular to the boundary. A mass term also leads to both velocity components being necessary. Let us consider the individual effects of damping and mass first separately, then later it is easy to conclude what their combined effects are.

For a concrete example (such as figure 9.1 rotated 90° clockwise), take the boundary to be the x-axis, with the vortex in the first quadrant at position $\mathbf{X}(t) = (X(t), \, Y(t))$ and velocity $\mathbf{V}(t) = (V_x(t), \, V_y(t))$. The outward normal is then $\hat{\mathbf{n}} = -\hat{\mathbf{y}}$, and the only force component is F_y. Define $f_y = \sigma^{-1}F_y$ to simplify the notation. Then the modified Thiele equation (9.46) in Cartesian components is written for this example as

$$-GV_y - \mathsf{D}V_x = \mathsf{M}\dot{V}_x \tag{9.154a}$$

$$f_y + GV_x - \mathsf{D}V_y = \mathsf{M}\dot{V}_y. \tag{9.154b}$$

The scaled force is

$$f_y = \sigma^{-1}F_y = \nu_{\mathrm{bc}}q^2\frac{\pi JS^2}{\sigma Y} = \frac{C}{Y}. \tag{9.155}$$

Now the distance to the boundary, Y, is not necessarily constant, due to $V_y \neq 0$. However, the velocity component V_x parallel to the boundary can be eliminated, solving (9.154b) as

$$GV_x = -f_y + \mathsf{D}V_y + \mathsf{M}\dot{V}_y. \tag{9.156}$$

This can be substituted into (9.154a) to give a separated equation for the component of the motion perpendicular to the boundary,

$$G^2V_y = \mathsf{D}\left(f_y - \mathsf{D}V_y - \mathsf{M}\dot{V}_y\right) + \mathsf{M}\left(\dot{f}_y - \mathsf{D}\dot{V}_y - \mathsf{M}\ddot{V}_y\right). \tag{9.157}$$

Due to the force varying with Y^{-1}, an exact solution for arbitrary D and M is difficult. At this point we consider separately the cases of damping without mass and mass without damping.

Damping without mass

Suppose the mass is dropped from (9.157), with the damping being the only effect to modify the gyrovector force. This could be considered the strong damping limit. Then the equation of motion is:

$$\left(G^2 + \mathsf{D}^2\right)V_y = \mathsf{D}f_y \qquad \Longrightarrow \qquad \frac{\mathrm{d}Y}{\mathrm{d}t} = \frac{\mathsf{D}C}{G^2 + \mathsf{D}^2}\frac{1}{Y} \tag{9.158}$$

or

$$\int_{Y_0}^{Y(t)} dY' \; Y' = \int_0^t dt' \; \frac{1}{2}\Gamma, \qquad \text{where } \Gamma \equiv \frac{2DC}{G^2 + D^2}. \qquad (9.159)$$

Starting at an initial distance from the boundary, Y_0, the exact solution is easily found,

$$Y(t) = \left(Y_0^2 + \Gamma t \right)^{1/2}. \qquad (9.160)$$

Within the approximations to arrive at this, it shows that the vortex accelerates as it approaches closer to the boundary, due to the increasing force. At the same time, (9.154a) for zero mass indicates that the trajectory has a constant slope:

$$\frac{V_y}{V_x} = -\frac{D}{G} \qquad \Longrightarrow \qquad \frac{dY}{dX} = -\frac{D}{G}. \qquad (9.161)$$

Then this shows that the vortex path is a straight line, with the constant $-D/G$ being the slope relative to the boundary. From this or by integration of (9.154a) the position along the boundary is

$$X(t) = X_0 - \frac{G}{D}\left[\left(Y_0^2 + \Gamma t \right)^{1/2} - Y_0 \right]. \qquad (9.162)$$

Figure 9.6 shows two examples of these results for free boundary conditions, one for a vortex with positive G (taking $q = p = +1$) and one with negative G (using $q = +1$ but $p = -1$), with different damping constants D. Note that the slope $-D/G$ does not depend on the type of boundary condition; D is positive while $G = 2\pi qp$, positive or negative, determines the slope. The force constant $C \propto \nu_{bc}$, however, is negative for free boundary conditions but positive for fixed boundary conditions, see (9.155). Then with $\Gamma \propto C$, the vortex approaches the boundary for free boundaries ($\Gamma < 0$) but it moves away from the boundary for fixed boundaries ($\Gamma > 0$). The translation
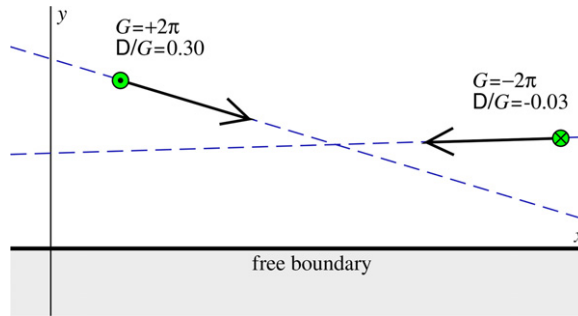

Figure 9.6. Examples of vortex motion near a boundary with free boundary conditions ($\nu_{bc} = -1$), damping parameter D and no mass, according to the results in (9.160) and (9.162). The vortex on the left has $q = +1$ (shown as green), $p = +1$ and $G = +2\pi$ (shown with $\odot$), being attracted to the boundary and moving at the descending slope $-D/G = -0.30$. The vortex on the right has $q = +1$ (green), $p = -1$ and then $G = -2\pi$ (shown with $\otimes$), but it is also attracted towards the boundary, moving in the reverse direction along the slope $-D/G = +0.03$.

parallel to the boundary can be seen to be in the direction of $-qp\nu_{bc}\hat{\mathbf{x}}$, as found without damping. For the examples in figure 9.6, both vortices are attracted to the boundary but move in opposite senses along the boundary because they have opposite signs of G.

Mass without damping

At this point suppose the mass is included, but not the damping. Later the correction $D > 0$ causes can be addressed. The force varies with position and hence with time, and we make an approximation,

$$\dot{f}_y = \frac{df_y}{dY}\frac{dY}{dt} = -\frac{C}{Y^2}\dot{Y} \approx -\frac{C}{Y_0^2}V_y, \tag{9.163}$$

where $Y_0 = Y(0)$ is the initial separation from the boundary. The vortex is assumed to be far enough from the boundary that this approximation of a nearly constant force makes sense. Then from (9.157), the transverse velocity component approximately satisfies a harmonic oscillator equation,

$$\ddot{V}_y \approx -\left(\frac{G^2}{M^2} + \frac{C}{MY_0^2}\right)V_y. \tag{9.164}$$

Assuming some initial velocity away from the boundary, $V_y(0)$, a solution with a convenient phase is

$$V_y(t) = V_y(0)\cos \omega_c t \tag{9.165a}$$

$$Y(t) = \int_0^t dt'\ V_y(t') = Y_0 + Y_1 \sin \omega_c t, \qquad Y_1 = V_y(0)/\omega_c, \tag{9.165b}$$

where the undamped cyclotron frequency is

$$\omega_c = \sqrt{\frac{G^2}{M^2} + \frac{C}{MY_0^2}}. \tag{9.166}$$

The corresponding motion parallel to the boundary is then found from (9.156),

$$V_x(t) = G^{-1}\left(-f_y + M\dot{V}_y\right) \approx -\frac{C}{GY_0} - V_y(0)\frac{M\omega_c}{G}\sin \omega_c t. \tag{9.167}$$

This is summarized as

$$V_x(t) = \bar{V}_x - V_y(0)\frac{M\omega_c}{G}\sin \omega_c t, \qquad \bar{V}_x = -C/\left(GY_0\right) \tag{9.168a}$$

$$X(t) = \int_0^t dt'\ V_x(t') = X_0 + \bar{V}_x t + X_1 \cos \omega_c t, \qquad X_1 = V_y(0)M/G. \tag{9.168b}$$

Note that $\bar{V}_x$ is the velocity $\bar{\mathbf{V}}$ of uniform motion found in (9.151). This is a rather interesting solution, because it shows that the vortex core makes a small-amplitude cycloidal motion on top of the uniform motion parallel to the boundary.
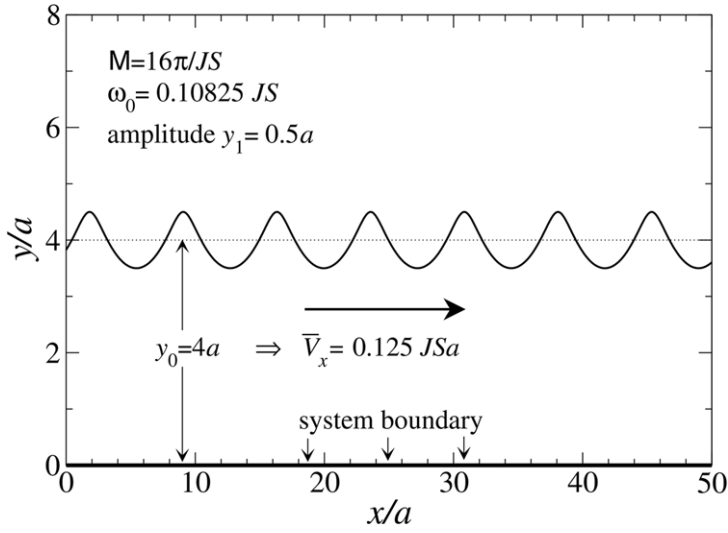
Figure 9.7. The type of undamped cycloidal oscillations expected for a vortex at distance $y_0 = 4a$ from a system boundary while interacting with its image across the boundary. The plot is made by assuming a typical vortex mass $M = 16\pi/JS$, gyrovector $G = 2\pi$, square lattice spin density $\sigma = S/a^2$ and force constant of magnitude $|C| = \pi JSa^2$, which gives the drift speed from $\bar{V}_x = -C/(GY_0)$ and cycloidal frequency from (9.166).

The cyclotron frequency becomes $\omega_c \to G/M$ if the vortex is far from the boundary; otherwise, $\omega_c < G/M$. Then, the amplitude Y_1 of the transverse oscillations is larger than the amplitude X_1 of the longitudinal oscillations, producing an elliptical oscillatory motion as the vortex translates parallel to the boundary. An example of the motion is shown in figure 9.7, for a vortex on a square lattice at an initial distance of $Y_0 = 4a$ from the boundary. The mass has been assumed to be the value $M = 16\pi/JS$, which is typical for small systems [8] with $R < 20a$. For this distance, the drift velocity is found to be $\bar{V}_x = 0.125JSa$, and the cycloidal frequency is $\omega_c = 0.10825JS$, whereas the limiting value of the frequency for a vortex very far from the boundary is $\omega_c \to G/M = 0.125JS$. Figure 9.7 is made for cycloidal oscillations in the counterclockwise sense, as would be the case for a vortex with $G = +2\pi$ and free boundary conditions. An amplitude $Y_1 = 0.5a$ was assumed; the amplitude of the cycloidal motion is not determined by this calculation. In a sense, it is a free parameter that represents something very similar to the amplitude of a classical spin wave mode.

Weak damping for a vortex with mass

Now consider if a weak damping $D \ll G$ is included together with the mass. First, we can see a simple mechanical law results from the modified Thiele equation, multiplying (9.154a) by V_x and (9.154b) by V_y, and adding, to give,

$$\frac{\mathrm{d}}{\mathrm{d}t}\mathrm{KE} = f_y V_y - \frac{2D}{M}\mathrm{KE}, \qquad \mathrm{KE} = \frac{1}{2}M\left(V_x^2 + V_y^2\right). \tag{9.169}$$

This indicates that a usual vortex kinetic energy associated with the mass changes in time either due to the damping, or due to the work done by the force. Without damping, we had $V_y = 0$ and there was no work, and the kinetic energy was constant. With damping, there could even be positive work, as in the case of a vortex moving towards its image across the boundary with free boundary conditions. The competition between the damping and the work will determine whether $\mathbf{V}^2$ is increasing or decreasing.

Going back to (9.157), and again assuming that the vortex is far from the boundary ($Y \approx Y_0$ plus oscillations), the first term on the RHS can be approximated (for weak damping),

$$\mathsf{D}f_y \approx \frac{\mathsf{D}C}{Y_0}. \tag{9.170}$$

The equation now is arranged as

$$\left(G^2 + \mathsf{D}^2 + \frac{\mathsf{M}C}{Y_0^2}\right)V_y = \frac{\mathsf{D}C}{Y_0} - 2\mathsf{D}\mathsf{M}\dot{V}_y - \mathsf{M}^2\,\ddot{V}_y. \tag{9.171}$$

Then one sees a quasi-steady-state solution with $\dot{V}_y \approx 0$ would be present with a slow drift velocity towards (away from) the boundary for free (fixed) boundary conditions,

$$\bar{V}_y = \frac{\mathsf{D}C/Y_0}{G^2 + \mathsf{D}^2 + \mathsf{M}C/Y_0^2}. \tag{9.172}$$

This drift can be taken out of $V_y(t) = \bar{V}_y + \tilde{V}_y(t)$ to obtain an equation for the oscillatory part, $\tilde{V}_y(t)$,

$$\mathsf{M}^2\,\ddot{\tilde{V}}_y + 2\mathsf{D}\mathsf{M}\,\dot{\tilde{V}}_y + \left(G^2 + \mathsf{D}^2 + \frac{\mathsf{M}C}{Y_0^2}\right)\tilde{V}_y = 0. \tag{9.173}$$

Then assuming a usual exponential type of solution, $\tilde{V}_y \propto \exp(-i\omega t)$, leads to an equation for the complex frequency,

$$-\mathsf{M}^2\omega^2 - 2\mathsf{D}\mathsf{M}i\omega + G^2 + \mathsf{D}^2 + \frac{\mathsf{M}C}{Y_0^2} = 0. \tag{9.174}$$

Using the definition (9.166) of the undamped frequency, this is

$$\omega^2 + \frac{2\mathsf{D}}{\mathsf{M}}i\omega - \omega_{\mathrm{c}}^2 - \frac{\mathsf{D}^2}{\mathsf{M}^2} = 0. \tag{9.175}$$

We obtain two solutions from the quadratic formula,

$$\omega = \frac{1}{2}\left[-\frac{2i\mathsf{D}}{\mathsf{M}} \pm \sqrt{\left(\frac{2i\mathsf{D}}{\mathsf{M}}\right)^2 + 4\left(\omega_{\mathrm{c}}^2 + \frac{\mathsf{D}^2}{\mathsf{M}^2}\right)}\,\right] = -\frac{i\mathsf{D}}{\mathsf{M}} \pm \omega_{\mathrm{c}}. \tag{9.176}$$

Then this will lead to decaying sine and cosine solutions, whose amplitudes diminish with $\exp(-\gamma_D t)$, where the decay constant is $\gamma_D = D/M$. We can see that the overall core motion will be described by

$$V_y(t) \approx \bar{V}_y + \tilde{V}_y(0)\mathrm{e}^{-\gamma_D t} \cos \omega_c t. \tag{9.177}$$

From this, one can go back and also find the motion $V_x(t)$ from (9.156). It exhibits a slight reduction in the uniform velocity parallel to the boundary and a damping of the oscillatory motion. For free boundary conditions, the vortex will indeed tend to move slowly towards its image of opposite vorticity on the other side of the boundary, as the damping takes out energy from the system. This causes the vortex to leave the system, eventually. For fixed or strong demagnetization boundary conditions, the tendency will be instead to move away from the boundary, but again in a process that lowers the energy, this time moving away from its image of the same vorticity. In that case, the damping effect will push the vortex back into the system and tend to stabilize it.

9.4.2 A pair of vortices in a large system

Consider a pair of vortices with charges q_1, p_1 and q_2, p_2 far from any boundaries in a large system, so that the forces due to images can be neglected, to leading order. The vortex locations are denoted as $\mathbf{X}_1$ and $\mathbf{X}_2$. They attract or repel each other with a Coulomb-like force given in (9.119). This situation was considered in [9] without damping. Here we show the main results, which are rather simple.

At first we seek uniform or stationary solutions, where the vortices move at constant speeds. Later we allow for possible small perturbations about these states. Looking at the Thiele equation for just one vortex affected by constant force, we know the steady-state velocity in (9.150) is in the direction of $\mathbf{G} \times \mathbf{F}$. The vortices exert equal and opposite forces on each other. Then the vortex velocities are in opposite directions if their gyrovectors are parallel, and conversely, the velocities are parallel (and equal) if the gyrovectors are anti-parallel. Figure 9.8 shows the result of
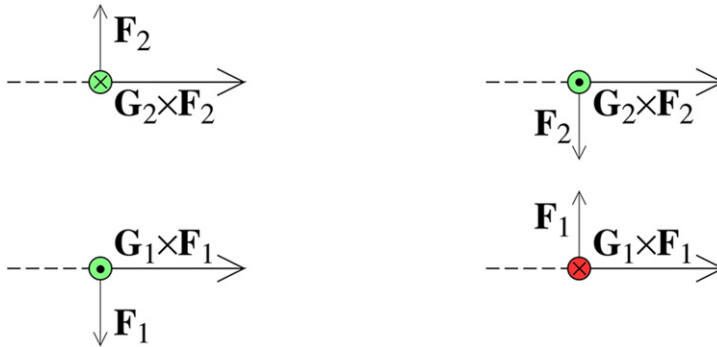

Figure 9.8. Examples of vortex pairs with anti-parallel gyrovectors performing linear translational motion. The gyrovector component out of the page is indicated by $\odot$ for $G = +2\pi$ and by $\otimes$ for $G = -2\pi$. The VV pair on the left has equal vorticities $q_1 = q_2 = +1$ (green) but opposite polarizations. The VA pair on the right has opposite vortices (red for $q = -1$) but equal polarizations. The translational velocity of a vortex is in the direction of $\mathbf{G} \times \mathbf{F}$, according to (9.150).
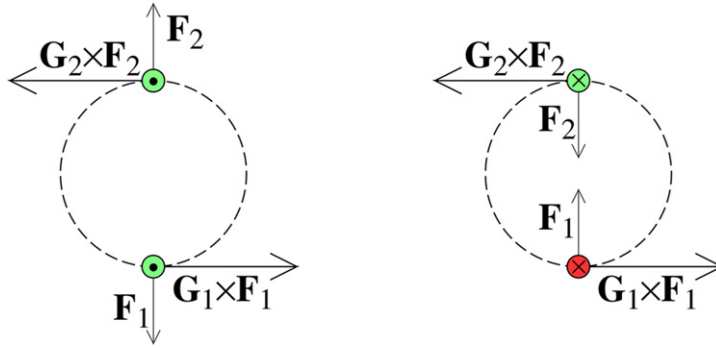
Figure 9.9. Examples of vortex pairs with parallel gyrovectors performing orbital motion. The gyrovector component $G = 2\pi q p$ out of the page is indicated by $\odot$ for $G = +2\pi$ and by $\otimes$ for $G = -2\pi$. The VV pair on the left has equal vorticities $q_1 = q_2 = +1$ (green) and equal polarizations ($p_1 = p_2 = +1$). The VA pair on the right has opposite vorticities (red for $q = -1$) and opposite polarizations. Each vortex moves instantaneously in the direction of $\mathbf{G} \times \mathbf{F}$, according to (9.150).

applying this rule to a vortex–vortex (VV) pair and a vortex–anti-vortex (VA) pair with opposite gyrovectors: the pair will translate together in a straight line. Figure 9.9 shows the result of this rule for a VV pair and a VA pair with parallel gyrovectors: the pair will orbit one about the other in uniform circular motion. This analysis leads to the conclusion that the motion has only these two possibilities:

$$\text{Anti-parallel } \mathbf{G}: q_1 p_1 = -q_2 p_2 \implies \text{ parallel translational motion} \quad (9.178a)$$

$$\text{Parallel } \mathbf{G}: q_1 p_1 = q_2 p_2 \implies \text{ circular orbital motion.} \quad (9.178b)$$

To make this result quantitative, we can calculate the speed in each case. It is convenient to let the separation of the pair be a parameter $2R_0$, and suppose that a unit vector $\hat{\mathbf{R}}_{12}$ points from vortex 2 towards vortex 1.

For *anti-parallel* gyrovectors, the parallel translation of the two vortices takes place at the steady-state velocity $\bar{\mathbf{V}} = \mathbf{V}_1 = \mathbf{V}_2$ with

$$\bar{\mathbf{V}} = \frac{\mathbf{G}_1 \times \mathbf{F}_1}{\sigma G_1^2} = \frac{2\pi J S^2 q_1 q_2 / (2R_0)}{\sigma 2\pi p_1 q_1} \left(\hat{\mathbf{z}} \times \hat{\mathbf{R}}_{12} \right) = \frac{C}{G_1 R_0} \left(\hat{\mathbf{z}} \times \hat{\mathbf{R}}_{12} \right). \quad (9.179)$$

This uses the generalized definition of the force constant in (9.152),

$$C = q_1 q_2 \pi \sigma^{-1} J S^2 \quad (9.180)$$

and the force is defined by

$$\mathbf{F}_1 = \frac{C}{R_0} \hat{\mathbf{R}}_{12}. \quad (9.181)$$

Compare with (9.147) for the force between a charge and its image outside the system, which points in the opposite direction. Of course, larger separation results in slower motion. Changing from a VV pair to a VA pair makes no difference once the polarizations are reversed to keep the gyrovectors anti-parallel, see figure 9.8.

When the gyrovectors are **parallel**, the resulting circular motion at some assumed steady-state frequency ω makes it necessary to include the acceleration term. The Thiele equation is applied just to vortex 1, while vortex 2 makes the same motion but half a period out-of-phase. We can write the acceleration as $\mathbf{A}_1 = -\omega^2 \mathbf{X}_1$, assuming $\mathbf{X}_1$ is relative to the center of the motion, and the velocity as $\mathbf{V}_1 = \omega\hat{\mathbf{z}} \times \mathbf{X}_1$, in

$$\sigma^{-1}\mathbf{F}_1 + \mathbf{G}_1 \times \mathbf{V}_1 = \mathsf{M}\mathbf{A}_1. \tag{9.182}$$

With $\mathbf{G}_1 \times \mathbf{V}_1 = -\omega G_1 \mathbf{X}_1$, this gives for the radial component,

$$\frac{C}{R_0} - G_1\omega R_0 = -\mathsf{M}\omega^2 R_0. \tag{9.183}$$

Note that in the limit of zero mass, the solution (of the original Thiele equation) must be

$$\omega_0 = \omega(\mathsf{M} = 0) = \frac{C}{G_1 R_0^2}. \tag{9.184}$$

The general quadratic equation with mass (9.183) can be rearranged as

$$\omega^2 - \frac{G_1}{\mathsf{M}}\omega + \frac{C}{\mathsf{M}R_0^2} = 0, \tag{9.185}$$

whose general solution is

$$\omega = \frac{G_1}{2\mathsf{M}} - \sqrt{\left(\frac{G_1}{2\mathsf{M}}\right)^2 - \frac{C}{\mathsf{M}R_0^2}}. \tag{9.186}$$

The negative root was selected to give the result (9.184) in the limit $\mathsf{M} \to 0$. This looks singular as far as the dependence on small M. Using the identity, $(a - \sqrt{a^2 - b})(a + \sqrt{a^2 - b}) = b$, another way to write it is

$$\omega = \frac{JS^2}{\sigma R_0^2}(q_2 p_1)\left(1 + \sqrt{1 - \frac{q_2}{q_1}\frac{JS^2\mathsf{M}}{\pi\sigma R_0^2}}\right)^{-1}. \tag{9.187}$$

Although small mass $\mathsf{M}JS \ll 1$ is probably not very likely [8], we can consider finding the small M limit (also because the ratio of M/R_0^2 is what is more relevant). An expansion leads to a result with a linear dependence on mass,

$$\omega \approx \omega_0\left(1 + \frac{q_2}{q_1}\frac{JS^2\mathsf{M}}{4\pi\sigma R_0^2}\right), \qquad \frac{JS^2\mathsf{M}}{4\pi\sigma R_0^2} \ll 1. \tag{9.188}$$

These are curious results, showing that a pair with equal vorticities (VV or AA) will have a faster steady-state rotation than a pair with opposite signs (VA). In order to have parallel gyrovectors, a VV or AA pair must have equal polarizations $p_1 = p_2$. For a VA pair, the polarizations would have to be in opposite directions. Then the VV or AA pair has a particularly different out-of-plane spin structure than a VA pair, which will be responsible for the change in the rotational frequency. Earlier we assumed a mass

$M = 16\pi/JS$, for a system around $R_0 = 20a$, which comes from studies of single vortex oscillations in circular systems [8]. For these parameters, the expansion parameter is

$$\frac{JS^2M}{4\pi\sigma R_0^2} \approx \frac{16\pi S}{4\pi S \cdot 20^2} = \frac{1}{100}. \qquad (9.189)$$

Therefore the mass effect on rotation rate can be expected to be rather small.

Exercise 9.8. (a) Verify that (9.183) results by application of the modified Thiele equation to a pair of vortices with parallel gyrovectors. (b) Show that the orbital frequency is given by general solution (9.186). (c) Make an appropriate expansion for small mass $MJS \ll 1$ and confirm the result (9.188), which shows that the relative vorticity of the pair q_2/q_1 affects the steady-state rate of rotation.

Cycloidal oscillations of a pair

Now consider fluctuations on the stationary solutions just found. Suppose there is an additional small-amplitude displacement superimposed. This extra displacement is taken to be in opposite directions for each vortex of the pair. To make this clear, define the half-separation vector $\mathbf{R}_{12}$ and the center vector $\mathbf{X}_c$ of the vortices as

$$\mathbf{R}_{12} = \frac{1}{2}\left(\mathbf{X}_1 - \mathbf{X}_2\right) \qquad (9.190a)$$

$$\mathbf{X}_c = \frac{1}{2}\left(\mathbf{X}_1 + \mathbf{X}_2\right). \qquad (9.190b)$$

Then $\mathbf{R}_{12}(t)$ measures the vortex positions relative to the center of the pair, i.e.

$$\mathbf{X}_1(t) = \mathbf{X}_c(t) + \mathbf{R}_{12}(t) \qquad (9.191a)$$

$$\mathbf{X}_2(t) = \mathbf{X}_c(t) - \mathbf{R}_{12}(t). \qquad (9.191b)$$

The center position translates uniformly at velocity $\bar{\mathbf{V}}$ for anti-parallel gyrovectors, see (9.179), or it is fixed in location for parallel gyrovectors. Either way, it does not contribute an acceleration. The half-separation can be assumed to be that from the stationary solution, $\mathbf{R}_0(t)$, combined with small oscillations $\mathbf{r}(t)$, writing,

$$\mathbf{R}_{12}(t) = \mathbf{R}_0(t) + \mathbf{r}(t). \qquad (9.192)$$

For *anti-parallel* gyrovectors, the stationary solution of parallel translation has $\mathbf{X}_c(t) = \mathbf{c}_0 + \bar{\mathbf{V}}t$, and constant separation $2\mathbf{R}_0$. Supposing that the translation is along the x-axis, $\bar{\mathbf{V}} = (\bar{V}_x, 0)$, one could take the vortex locations described by $\mathbf{R}_0 = (0, Y_0)$ and fluctuations $\mathbf{r}(t) = (X(t), Y(t))$. The velocity of vortex 1 is then $\mathbf{V}_1 = (\bar{V}_x + \dot{X}, \dot{Y})$, and for vortex 2 the velocity is $\mathbf{V}_2 = (\bar{V}_x - \dot{X}, -\dot{Y})$. To leading order in the small fluctuations, this physical situation is the same as that already considered in section 9.4.1, for a vortex interacting with its image, moving along a boundary parallel to the x-axis. When the vortex moves to slightly larger Y, its image moves farther away in the opposite direction. The corresponding small displacements in X do not affect the force, and play a limited role. Therefore we already have solved

for the frequency of the oscillations, in (9.166). Using the force constant in (9.180), the small-amplitude cycloidal oscillations have the undamped frequency,

$$\omega_c = \sqrt{\frac{G^2}{\mathsf{M}^2} + \frac{C}{\mathsf{M}y_0^2}} = \frac{G}{\mathsf{M}}\sqrt{1 + \frac{q_1 q_2 J S^2 \mathsf{M}}{\pi\sigma\left(2R_0\right)^2}} . \tag{9.193}$$

Note that this depends on $2R_0$, the average separation of the pair, and the relative signs of the vorticities $q_1 q_2$. A VV or AA pair will have a higher frequency than a VA pair. The resulting trajectories for this parallel translation in the x-direction are still given by (9.165) and (9.168).

For **parallel** gyrovectors, the stationary solution of rotational motion is described with a fixed center $\mathbf{X}_c = \mathbf{c}$, and a constant separation distance $2R_0$. Of course, the half-separation vector itself is rotating at the steady-state frequency ω in (9.187), with $\dot{\mathbf{R}}_0 = \omega\hat{\mathbf{z}} \times \mathbf{R}_0$. Therefore suppose this part of the motion has components,

$$\mathbf{R}_0 = R_0(\cos\omega t, \ \sin\omega t) \tag{9.194a}$$

$$\dot{\mathbf{R}}_0 = \omega R_0(-\sin\omega t, \ \cos\omega t). \tag{9.194b}$$

The components of the modified Thiele equation (for vortex 1) are

$$f_x - G_1 V_y = \mathsf{M}\dot{V}_x \tag{9.195a}$$

$$f_y + G_1 V_x = \mathsf{M}\dot{V}_y, \tag{9.195b}$$

where the scaled force, using C of (9.180), is

$$\mathbf{f} = \sigma^{-1}\mathbf{F} = \frac{C}{R_{12}^2}\mathbf{R}_{12}. \tag{9.196}$$

It is assumed that $\mathbf{R}_0(t)$ keeps a fixed length, whereas $\mathbf{r}(t)$ must make an elliptical cycloidal motion to solve the equations. It is somewhat tedious but with appropriate expansions and keeping the leading linear terms in $\mathbf{r}(t)$ and its time derivatives, one can find the small-amplitude oscillations at a frequency ω_c about the uniform rotational motion at frequency ω. The resulting cyclotron frequency for those oscillations is similar to that for the case of parallel translation, becoming

$$\omega_c = \frac{G}{\mathsf{M}}\sqrt{1 - \frac{q_1 q_2 J S^2 \mathsf{M}}{2\pi\sigma R_0^2}} . \tag{9.197}$$

Compare (9.193) for the case of anti-parallel gyrovectors, which has the opposite sign in the radical and an extra factor of 2 dividing the mass. Of course, these mass effects can be expected to be rather small; the dominant contribution to this cyclotron oscillation frequency is G/M. These types of oscillations can be reproduced in simulations of vortex pairs, especially for parallel gyrovectors, such as seen in the work of Mertens *et al* [9]. Further discussion of a more elaborate *collective coordinate* theory for describing the motion of vortex pairs can be found in Völkel *et al* [7]. In this collective coordinate theory, the ideas on vortex mass presented here have been extended to a more general

theory where a mass tensor is developed that is a multi-vortex object, rather than the mass discussed here, which has been a single vortex property.

9.4.3 An individual vortex in a circular system

A situation of great interest is a single vortex within a circular system of radius R, especially because this can be the ground state in the case where demagnetization effects are included. At this point, we do not explicitly include demagnetization, but instead, consider how a vortex moves in a circular quasi-2D magnet with either free ($\nu_{bc} = -1$) or fixed ($\nu_{bc} = +1$) boundary conditions. Recall that the latter type, which forces the spins to point along the edge of the circle on the boundary, is the limit of strong demagnetization. It also can be satisfied only if the vortex has a positive charge $q = +1$.

Suppose a vortex q is inside the circle, at time-varying position $\mathbf{X}(t)$ measured from the center of the circle. For either type of boundary condition, there is an image vortex $q' = \nu_{bc}q$ outside the system at a radius $X' = R^2/X$. The vortex will move in a circle of radius X, under the force caused by its image. From the earlier result (9.133), the radial component of force scaled by σ is

$$f_r = -qq'\frac{2\pi JS^2/\sigma}{R^2/X - X} = \frac{-2CX}{R^2 - X^2}. \tag{9.198}$$

This is equivalent to using the force definition (9.147) with $\hat{\mathbf{n}} = \hat{\mathbf{r}}$, with the definition of C in (9.152). If the vortex is very close to the center of the circle, with $X \ll R$, the force will be linear in X. For free (fixed) boundary conditions the force points outward (inward), with $C < 0$ ($C > 0$). The direction of the force is *opposite* to that when we considered a pair of vortices rotating about each other, because the image charge is outside the system, on the same radius as the charge q itself. Either boundary condition will have a stationary solution that is an orbital motion around the center of the circle, although the outward force might be expected to lead to an unstable orbit.

Let the stationary solutions have a constant speed with velocity given by

$$\mathbf{V} = \omega\hat{\mathbf{z}} \times \mathbf{X} \tag{9.199}$$

similar to the pair of vortices with parallel gyrovectors orbiting about each other. The modified Thiele equation (9.46) requires $\mathbf{G} \times \mathbf{V} = -\omega G\mathbf{X}$. Then the modified Thiele equation without damping is

$$\frac{-2C}{R^2 - X^2}\mathbf{X} - \omega G\mathbf{X} = -\mathsf{M}\omega^2\mathbf{X}. \tag{9.200}$$

The sign on C is opposite to that in (9.183) for the rotating vortex pair, again because now q interacts with its image which is outside the system. For a chosen orbital radius X the frequency is determined, similar to the result (9.187) for a rotating vortex pair,

$$\omega = 2\omega_0\left(1 + \sqrt{1 - 4\mathsf{M}\omega_0/G}\right)^{-1} \tag{9.201a}$$

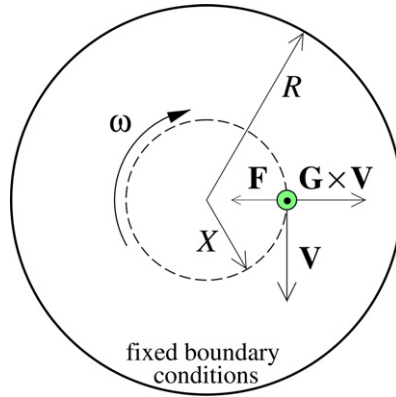$$\omega_0 = \frac{-2C/G}{R^2 - X^2}. \tag{9.201b}$$

Figure 9.10. Circular path of a vortex with $q = +1$, $G = +2\pi$ (indicated by $\odot$) moving in a circular orbit of radius X in a circular system of radius R. Assuming fixed boundary conditions ($\nu_{bc} = +1$), the image vortex produces a force towards the center. The sense of the velocity is in the direction of $\mathbf{G} \times \mathbf{F}$. The gyrotropic orbital frequency $\omega = V/X$ is given in (9.201), using a positive force constant C, leading to clockwise rotation ($\omega < 0$). The rotation would be reversed for free boundary conditions or by reversing the sign of G.

The frequency ω_0 is the result at zero mass. The root from the quadratic formula was chosen to give the correct result at zero mass. The force constant $C \propto qq' = \nu_{bc}q^2$ is negative for free boundary conditions ($\nu_{bc} = -1$). This then leads to a positive value of ω_0 when $G = +2\pi$, corresponding to a counterclockwise vortex motion. The outward force on the vortex is balanced by $\mathbf{G} \times \mathbf{V}$ and $-M\omega^2\hat{\mathbf{r}}$ both pointing inward. For the other case of fixed boundary conditions ($\nu_{bc} = +1$), the constant C is positive and $\omega_0 < 0$ for $G = +2\pi$, and the vortex rotates in the clockwise sense. This is sketched in figure 9.10. Now the force and $-M\omega^2\hat{\mathbf{r}}$ are both inward but $\mathbf{G} \times \mathbf{V}$ is outward. The velocity is in the same sense as the cross product $\mathbf{G} \times \mathbf{F}$, see figure 9.10.

If the mass is small relative to G/ω_0, an expansion then gives the approximate result,

$$\omega \approx \omega_0\left(1 + \frac{M\omega_0}{G}\right) = \omega_0\left[1 - \frac{q'}{q}\frac{JS^2M}{2\pi\sigma(R^2 - X^2)}\right], \qquad \frac{JS^2M}{2\pi\sigma(R^2 - X^2)} \ll 1. \quad (9.202)$$

The last form is written to compare with (9.188) obtained for a rotating pair of vortices. The main difference is the opposite sign on the mass term, due to the location of the image. The other important difference is the dependence on radial location of the vortex, which must subtract from the size of the circle. However, in the limit $X \to 0$, this gyrotropic frequency reaches a finite limit inversely proportional to the squared radius of the circle. Thus these results are important for the development of magnetic oscillators based on this gyrotropic mode of oscillation.

A real system will have some small damping. As seen earlier in the case of a vortex near a straight boundary, the damping will tend to cause the vortex to drift towards the boundary for free boundary conditions. In that case, the vortex is unstable in the system, and after some number of revolutions, it will leave the system, as it moves to lower energy (being attracted to its image). Therefore, the case of an outward force on the vortex is certainly unstable. On the other hand, for fixed

boundary conditions (strong demagnetization), damping will cause the vortex to move away from the boundary, towards the center of the system. The system will be stable. This is the situation needed for the design of a stable oscillator.

9.5 Vortex–spin wave interactions and normal modes

Up to this point a magnetic vortex has been treated almost as if it has a fixed structure, for a given magnetic anisotropy described by parameter λ. The only variations considered in the structure were those due to a change in velocity, which led to the idea of a vortex mass. In this section we consider more general natural oscillatory changes in vortex structure associated with the fact that it has a certain flexibility, just as a guitar string or the membrane of a drum. If the spin field of a vortex is slightly perturbed, say, by thermal fluctuations, it has natural modes of oscillation about the original structure. These oscillations make up what might be called the vortex *internal dynamics*. These normal modes of a vortex also characterize the interaction of the vortex with the spin waves of the system.

The mode spectrum was first calculated numerically for small ferromagnetic (FM) systems in [10] and extended to the case of antiferromagnetic systems in [11] and [12]. Some of the modes of oscillation appear as a result of imparting motion to the vortex; these are called *translational modes*. They tend to have a fairly low frequency, perhaps inversely proportional to the system size, basically because the energy associated with a shift of vortex position is close to zero. Then, other *instability modes* are possible that become strong when the anisotropy parameter λ is close to the critical value λ_c for crossover from stable in-plane vortices to stable out-of-plane vortices. This type of mode has a wave function concentrated near the vortex core region, where the out-of-plane fluctuations become strong. Finally there are many other modes that correspond in general to a continuum of spin waves *scattered* from the vortex. Far from the vortex, they may be nearly the same as found without a vortex; the core region of the vortex changes the spectrum. As in quantum scattering problems, one can analyze the modes in terms of radial and azimuthal dependencies and quantum numbers. The FM system has also been analyzed with the presence of an applied field perpendicular to the easy plane, in the so-called cone state [13].

Here the calculational procedure will be described for FM systems, and then some results described for the FM easy-plane model without applied fields. The easy-plane model is studied on a square lattice, for the discrete Hamiltonian,

$$H = -J \sum_{\mathbf{n}} \sum_{j=1}^{z} \left(S_{\mathbf{n}}^x S_{\mathbf{n}+\mathbf{a}_j}^x + S_{\mathbf{n}}^y S_{\mathbf{n}+\mathbf{a}_j}^y + \lambda S_{\mathbf{n}}^z S_{\mathbf{n}+\mathbf{a}_j}^z \right). \tag{9.203}$$

The spectrum of modes will be computed for small systems by numerical diagonalization of a linearized perturbation problem. Results will be analyzed for the system with and without a vortex, for a full range of the anisotropy parameter λ. The calculations are performed on a circular system of radius R, with the sites on a square lattice grid, for a static vortex. Fixed or vortex-Dirichlet boundary conditions (as in strong demagnetization) are assumed, which makes the vortex have its minimum energy when centered in the circular system.

9.5.1 The initial discrete lattice vortex solution

To initiate the perturbation calculations, first a static in-plane or out-of-plane vortex solution on the lattice is required. It may be close to the approximate analytic solutions already described, such as (8.7) for the in-plane angle, and (8.19) for the out-of-plane component if $\lambda > \lambda_c$. As mentioned earlier, these become modified slightly on a grid, and we need to use the grid solution, which will be a local minimum energy configuration. The discrete structure can be calculated by the spin alignment technique, see for examples the curves found in figure 8.1. Even for an in-plane vortex, the in-plane angles in the discrete vortex change in the core region, when compared to the continuum arctangent solution of (8.7). The discrete structure can be found just as well for triangular and hexagonal lattices just as for a square lattice, without extra complications.

The static state achieved is described by the set of planar spherical in-plane and out-of-plane angles $(\phi_{\mathbf{n}}^0, \theta_{\mathbf{n}}^0)$, or the corresponding spins $\mathbf{S}_{\mathbf{n}}^0 = (S_{\mathbf{n}}^{0\,x}, S_{\mathbf{n}}^{0\,y}, S_{\mathbf{n}}^{0\,z})$. To simplify some notation, it is helpful in the perturbation analysis to define some variables that appear repeatedly,

$$m_{\mathbf{n}}^0 = \sin\theta_{\mathbf{n}}^0, \qquad p_{\mathbf{n}}^0 = \cos\theta_{\mathbf{n}}^0. \tag{9.204}$$

Profiles of $m_{\mathbf{n}}^0$ as obtained by spin alignment relaxation were given in figure 8.1. The factors $p_{\mathbf{n}}^0$ represent the projection of the spins onto the xy-plane. In the core region where $m_{\mathbf{n}}^0$ is large, the deviation of $p_{\mathbf{n}}^0$ below unity becomes important.

9.5.2 Perturbations of a static vortex

The oscillations about the static vortex solution are found from perturbation analysis, just as spin waves were analyzed in chapter 6. There are two main differences here. First, the unperturbed state is not uniform, so we need to define different local axes at each site. Second, we consider a finite system, so that translational symmetry is not present. The modes will not be simply distinguished by wave vectors.

To deal with the non-uniform unperturbed state, we use the static directions $\mathbf{S}_{\mathbf{n}}^0$ as the local quantization axes $\tilde{\mathbf{z}}$ for each site. The spins make small fluctuations about those directions. Therefore only the spin components perpendicular to each $\mathbf{S}_{\mathbf{n}}^0$ will be involved in the oscillations. It is those spin components for which the equations of motion will be linearized. As in [10], one can make a transformation to new site-dependent coordinate axes $\tilde{\mathbf{x}}, \tilde{\mathbf{y}}, \tilde{\mathbf{z}}$, where $\tilde{\mathbf{z}}$ is along $\mathbf{S}_{\mathbf{n}}^0$, $\tilde{\mathbf{x}}$ is in the original xy-plane and perpendicular to $\tilde{\mathbf{z}}$, and then $\tilde{\mathbf{y}} = \tilde{\mathbf{z}} \times \tilde{\mathbf{x}}$ is the third member of the mutually orthogonal triplet. These local axes are given in terms of the global $\hat{\mathbf{x}}, \hat{\mathbf{y}}, \hat{\mathbf{z}}$ basis as (see figure 9.11)

$$\begin{pmatrix} \tilde{\mathbf{x}} \\ \tilde{\mathbf{y}} \\ \tilde{\mathbf{z}} \end{pmatrix} = \begin{pmatrix} -\sin\phi_{\mathbf{n}}^0 & \cos\phi_{\mathbf{n}}^0 & 0 \\ -m_{\mathbf{n}}^0\cos\phi_{\mathbf{n}}^0 & -m_{\mathbf{n}}^0\sin\phi_{\mathbf{n}}^0 & p_{\mathbf{n}}^0 \\ p_{\mathbf{n}}^0\cos\phi_{\mathbf{n}}^0 & p_{\mathbf{n}}^0\sin\phi_{\mathbf{n}}^0 & m_{\mathbf{n}}^0 \end{pmatrix} \begin{pmatrix} \hat{\mathbf{x}} \\ \hat{\mathbf{y}} \\ \hat{\mathbf{z}} \end{pmatrix}. \tag{9.205}$$
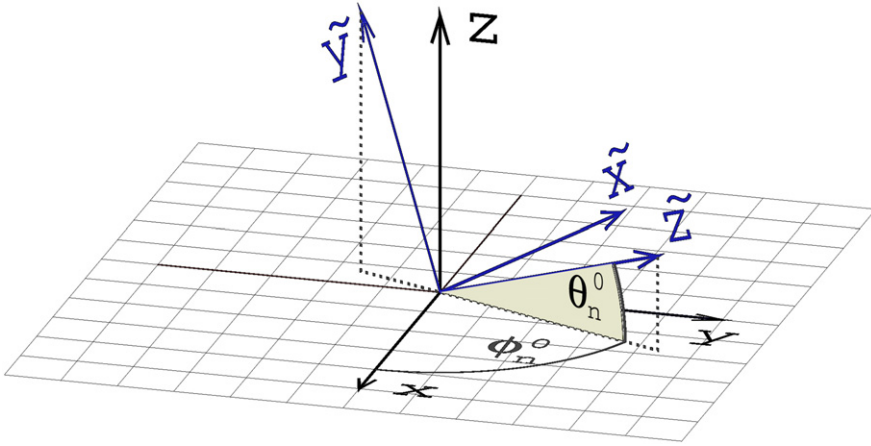
Figure 9.11. Sketch of the relation between the original global xyz-coordinate axes and the local $\tilde{x}\tilde{y}\tilde{z}$-coordinate axes for a particular spin site, as defined in (9.205). The $\tilde{z}$-axis is taken along the direction (ϕ_n^0, θ_n^0) of the unperturbed spin at the site. Then $\tilde{x}$ is perpendicular to $\tilde{z}$ and in the xy-plane, while $\tilde{y} = \tilde{z} \times \tilde{x}$ to make the third member of the right-handed triplet.

With $(p_n^0)^2 + (m_n^0)^2 = 1$, the matrix here is of orthogonal form and the transpose is its inverse. The local spin components are obtained by $S_n^{\tilde{x}} = \mathbf{S_n} \cdot \tilde{x}$, and so on, which shows that the spins are transformed the same way,

$$\begin{pmatrix} S_n^{\tilde{x}} \\ S_n^{\tilde{y}} \\ S_n^{\tilde{z}} \end{pmatrix} = \begin{pmatrix} -\sin\phi_n^0 & \cos\phi_n^0 & 0 \\ -m_n^0\cos\phi_n^0 & -m_n^0\sin\phi_n^0 & p_n^0 \\ p_n^0\cos\phi_n^0 & p_n^0\sin\phi_n^0 & m_n^0 \end{pmatrix} \begin{pmatrix} S_n^x \\ S_n^y \\ S_n^z \end{pmatrix}. \tag{9.206}$$

The dynamic equations of motion without damping are $\dot{\mathbf{S}}_n = \mathbf{S}_n \times \mathcal{F}_n$. These can be written out in the local coordinates, which are transformed into the global coordinates as needed, by the previous equation. The time derivatives should be linearized in $S_n^{\tilde{x}}, S_n^{\tilde{y}}, S_n^{\tilde{z}}$. The derivation of the equations of motion is a simple but tedious exercise.

Exercise 9.9. Starting from the equations of motion from Hamiltonian (9.203), transform them to the local rotated coordinates (9.206). Show that after linearization in all spin components, the components along the quantization axes are nearly conserved quantities, $S_n^{\tilde{z}}$, while the transverse components form a set of linear differential equations,

$$\dot{S}_n^{\tilde{x}} = JS \sum_{\mathbf{m=n+a}} \left\{ m_n^0 \sin(\phi_n^0 - \phi_m^0)S_m^{\tilde{x}} + \left[p_n^0 p_m^0 \cos(\phi_n^0 - \phi_m^0) + \lambda m_n^0 m_m^0 \right]S_n^{\tilde{y}} \right.$$
$$\left. - \left[m_n^0 m_m^0 \cos(\phi_n^0 - \phi_m^0) + \lambda p_n^0 p_m^0 \right]S_m^{\tilde{y}} \right\} \tag{9.207a}$$

$$\dot{S}_{\mathbf{n}}^{\tilde{y}} = JS \sum_{\mathbf{m}=\mathbf{n}+\mathbf{a}} \left\{ m_{\mathbf{m}}^{0} \sin\!\left(\phi_{\mathbf{n}}^{0} - \phi_{\mathbf{m}}^{0}\right) S_{\mathbf{m}}^{\tilde{y}} - \left[p_{\mathbf{n}}^{0} p_{\mathbf{m}}^{0} \cos\!\left(\phi_{\mathbf{n}}^{0} - \phi_{\mathbf{m}}^{0}\right) + \lambda m_{\mathbf{n}}^{0} m_{\mathbf{m}}^{0} \right] S_{\mathbf{n}}^{\tilde{x}} \right.$$
$$\left. + \cos\!\left(\phi_{\mathbf{n}}^{0} - \phi_{\mathbf{m}}^{0}\right) S_{\mathbf{m}}^{\tilde{x}} \right\}. \qquad (9.207b)$$

These equations (9.207) can be solved by assuming oscillatory time-dependence, after which they become an eigenvalue problem. Wysin and Völkel [10] analyzed and solved the problem in the language of quantum eigenmodes, by supposing there are linear combinations of the local spin coordinates that form creation and annihilation operators. While that is not essential it makes a closer connection to the problem as studied in quantum terminology. The creation operator for a mode labeled by some index k is

$$B_{k}^{\dagger} = \sum_{\mathbf{n}} \left(w_{k,\mathbf{n}}^{(1)} S_{\mathbf{n}}^{\tilde{x}} + w_{k,\mathbf{n}}^{(2)} S_{\mathbf{n}}^{\tilde{y}} \right), \qquad (9.208)$$

where pairs $w_{k,\mathbf{n}}^{(1)}$, $w_{k,\mathbf{n}}^{(2)}$ are complex numbers that give amplitudes of the oscillations at each site, and now $S_{\mathbf{n}}^{\tilde{x}}$ and $S_{\mathbf{n}}^{\tilde{y}}$ are treated as operators. There is a corresponding annihilation operator, which is just the conjugate,

$$B_{k} = \sum_{\mathbf{n}} \left(w_{k,\mathbf{n}}^{(1)*} S_{\mathbf{n}}^{\tilde{x}} + w_{k,\mathbf{n}}^{(2)*} S_{\mathbf{n}}^{\tilde{y}} \right). \qquad (9.209)$$

For the creation operator, a time-dependence of the form $\exp(i\omega_k t)$ is assumed, so that its time derivative is

$$\dot{B}_{k}^{\dagger} = i\omega_k B_{k}^{\dagger}. \qquad (9.210)$$

The annihilation operator has the negative of this frequency, $-\omega_k$. With this time-dependence, the linearized equations (9.207) become an eigenvalue problem of similar structure involving the amplitudes,

$$i\omega_k w_{k,\mathbf{n}}^{(1)} = JS \sum_{\mathbf{m}=\mathbf{n}+\mathbf{a}} \left\{ -m_{\mathbf{m}}^{0} \sin\!\left(\phi_{\mathbf{n}}^{0} - \phi_{\mathbf{m}}^{0}\right) w_{k,\mathbf{m}}^{(1)} + \cos\!\left(\phi_{\mathbf{n}}^{0} - \phi_{\mathbf{m}}^{0}\right) w_{k,\mathbf{m}}^{(2)} \right.$$
$$\left. - \left[p_{\mathbf{n}}^{0} p_{\mathbf{m}}^{0} \cos\!\left(\phi_{\mathbf{n}}^{0} - \phi_{\mathbf{m}}^{0}\right) + \lambda m_{\mathbf{n}}^{0} m_{\mathbf{m}}^{0} \right] w_{k,\mathbf{n}}^{(2)} \right\} \qquad (9.211a)$$

$$i\omega_k w_{k,\mathbf{n}}^{(2)} = JS \sum_{\mathbf{m}=\mathbf{n}+\mathbf{a}} \left\{ -m_{\mathbf{n}}^{0} \sin\!\left(\phi_{\mathbf{n}}^{0} - \phi_{\mathbf{m}}^{0}\right) w_{k,\mathbf{m}}^{(2)} - \left[m_{\mathbf{n}}^{0} m_{\mathbf{m}}^{0} \cos\!\left(\phi_{\mathbf{n}}^{0} - \phi_{\mathbf{m}}^{0}\right) + \lambda p_{\mathbf{n}}^{0} p_{\mathbf{m}}^{0} \right] w_{k,\mathbf{m}}^{(1)} \right.$$
$$\left. + \left[p_{\mathbf{n}}^{0} p_{\mathbf{m}}^{0} \cos\!\left(\phi_{\mathbf{n}}^{0} - \phi_{\mathbf{m}}^{0}\right) + \lambda m_{\mathbf{n}}^{0} m_{\mathbf{m}}^{0} \right] w_{k,\mathbf{n}}^{(1)} \right\}. \qquad (9.211b)$$

This sets up the eigenvalue problem. The matrix on the RHS has all real elements, but it is not Hermitian. The problem, however, has real eigenfrequencies ω_k, hence the matrix on the RHS is expected to have pure imaginary eigenvalues. The system can be solved by a routine such as RG (real general matrix) from the EISPACK eigensystem subroutine package, although the system size that can be solved will be rather limited (say, a maximum $R \sim 20a$ on a laptop, due to memory restrictions). In

other work by Ivanov *et al* [14] one can find a better way to describe the matrix and use its symmetries to solve it on larger systems up to $R \sim 100a$. Also, that work showed that the eigenvalues are indeed pure imaginary and hence give real eigenfrequencies. However, such large systems may lead to numerical instabilities and even if the memory issue is resolved the required CPU time may be prohibitive. Whatever numerical diagonalization is used, double precision is necessary for stability. The full set of $w_{k,\mathbf{n}}^{(1)}$, $w_{k,\mathbf{n}}^{(2)}$ over the lattice then is the eigenvector associated with a mode of frequency ω_k. While diagonalization could give a large number of modes, in usual practice we are interested more so in those of the lowest frequencies.

Once a mode has been determined, normalization for quantum creation/annihilation operators requires a unit commutator, $[B_k, B_{k'}^{\dagger}] = \delta_{k,k'}$. Based on a canonical commutator,

$$\left[S_{\mathbf{n}}^{\tilde{x}}, S_{\mathbf{m}}^{\tilde{y}} \right] = i\hbar S_{\mathbf{n}}^{z} \delta_{\mathbf{n,m}} \to i\hbar S \delta_{\mathbf{n,m}}, \qquad (9.212)$$

this results in the normalization condition,

$$\left[B_k, B_{k'}^{\dagger} \right] = \hbar S \sum_{\mathbf{n}} \left[\left(iw_{k,\mathbf{n}}^{(1)*} w_{k',\mathbf{n}}^{(2)} \right) + \left(iw_{k',\mathbf{n}}^{(1)*} w_{k,\mathbf{n}}^{(2)} \right)^{*} \right] = \delta_{k,k'}. \qquad (9.213)$$

Although for classical modes the normalization is somewhat arbitrary, for the quantum system a correct normalization is needed if one wants to use these results to give the spin fluctuations in thermal equilibrium. Once the modes are known and correctly normalized, the original spin operators in the local coordinates can be recovered. Inverting (9.208) and (9.209), they are

$$S_{\mathbf{n}}^{\tilde{x}} = iS \sum_{k} \left(w_{k,\mathbf{n}}^{(2)} B_k - w_{k,\mathbf{n}}^{(2)*} B_k^{\dagger} \right) \qquad (9.214a)$$

$$S_{\mathbf{n}}^{\tilde{y}} = -iS \sum_{k} \left(w_{k,\mathbf{n}}^{(1)} B_k - w_{k,\mathbf{n}}^{(1)*} B_k^{\dagger} \right). \qquad (9.214b)$$

These can be used to analyze the spin fluctuations caused by a given pure mode or in a combination of the modes.

The original unperturbed vortex state can be denoted $|0\rangle$, being like the ground state of the spin wave modes being found here. A state with a single mode excited is created by its creation operator, acting on the ground state,

$$|k\rangle = B_k^{\dagger}|0\rangle. \qquad (9.215)$$

With these being normalized operators with unit commutator (9.212), the excited states are also unit normalized:

$$\langle k|k \rangle = \langle 0|B_k B_k^{\dagger}|0\rangle = 1. \qquad (9.216)$$

Using as reference the vortex ground state, there is also the relation for the expectation value of the number operator, $N_k \equiv B_k^{\dagger} B_k$, $\langle 0|B_k^{\dagger} B_k|0\rangle = 0$, because $|0\rangle$ has no excitations present. However, if the state of the system is a *mixed state*, corresponding

to thermal equilibrium, then it is important to realize that some population of the modes will be present. In thermal equilibrium, the expectation value of the number operator leads to the well-known Bose–Einstein occupation number, and we write

$$\langle N_k \rangle = \langle B_k^\dagger B_k \rangle = \frac{1}{\exp(\beta\hbar\omega_k) - 1}. \tag{9.217}$$

Generally, we can discuss the spin fluctuations in a state of thermal equilibrium, but then isolate each contribution of each particular mode k.

The spin fluctuations take place transverse to the $\tilde{z}$-directions at each site, but average out to zero so that $\langle S_\mathbf{n}^{\tilde{x}} \rangle = \langle S_\mathbf{n}^{\tilde{y}} \rangle = 0$ in any state. The expectation value of the longitudinal component, however, can be estimated using the Holstein–Primakoff transformation [15], which is used to ensure a conserved total spin length when fluctuations are present,

$$S_\mathbf{n}^{\tilde{z}} = S - \frac{1}{2S}\left(S_\mathbf{n}^{\tilde{x}} - iS_\mathbf{n}^{\tilde{y}}\right)\left(S_\mathbf{n}^{\tilde{x}} + iS_\mathbf{n}^{\tilde{y}}\right). \tag{9.218}$$

The last term involves the product of the spin lowering and raising operators, $S_\mathbf{n}^-$ and $S_\mathbf{n}^+$. After expressing this in terms of B_k and $B_k^\dagger$ by (9.209) and (9.208), a short exercise leads to the result

$$\langle S_\mathbf{n}^{\tilde{z}} \rangle = S - \frac{1}{2}S\sum_k\left[\left|w_{k,\mathbf{n}}^{(1)} + iw_{k,\mathbf{n}}^{(2)}\right|^2\langle B_k^\dagger B_k \rangle + \left|w_{k,\mathbf{n}}^{(1)} - iw_{k,\mathbf{n}}^{(2)}\right|^2\langle B_k B_k^\dagger \rangle\right]. \tag{9.219}$$

To arrive at this result, one uses the fact that $\langle B_k \rangle = \langle B_k^\dagger \rangle = 0$ as well as $\langle B_k B_{k'} \rangle = \langle B_k^\dagger B_{k'}^\dagger \rangle = 0$. This shows that the spin length along $\tilde{z}$ is slightly reduced by the fluctuations.

Eventually the squared fluctuations away from the mean, in the original global coordinates xyz, are desired. They can be partitioned into in-plane and out-of-plane types, from the definitions,

$$\left\langle \left(\delta S_\mathbf{n}^{\text{in}}\right)^2 \right\rangle = \left\langle \left(S_\mathbf{n}^x - \langle S_\mathbf{n}^x \rangle\right)^2 + \left(S_\mathbf{n}^y - \langle S_\mathbf{n}^y \rangle\right)^2 \right\rangle \tag{9.220a}$$

$$\left\langle \left(\delta S_\mathbf{n}^{\text{out}}\right)^2 \right\rangle = \left\langle \left(S_\mathbf{n}^z - \langle S_\mathbf{n}^z \rangle\right)^2 \right\rangle. \tag{9.220b}$$

By using the inverse of the coordinate transformation in (9.206), these can be expressed using the local coordinates,

$$\left\langle \left(\delta S_\mathbf{n}^{\text{in}}\right)^2 \right\rangle = \left\langle S_\mathbf{n}^{\tilde{x}2} \right\rangle + \left\langle S_\mathbf{n}^{\tilde{y}2} \right\rangle \sin^2\theta_\mathbf{n}^0 \tag{9.221a}$$

$$\left\langle \left(\delta S_\mathbf{n}^{\text{out}}\right)^2 \right\rangle = \left\langle S_\mathbf{n}^{\tilde{y}2} \right\rangle \cos^2\theta_\mathbf{n}^0. \tag{9.221b}$$

This is reasonable; the $\tilde{\mathbf{y}}$-axis makes an angle $\theta_\mathbf{n}^0$ to the $\hat{\mathbf{z}}$-axis, and all the out-of-plane motions take place in $S_\mathbf{n}^{\tilde{y}}$. The $\tilde{\mathbf{x}}$-axis lies in the original xy-plane, and so $S_\mathbf{n}^{\tilde{x}}$ contributes only to in-plane fluctuations. There is also a contribution to in-plane

fluctuations from the component of $S_{\mathbf{n}}^{\widetilde{y}}$ projected onto the xy-plane. Now, the expectations contained here can be found from using (9.214) to express all parts in terms of the creation/annihilation operators,

$$\left\langle S_{\mathbf{n}}^{\widetilde{x}2} \right\rangle = (\hbar S)^2 \sum_k \left| w_{k,\mathbf{n}}^{(2)} \right|^2 \left\langle 2B_k^\dagger B_k + 1 \right\rangle \qquad (9.222a)$$

$$\left\langle S_{\mathbf{n}}^{\widetilde{y}2} \right\rangle = (\hbar S)^2 \sum_k \left| w_{k,\mathbf{n}}^{(1)} \right|^2 \left\langle 2B_k^\dagger B_k + 1 \right\rangle. \qquad (9.222b)$$

Consistent with (9.214), these show how the $w^{(1)}$ amplitudes give a sense of the $S_{\mathbf{n}}^{\widetilde{y}}$ variations and the $w^{(2)}$ amplitudes relate to the $S_{\mathbf{n}}^{\widetilde{x}}$ variations. Then, the expressions of (9.221) become

$$\left\langle \left(\delta S_{\mathbf{n}}^{\text{in}} \right)^2 \right\rangle = (\hbar S)^2 \sum_k \left(\left| w_{k,\mathbf{n}}^{(2)} \right|^2 + \left| w_{k,\mathbf{n}}^{(1)} \right|^2 \sin^2 \theta_{\mathbf{n}}^0 \right) \left\langle 2B_k^\dagger B_k + 1 \right\rangle \qquad (9.223a)$$

$$\left\langle \left(\delta S_{\mathbf{n}}^{\text{out}} \right)^2 \right\rangle = (\hbar S)^2 \sum_k \left| w_{k,\mathbf{n}}^{(1)} \right|^2 \cos^2 \theta_{\mathbf{n}}^0 \left\langle 2B_k^\dagger B_k + 1 \right\rangle. \qquad (9.223b)$$

Each mode contributes a separate term on a chosen spin site. Because this has been obtained through a semiclassical approach, the last '1' after the number operator $B_k^\dagger B_k$ actually is the zero-point term, present even when the mode is not excited. It might be ignored for the analysis of the classical system.

9.5.3 Examples of the spin wave mode spectrum on a vortex

An example of these exact diagonalization calculations is to use a circular system of radius $R = 15a$, discretized on a square lattice, see figure 9.12 for the frequency spectrum. This results in a system with $N = 716$ sites, which means that with two variables at each site, the exact diagonalization involves a real matrix of size 1432×1432, with 1432 eigenstates. One must also save the 1432 complex eigenvectors, all with 1432 elements. This size is easily solved for a selected value of λ on a laptop computer, and it is not too difficult to go to larger sizes. Of course, we are mostly interested in some subset, usually only the lowest few dozen modes. To obtain a complete understanding of the properties or symmetries of the modes, one should calculate the spectrum at a sequence of anisotropies λ. Then with the repetition of the calculations over a range of λ the total CPU time can grow to become less convenient.

When the calculations are performed for two closely spaced values of λ, it is important to be able to identify the eigenmodes at the first value of λ with the same modes (of the same symmetry) at the next value of λ. This process can be achieved by calculating the overlaps of the two sets of eigenvectors with each other, and looking for the values closest to unity. For fixed λ, modes at distinct eigenfrequencies are orthogonal. The normalization integral or overlap is the sum that one finds in (9.213) for the expression of the commutator, $[B_k, B_{k'}^\dagger]$. When modes at two different
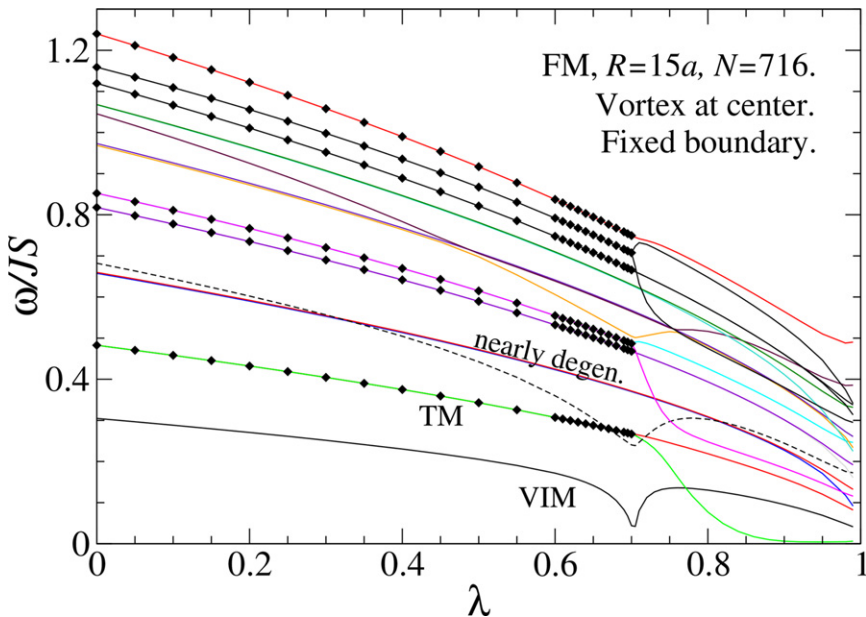
Figure 9.12. Spectrum of normal modes on a static vortex at the center of a circular square lattice system of radius $R = 15a$ (with 716 sites, fixed boundary conditions), obtained by exact diagonalization of the equations (9.211a). Modes marked with diamonds are doubly degenerate. All of those appear for $\lambda < \lambda_c$. A near degeneracy (split slightly by the lattice) is also marked. The lowest mode for $\lambda < \lambda_c$ is associated with the instability of in-plane vortices (VIM), seen by the downward cusp at $\lambda = \lambda_c \approx 0.7$. The lowest doubly degenerate mode contains the translational modes (TM), which split for $\lambda > \lambda_c$.

λ are compared, their overlaps do not need to be very close to unity, so it is important to avoid changing λ by a step that is too large. This technical detail can be difficult to apply because some modes are degenerate and become split in frequency and, as well, some modes cross over other modes.

The changing spectrum of frequencies with λ for the $R = 15a$ system with a vortex is shown in figure 9.12. Mostly the anisotropy constant was incremented by $\Delta\lambda = 0.05$, except for values near the critical value around $\lambda_c \approx 0.7$, where smaller increments were used. Only the lowest 20 modes have been kept here. When more modes are tracked with changing λ, it becomes more difficult to unambiguously identify them as λ changes. There are doubly degenerate modes that have been marked with diamond symbols in figure 9.12; solid curves without symbols are non-degenerate modes.

The eigenvectors or wave functions of some of the modes are presented in figures 9.13 through 9.24, using red line arrows (such as $\rightarrow$) to represent the complex amplitudes $w_{k,\mathbf{n}}^{(1)}$ and blue hollow head arrows (such as $\longrightarrow\!\!\triangleright$) to represent the complex amplitudes $w_{k,\mathbf{n}}^{(2)}$. The horizontal (vertical) components of the arrows are the real (imaginary) parts. For the simplest case of an in-plane unperturbed vortex, recall that $w_{k,\mathbf{n}}^{(1)}$ gives out-of-plane oscillations and $w_{k,\mathbf{n}}^{(2)}$ gives in-plane oscillations. If the unperturbed vortex is of out-of-plane type, however, then out-of-plane oscillations are

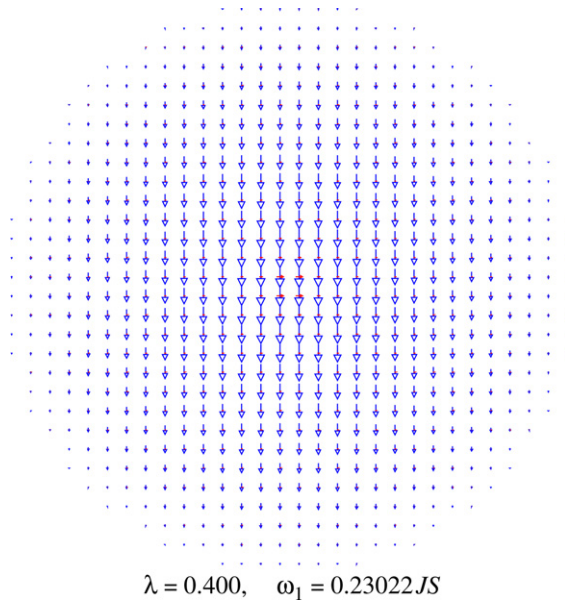$$\lambda = 0.400, \quad \omega_1 = 0.23022\,JS$$

Figure 9.13. Eigenvector of the lowest mode for a vortex in the $R = 15a$ system, at $\lambda = 0.40$. The red line arrows ($\rightarrow$) represent the amplitude and phase of the complex values $w_{k,\mathbf{n}}^{(1)}$ (mostly out-of-plane oscillations). Blue hollow arrows ($\longrightarrow$) represent $w_{k,\mathbf{n}}^{(2)}$ in the same scale (in-plane oscillations). This is the mode labeled as VIM in figure 9.12. It has rotational symmetry and is predominantly of in-plane fluctuations at this value of λ.

determined only by $w_{k,\mathbf{n}}^{(1)}$, but in-plane oscillations are determined by both $w_{k,\mathbf{n}}^{(1)}$ and $w_{k,\mathbf{n}}^{(2)}$, depending on $\theta_{\mathbf{n}}^0$ at the site, see (9.223).

The lowest mode frequency for $\lambda < \lambda_c$ has a strong downward cusp at $\lambda = \lambda_c$, which is associated with the instability of in-plane vortices found earlier. It is marked as VIM for *vortex instability mode*. The cusp does not go exactly to zero frequency here only because the calculations were not performed at the exact λ_c for the given system size. The presence of this soft mode in the spectrum is a significant confirmation of the vortex instability calculations. Its eigenfunction is shown for $\lambda = 0.40, 0.705, 0.90$ in figures 9.13, 9.17 and 9.21, respectively. Note that the mode is circularly symmetric and very strongly dominated by out-of-plane fluctuations, especially at $\lambda = 0.705 \approx \lambda_c$, as expected from vortex stability analysis. Interestingly, there are a number of higher modes that also have downward cusps at the same λ, but it is not likely that these would go to zero frequency at the exact value of λ_c. An example is 'mode 6' (the sixth lowest mode at $\lambda = 0$), whose eigenvectors are shown at the same values of λ in figures 9.16, 9.20 and 9.24. Mode 6 is also circularly symmetric, but reverses sign at a particular radius: it has a circular nodal line. This is very similar to higher states in any quantum system, such as hydrogen atom wave functions. At $\lambda = 0.705 \approx \lambda_c$, mode 6 reaches its minimum frequency and has a strong central amplitude in $w_{k,\mathbf{n}}^{(1)}$, see figure 9.20.

The lowest of the doubly degenerate modes contains the pair of *translational modes*, marked as TM in the spectrum, figure 9.12. For $\lambda < \lambda_c$, the wave functions of these

translational modes have structures comparable to the moving vortex solution (8.40) found earlier, see figures 9.14 and 9.15. Double degeneracy of the TM modes makes sense as there are two independent directions of motion possible. The degeneracy is split once $\lambda > \lambda_c$, with one mode of the doublet moving to very low frequency as $\lambda \to 1$. The eigenfunctions are shown just above the critical anisotropy in figures 9.18 and 9.19. Now they have a dependence on the azimuthal angle φ of the forms $\exp(+i\varphi)$ for the TM mode with higher frequency, and $\exp(-i\varphi)$ for the TM mode of lower frequency. These two functions were mixed in the eigenvectors for $\lambda < \lambda_c$. The splitting becomes much stronger at $\lambda = 0.90$, see the eigenvectors in figures 9.22 and 9.23. The lower of the two modes moves to a very low frequency, and its eigenvector is strongly concentrated in the vortex core.

The other doubly degenerate modes for $\lambda < \lambda_c$ also split once the anisotropy constant surpasses λ_c. This effect is reasonable, because the combination of a vorticity $q = +1$ and a polarization $p = +1$, giving non-zero G, breaks the *rotational symmetry* of the spin structure. To state this in other words, translational modes could also be combined into circular motions of two opposite senses. Once there is a non-zero gyrovector present, the two rotational senses of motions have different energies or frequencies. The Thiele equation shows that non-zero G gives motion in a well-defined direction in response to a force. If $G \neq 0$, functions of the form $\exp(im\varphi)$ with integer quantum numbers $m = 0, \pm1, \pm2, \ldots$ become the good eigenstates. They were degenerate and therefore mixed when $G = 0$ for in-plane vortices.

The presence of these features such as the vortex instability mode and mode 6, together with the translational modes, can be considered the internal dynamics of

$$\lambda = 0.400, \quad \omega_2 = 0.37496\,JS$$
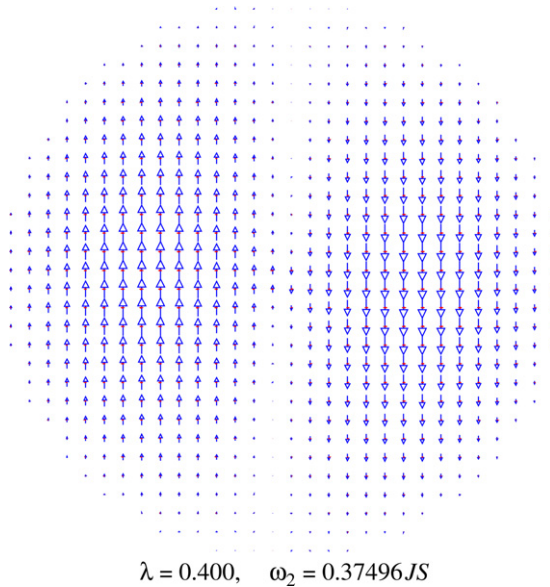
Figure 9.14. Eigenvector of one of the translational modes (TM in figure 9.12) for a vortex in the $R = 15a$ system, at $\lambda = 0.40$, with notation as in figure 9.13. It would be a linear combination of functions $\exp(i\varphi)$ and $\exp(-i\varphi)$.
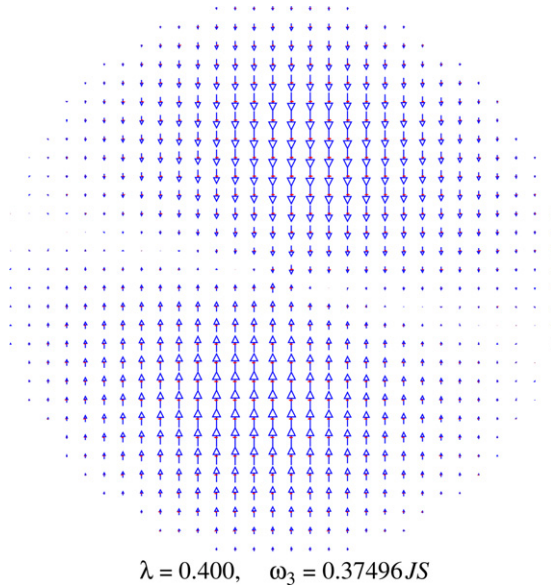
$$\lambda = 0.400, \quad \omega_3 = 0.37496\,JS$$

Figure 9.15. Eigenvector of the second of the translational modes (TM) for a vortex in the $R = 15a$ system, at $\lambda = 0.40$, with notation as in figure 9.13. It is degenerate with mode 2 shown in figure 9.14, but as a different linear combination of functions $\exp(i\varphi)$ and $\exp(-i\varphi)$.
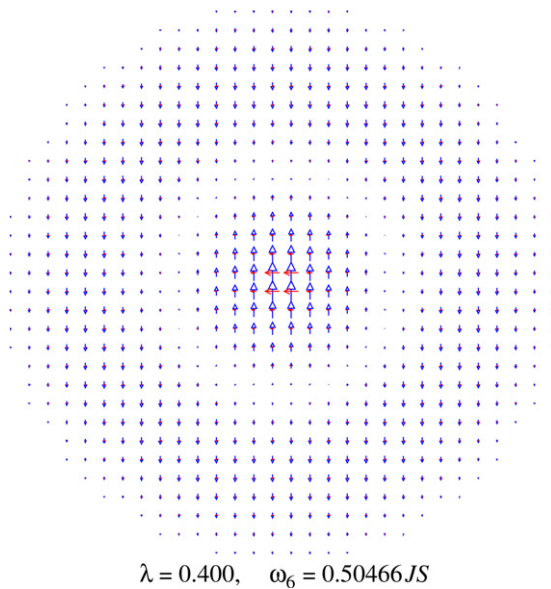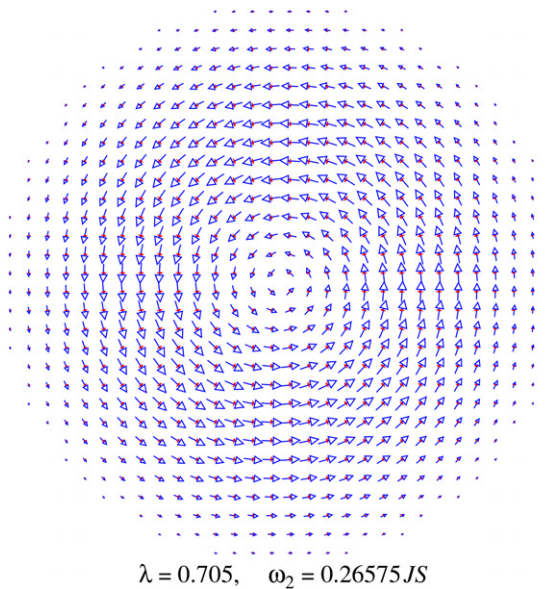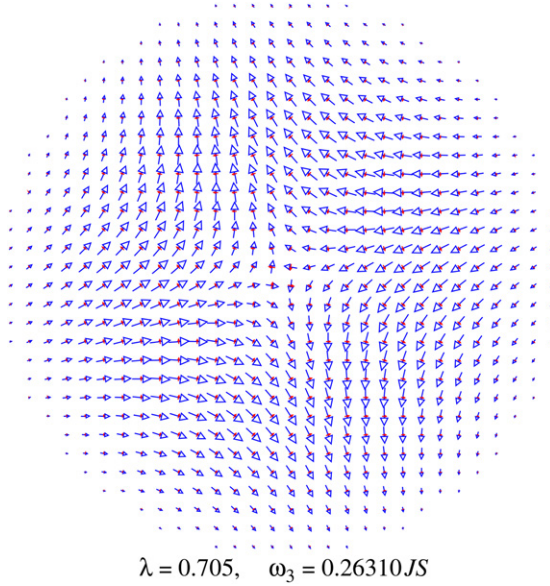

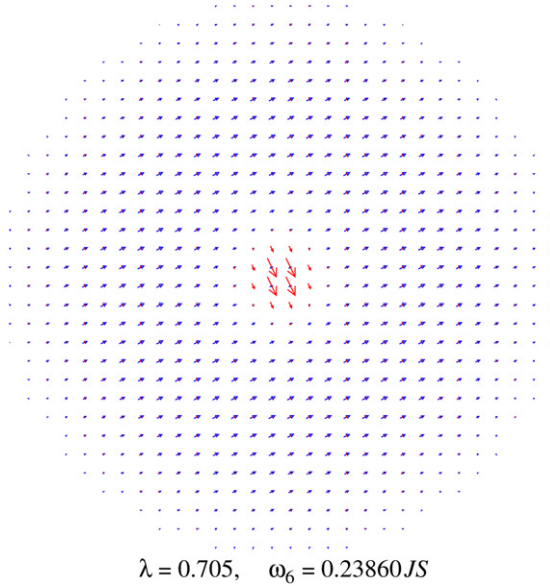$$\lambda = 0.400, \quad \omega_6 = 0.50466\,JS$$

Figure 9.16. Eigenvector of mode 6 for a vortex in the $R = 15a$ system, at $\lambda = 0.40$, with notation as in figure 9.13. It is the second of the modes in the spectrum of figure 9.12 that exhibits a downward cusp at λ_c. It has rotational symmetry but a circular node where the sign reverses.

$$\lambda = 0.705, \quad \omega_1 = 0.04207\,JS$$
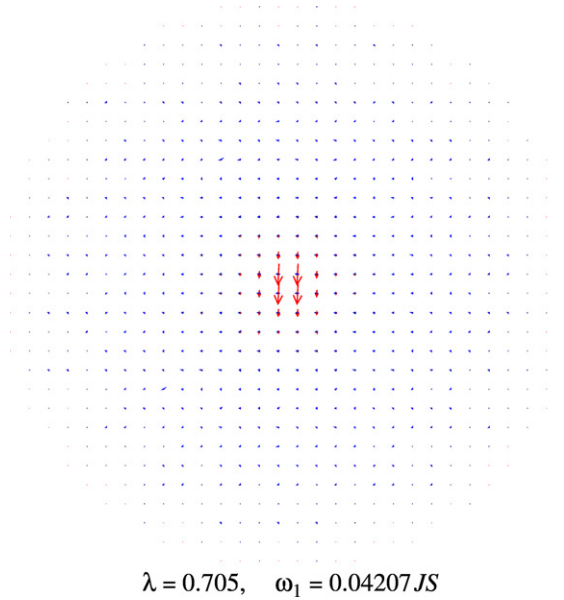
Figure 9.17. Eigenvector of the lowest mode for a vortex in the $R = 15a$ system, at $\lambda = 0.705 \approx \lambda_c$ with notation as in figure 9.13. This is the VIM in figure 9.12. Here it is predominantly of out-of-plane fluctuations concentrated in the vortex core.

$$\lambda = 0.705, \quad \omega_2 = 0.26575\,JS$$

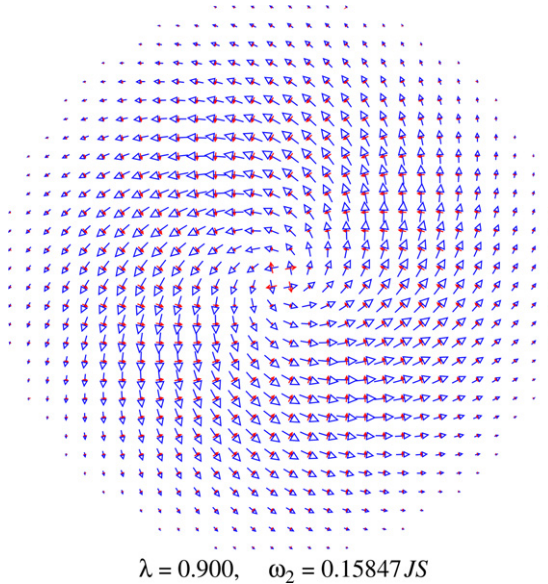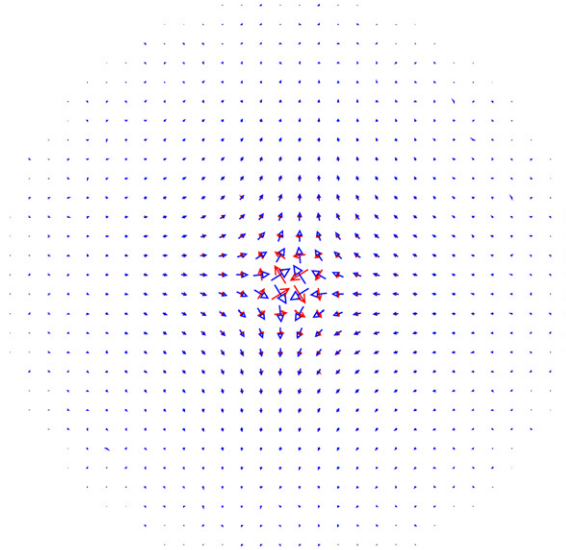**Figure 9.18.** Eigenvector of one of the translational modes (TM in figure 9.12) for a vortex in the $R = 15a$ system, at $\lambda = 0.705$, with notation as in figure 9.13. The mode's amplitude varies as $\exp(i\varphi)$. It is named mode T_+ later in figure 9.28.

$$\lambda = 0.705, \quad \omega_3 = 0.26310\,JS$$

Figure 9.19. Eigenvector of the second translational mode (TM) for a vortex in the $R = 15a$ system, at $\lambda = 0.705$, with notation as in figure 9.13. The degeneracy with mode 2 has been split, see figure 9.18. The mode's amplitude varies as $\exp(-i\varphi)$. It is named mode T_ later in figure 9.28.

$$\lambda = 0.705, \quad \omega_6 = 0.23860\,JS$$

Figure 9.20. Eigenvector of mode 6 for a vortex in the $R = 15a$ system, at $\lambda = 0.705$, with notation as in figure 9.13. In the spectrum of figure 9.12, it is the second downward cusp at λ_c.

$$\lambda = 0.900, \quad \omega_1 = 0.09535\,JS$$
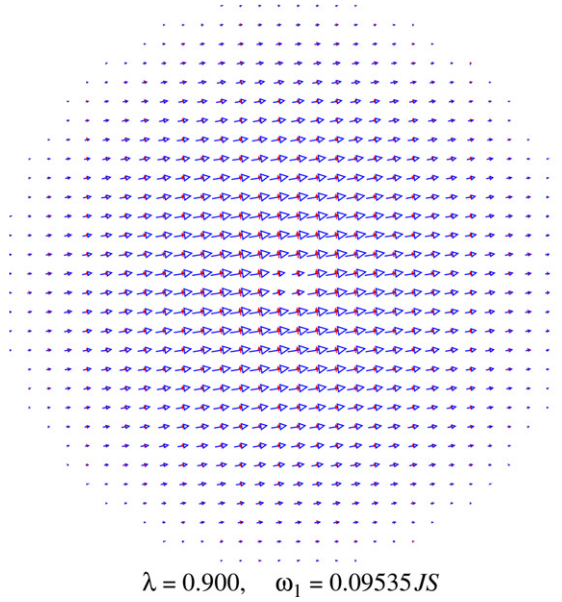
Figure 9.21. The VIM eigenvector for a vortex in the $R = 15a$ system, at $\lambda = 0.90$, with notation as in figure 9.13.

$$\lambda = 0.900, \quad \omega_2 = 0.15847\,JS$$

Figure 9.22. Eigenvector of the higher translational mode (TM in figure 9.12 or T_+ in figure 9.28) for a vortex in the $R = 15a$ system, at $\lambda = 0.90$, with notation as in figure 9.13. The mode's amplitude varies as $\exp(i\varphi)$.

the vortex. These features show how a vortex should not be considered an object with a fixed structure as it is moving.

For comparison, the spectrum for the same system but without a vortex present is shown in figure 9.25. In this case, the unperturbed state is the state of ferromagnetically

$$\lambda = 0.900, \quad \omega_3 = 0.00614\,JS$$

Figure 9.23. Eigenvector of the lower translational mode (TM if figure 9.12 or T₋ in figure 9.28) for a vortex in the $R = 15a$ system, at $\lambda = 0.90$, with notation as in figure 9.13. The mode's amplitude varies as $\exp(-i\varphi)$. Compare to figure 9.22, which has the opposite azimuthal symmetry and is more spread out.
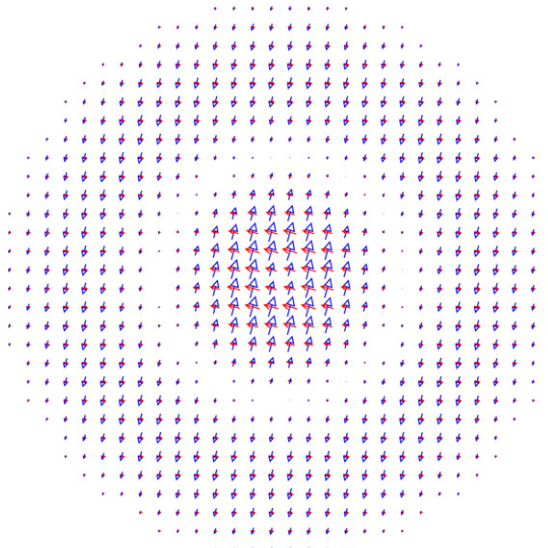
$$\lambda = 0.900, \quad \omega_6 = 0.24446\,JS$$

Figure 9.24. Eigenvector of mode 6 for a vortex in the $R = 15a$ system, at $\lambda = 0.90$, with notation as in figure 9.13. The sign reversal through the circular node is more obvious.
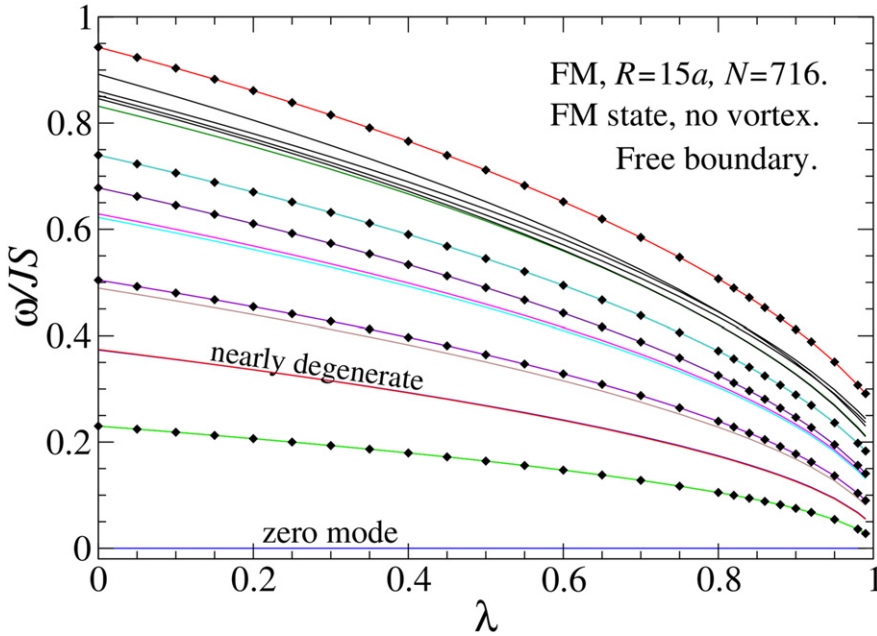
Figure 9.25. Spectrum of normal modes in a square lattice system of radius $R = 15a$ (716 sites) without a vortex, obtained by exact diagonalization of the equations (9.211a). The unperturbed state is that of aligned spins in the xy-plane, free boundary conditions must be used here. Modes marked with diamonds are doubly degenerate. The *zero mode* with $\omega = 0$ appears due to the freedom to rotate all spins together at no energy cost.

aligned spins, with free boundary conditions then being necessary. While there are still certain doubly degenerate modes among the predominantly non-degenerate ones, the spectrum is rather uniform and featureless. Nothing in particular happens around λ_c, because there is no vortex present. There is, however, an extra mode at zero frequency. This is due to the freedom of rotating all spins together around the z-axis, without any energy cost. It is a direct consequence of the free boundary conditions.

A further comparison can be made by looking at the spectrum with a vortex present, but with *free boundary conditions*, see figure 9.26, again for the vortex in a square lattice system of radius $R = 15a$. If damping were present, the vortex would probably be unstable, and its dynamics would cause it to move towards the boundary. The diagonalization calculations, however, do not include damping, and only give a measure of the small-amplitude harmonic oscillations that can appear. Even so, the spectrum changes slightly from that for fixed boundary conditions. First, the zero frequency mode now appears, because the free boundary condition allows all spins to rotate together around the z-axis, with no energy cost, even when a (centered) vortex is present. Second, the translational mode frequencies acquire a small imaginary part, on the order of $10^{-6}JS$, due to round-off errors, that would correspond to the same effect expected if damping were present. This shows that the instability of the vortex remaining at the system center actually does appear in the calculation. Third, the vortex instability mode that would go to $\omega = 0$ at λ_c
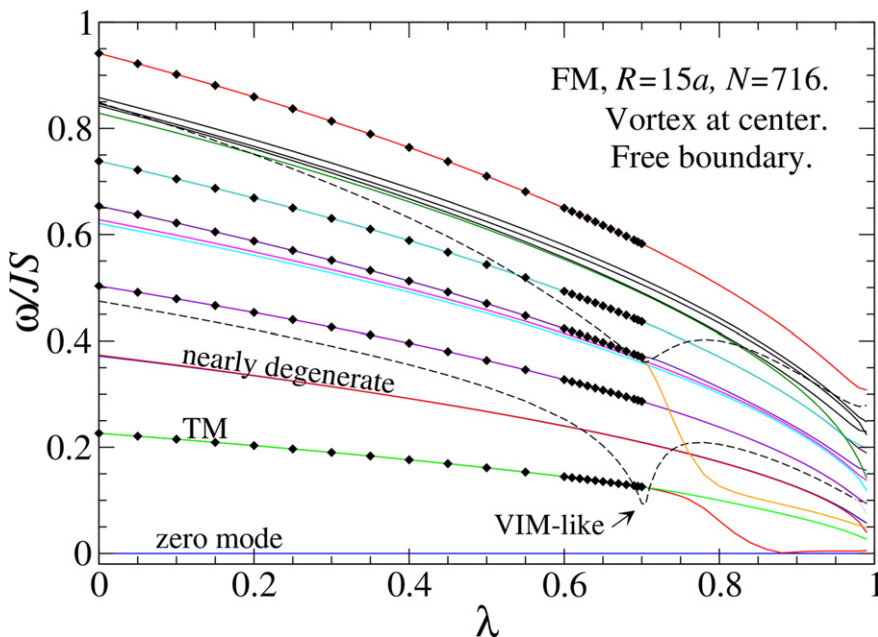
Figure 9.26. Spectrum of normal modes on a vortex in a square lattice system of radius $R = 15a$ (716 sites, free boundary conditions), obtained by exact diagonalization of the equations (9.211a). Modes marked with diamonds are doubly degenerate. Modes shown as dashed are similar to the VIM but do not go to zero frequency at λ_c. The *zero mode* with $\omega = 0$ appears due to the freedom to rotate all spins together at no energy cost. Note how all modes tend to have lower frequencies than for fixed boundary conditions, figure 9.12. The translational modes and others degenerate for $\lambda < \lambda_c$ become split for $\lambda > \lambda_c$, due to non-zero G.

now is not present, however, there are other higher modes with a strong downward cusp at λ_c (shown as dashed curves). The free boundary condition is softer than a fixed boundary, and that is responsible for this change.

It is very clear that the presence or absence of a vortex, together with the type of boundary conditions, has a substantial effect on the spin wave spectrum.

9.6 Vortex mass obtained from vortex normal modes

The normal mode spectrum can be connected to calculations of the vortex mass [8], for an isolated vortex in a small circular system such as that just considered above. The idea is that the translational modes are directly related to the vortex motion and, hence, their eigenfrequencies are connected to the frequencies one finds for gyrotropic motion of the vortex in the circular system. The mass can be estimated by making the results of the modified Thiele equation consistent with the eigenfrequencies found from the perturbation analysis.

We have already considered the motion of a vortex in a circular system, from the point of view of the modified Thiele equation (9.46). The force was assumed to be the force due to an image vortex. For a system discretized on a lattice, the force may

be somewhat different from the analytic expressions already found. For the moment, assume that with fixed boundary conditions, the force is a radial restoring force with some force constant k_F,

$$\mathbf{F} = -k_F \mathbf{X}, \tag{9.224}$$

where $\mathbf{X}(t)$ is the instantaneous vortex location, measured from the center of the circular system. With an assumed rotational motion $\mathbf{V} = \omega \hat{\mathbf{z}} \times \mathbf{X}$ and then $\ddot{\mathbf{X}} = -\omega^2 \mathbf{X}$, the equation of motion is just like (9.200) found earlier,

$$-k_F \mathbf{X} - \omega G \mathbf{X} = -\mathsf{M}\omega^2 \mathbf{X}. \tag{9.225}$$

The two frequencies that result for orbital motion are written here as

$$\omega_{\pm} = \frac{1}{2\mathsf{M}}\left(G \pm \sqrt{G^2 + 4k_F \mathsf{M}}\right), \qquad \text{for } \mathsf{M} > 0, \, k_F > 0. \tag{9.226}$$

At this point we allow both possible solutions, which are assumed to be mapped to the two possible translational modes. For an out-of-plane vortex, these connect to different rates and senses of rotation around the system center. One can see that with $\mathsf{M} > 0$ and $k_F > 0$, one obtains $\omega_+ > 0$ (counterclockwise motion) but $\omega_- < 0$ (clockwise motion), regardless of the sign of G. If instead an in-plane vortex is considered, with $G = 0$, the solutions are those for simple harmonic motion,

$$\omega_{\pm} = \pm\sqrt{k_F/\mathsf{M}}, \qquad \text{for } G = 0. \tag{9.227}$$

This can also be interpreted as saying that circular motions in opposite senses will have the same frequencies. The results so far have required a mass. If the mass were not present, the Thiele equation then gives only one frequency,

$$\omega_0 = -k_F/G, \qquad \text{for } \mathsf{M} = 0. \tag{9.228}$$

If both $\mathsf{M} = 0$ and $G = 0$, as would be the case for massless in-plane vortices, there is no solution. Thus, we suppose that a mass is always present, in order to have consistency between the Thiele dynamics and the spin wave spectrum.

From the quadratic equation that leads to $\omega_{\pm}$, one has a relation for the product of the two frequencies, that can be solved for an estimate of the mass,

$$\omega_+ \omega_- = -\frac{k_F}{\mathsf{M}} \qquad \Longrightarrow \qquad \mathsf{M} = -\frac{k_F}{\omega_+ \omega_-}. \tag{9.229}$$

Therefore, this can be used to estimate M if the force constant is already known, assuming that the frequencies are taken to be the translational mode frequencies from the perturbation analysis.

We can estimate the force constant essentially by a variation of the spin alignment iteration approach, but enforcing a constraint on the vortex position. The total quasi-static energy of the vortex might be expected to be of a quadratic potential form,

$$U(\mathbf{X}) \approx \frac{1}{2}k_F X^2. \tag{9.230}$$

To impose a desired position, the in-plane angles ϕ_i for four sites in the core of the vortex can be fixed to have the values given by (8.7), for a desired location, not exactly at the system center. The spin configuration can be relaxed by the spin alignment technique, resulting in a calculation of $U(\mathbf{X})$ for that position. This can be repeated for different small displacements (fractions of a lattice constant) away from the system center. As a result, one finds an approximate quadratic dependence on the displacement from the center, and the force constant k_F is easily determined. This is performed for the same boundary conditions (fixed) as those applied to obtain the normal modes. Results for k_F are shown in figure 9.27, which are rather surprising. For $\lambda < \lambda_c$, the force constant is very close to constant, independent of the system size. This is in contrast to what we could expect from the continuum expression (9.198) based on the forces due to vorticity between the vortex and its image. Expression (9.198) would predict that $k_F \propto R^{-2}$ as $X \to 0$. But that is not what is found for the system on a square lattice. This may be because there are discrete pinning forces, especially in the core region, that dominate the force. As $\lambda \to 1$ for out-of-plane vortices, the force constant shown in figure 9.27 decreases considerably, and is all the smaller for larger R, but not as an inverse square law.
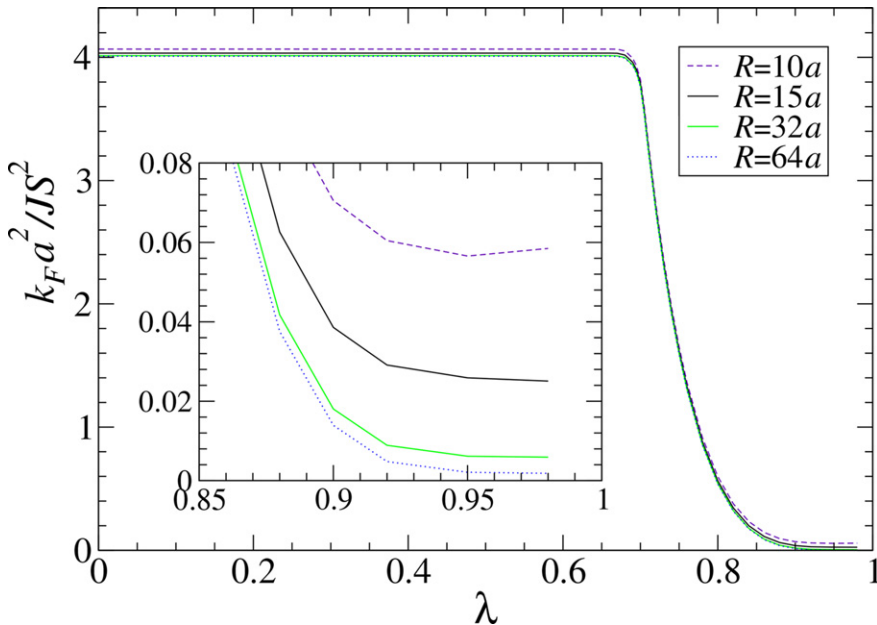

Figure 9.27. The effective vortex force constant k_F as estimated from (9.230) and energy calculated from the spin alignment relaxation scheme, for indicated system radii. The inset gives an indication of the dependence on system radius for out-of-plane vortices.
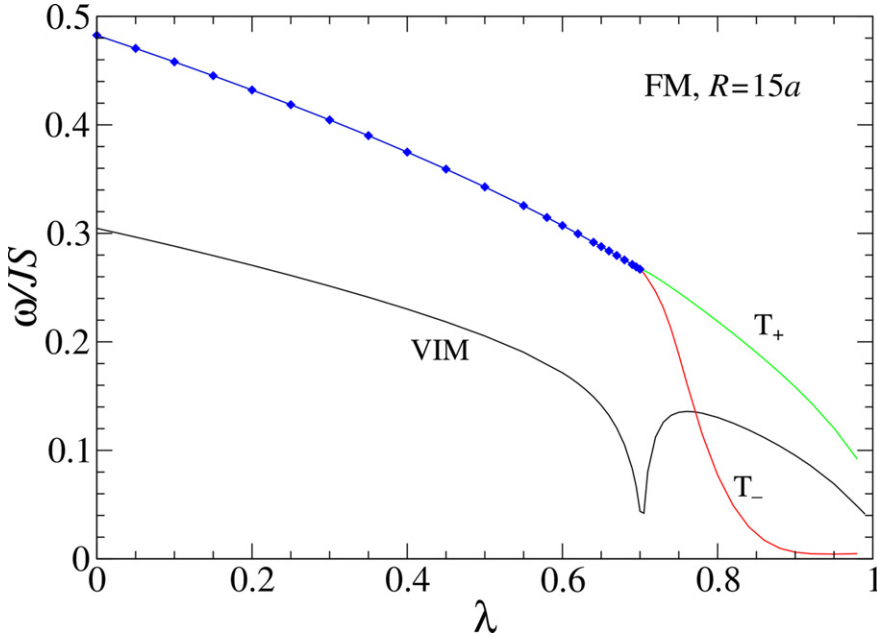
Figure 9.28. Three of the lowest modes in an FM square lattice system of radius $R = 15a$ with a vortex with fixed boundary conditions, obtained by exact diagonalization of equations (9.211a). The VIM is responsible for the transformation of an in-plane vortex into out-of-plane form at $\lambda_c \approx 0.70$. The translational modes T_+ and T_- are degenerate for in-plane vortices but become distinctly split in out-of-plane vortices, due to the non-zero gyrovector that plays such an important role in the dynamics.

The translational mode frequencies for the $R = 15a$ system are shown again in figure 9.28, together with the vortex instability mode as a reference. The lower of the translational modes, labeled as T_-, goes to very low frequency as λ approaches unity. That is the mode whose frequency becomes $\omega_0 = -k_F/G$ in the limit of zero mass; it is the more 'natural' motion for a vortex in a confined circular system. Examples of its wave function were given in figures 9.19 and 9.23. The higher mode T_+ has wave functions such as those in figures 9.22 and 9.18. Based on the result (9.229) above, the translational mode frequencies are identified as ω_+ and ω_-, and used to estimate the mass, whose result is shown in figure 9.29 for various system sizes, all with fixed boundary conditions. Note that M has been calculated in units of $(JS)^{-1}$; the physical mass would be $m = \sigma M$, which has units of $(Ja^2)^{-1}$, which can be expressed in kilograms. The mass has a considerable variation with λ, especially a large peak around λ_c. Also, M increases with system radius, but not according to the logarithmic form in (9.35). It is difficult to reconcile this calculation of M on the discrete lattice system with that continuum theory expression. One can suspect that there are intense discreteness effects that could be responsible for the considerable differences. The continuum expression employed an artificial cutoff in the core region, but that is probably the region with the most important dynamics, which has somehow been over-approximated in the continuum limit.
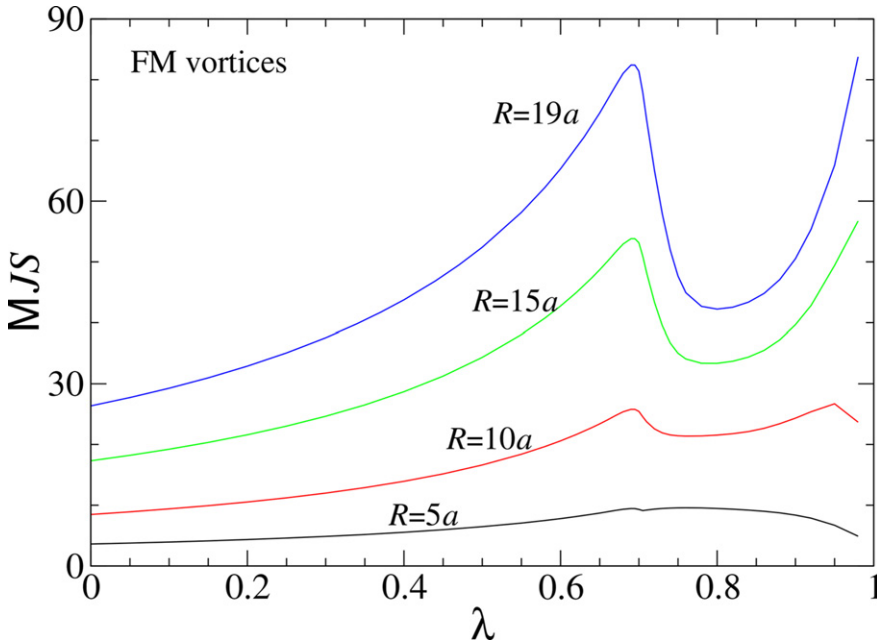
Figure 9.29. FM vortex masses as estimated from expression (9.229), which uses the translational mode eigenfrequencies, calculated on circular square lattice systems of the indicated radii. These values tend to be considerably larger than the predictions of the continuum theory, expression (9.35). The physical mass m is obtained by scaling with the spin density, $m = \sigma M$.

Bibliography

[1] Thiele A A 1973 Steady-state motion of magnetic domains *Phys. Rev. Lett.* **30** 230

[2] Thiele A A 1974 Applications of the gyrocoupling vector and dissipation dyadic in the dynamics of magnetic domains *J. Appl. Phys.* **45** 377

[3] Huber D L 1982 Dynamics of spin vortices in two-dimensional planar magnets *Phys. Rev.* B **26** 3758

[4] Wysin G M and Mertens F G 1991 Equations of motion for vortices in 2D easy-plane magnets *Nonlinear Coherent Structures in Physics and Biology* vol 393. In ed M Remoissenet and M Peyrard (Berlin: Springer) pp 1–4

[5] Wysin G M, Mertens F G, Völkel A R and Bishop A R 1994 Mass and momentum for vortices in two-dimensional easy-plane magnets *Nonlinear Coherent Structures in Physics and Biology* vol 329. In ed K H Spatschek and F G Mertens (New York: Plenum) pp 177–86

[6] Tjon J and Wright J 1977 Solitons in the continuous Heisenberg spin chain *Phys. Rev.* B **15** 3470

[7] Völkel A R, Wysin G M, Mertens F G, Bishop A R and Schnitzer H J 1994 Collective variable approach to the dynamics of nonlinear magnetic excitations with application to vortices *Phys. Rev.* B **50** 12711

[8] Wysin G M 1996 Magnetic vortex mass in two-dimensional easy-plane magnets *Phys. Rev.* B **54** 15156

 [9] Mertens F G, Wysin G M, Völkel A R, Bishop A R and Schnitzer H J 1994 Cyclotron-like oscillations and boundary effects in the 2-vortex dynamics of easy-plane magnets *Nonlinear Coherent Structures in Physics and Biology* vol 329. In ed K H Spatschek and F G Mertens (New York: Plenum) pp 191–8

[10] Wysin G M and Völkel A R 1995 Normal modes of vortices in easy-plane ferromagnets *Phys. Rev.* B **52** 7412

[11] Wysin G M and Völkel A R 1996 Comparison of vortex normal modes in easy-plane ferromagnets and antiferromagnets *Phys. Rev.* B **54** 12921

[12] Ivanov A K, Kolezhuk B A and Wysin G M 1996 Normal modes and soliton resonance for vortices in 2D classical antiferromagnets *Phys. Rev. Lett.* **76** 511

[13] Ivanov B A and Wysin G M 2002 Magnon modes for a circular two-dimensional easy-plane ferromagnet in the cone state *Phys. Rev.* B **65** 134434

[14] Ivanov B A, Schnitzer H J, Mertens F G and Wysin G M 1998 Magnon modes and magnon-vortex scattering in two-dimensional easy-plane ferromagnets *Phys. Rev.* B **58** 8464

[15] Holstein T and Primakoff H 1940 Field dependence of the intrinsic domain magnetization of a ferromagnet *Phys. Rev.* **58** 1098